ELECTROCHEMISTRY COUPLED ONLINE WITH MASS SPECTROMETRY AND ITS APPLICATIONS

By

TIANYI ZHANG

A DISSERTATION PRESENTED TO THE GRADUATE SCHOOL
OF THE UNIVERSITY OF FLORIDA IN PARTIAL FULFILLMENT
OF THE REQUIREMENTS FOR THE DEGREE OF
DOCTOR OF PHILOSOPHY

UNIVERSITY OF FLORIDA

2001

To my wonderful parents, my dear wife and my lovely son

ACKNOWLEDGMENTS

I would like to sincerely thank Dr Anna Brajter-Toth for her guidance and total support. I would like to give my sincere appreciation to Dr John P Toth for helpful discussions MS training, and unlimited access to the particle beam MS

I would like to thank Dr John R. Eyler for giving me a chance to play with the ESI-FTICR MS His help with my research is gratefully acknowledged The friendship and assistance from the members of the Eyler group are also acknowledged

I would like to thank Dr Weihong Tan, Dr Jon Stewart, Dr John R Eyler and Dr John P Toth for the time and willingness to serve on my committee Many thanks go to Dr Kathryn Williams for her help and support The help from the departmental machine shop and electronic shop is also acknowledged I also would like to thank Roberto Bravo and Weijun Qian for their friendship and help

I would like to thank my parents and my parents-in-law for their consistent support, encouragement and love. Finally I would like to express my sincerest gratitude to my dear wife for her understanding, full support and love

TABLE OF CONTENTS

page

ACKNOWLEDGMENTS iii

KEY TO ABBREVIATIONS viii

ABSTRACT x

CHAPTERS

- 1 INTRODUCTION 1
  - Electrochemistry Online with Mass Spectrometry (EC/MS) 1
  - Design of EC Cell for Online EC/MS 3
  - Detection of Cation Radicals 6
  - Aromatic Amines 8
    - Electrochemistry of Triphenylamine (TPA) 9
    - Mass Spectrometry of Aromatic Amines 12
  - Polycyclic Aromatic Hydrocarbons (PAHs) 13
    - Electrochemistry of PAHs 14
    - MS Investigation of Nucleophilic Reactions 16
  - LC/MS Interfaces for EC/MS 16
    - Evolution of LC/MS Interfaces 17
    - PB Interface for EC/MS 18
    - Electrolytic Nature of ESI Interface 19
    - Use of Electrolyte in ESI-MS 20
    - Coupling EC Cell to ESI-MS 21
  - Analytical Applications 23
  - Overview of Thesis 25
- 2 EXPERIMENTAL METHODS 32
  - Methods and Instrumentation 32
    - EC Flow Cell 32
    - Cyclic Voltammetry 33
    - Chronocoulometry 33
    - Flow Injection/Electrochemical Detection 33
    - EC/PB/MS 34
    - EC/ESI-FTICR MS 34
  - Methods Fundamentals 34
    - Cyclic Voltammetry (CV) 34

        Flow Injection/EC Detection 37
        PB/MS 38
        ESI/MS 39
        FTICR MS 42
    Experimental Conditions 44
        Reagents and Chemicals 44
        CV Experiment 45
        Chronocoulometry (CC) 45
        Flow Injection/Electrochemical Detection 46
        PB and MS Conditions 46
        EC/PB/MS 47
        PB/MS Analysis of TPA 48
        Solutions for EC/ESI-FTICR MS 49
        EC/ESI-FTICR MS Conditions 49
        Regeneration of the EC Cell 51
        Data Handling in FTICR MS 51

3 INVESTIGATION OF THE GENERATION OF NONAQUEOUS INTERMEDIATE RADICAL CATIONS IN THE OXIDATION OF TRIPHENYLAMINE BY ELECTROCHEMISTRY/PARTICLE BEAM MASS SPECTROMETRY 61
    Introduction 61
    Results and Discussion 62
        Cyclic Voltammetry of TPA 62
        Offline Flow Injection Analysis (FIA) 63
        Online FIA in EC/PB/MS 65
        Direct EC/PB/MS Monitoring of Radical Intermediate and Product 66
        Ion Formation in EC/PB/MS 67
        Ion Formation by EI 68
        Ion Intensity Ratio for Ion Monitoring 69
        Concentrations of TPA and TBAP 70
        Signal Enhancement with TBAP 71
    Conclusions 72

4 HIGH SENSITIVITY IN PARTICLE BEAM MASS SPECTROMETRY WITH A NONVOLATILE ELECTROLYTE 83
    Introduction 83
    Results and Discussion 85
        Change to the EI Mass Spectrum of TPA 85
        Formation of TPA/TBAP Aggregates 87
        Effect of TBAP Concentration 88
        TPA Calibration Curves 89
        Effect of Different Electrolyte Additives on TPA Signal 91
        Effect of Neutral Additives 92
        Effect of TBAP on Signals of Different Analytes 93
        Effect of Ionization Mode on Signal Enhancement 94
    Conclusions 94

5 ENHANCEMENT OF IONIZATION EFFICIENCY BY ELECTROCHEMICAL REACTION PRODUCTS IN ELECTROCHEMISTRY/ELECTROSPRAY FOURIER TRANSFORM ION CYCLOTRON RESONANCE MASS SPECTROMETROMETRY 103
Introduction 103
Results and Discussion 105
  EC Cell 105
  ESI and EC/ESI-MS of TPA 105
  Ion Assignments 106
  Ion Formation in the EC Cell 108
  Protonation of TPA in EC/ESI MS 109
  EC/ESI-MS with the ss(2)–ss(3) Electrodes 110
  Effect of Flow Rate 111
  Limited Signal Suppression by TBAP in EC/ESI-FTICR MS 111
Conclusions 112

6 EXPERIMENTAL FACTORS CONTROLLING DETECTION SENSITIVITY IN THE OXIDATION OF TRIPHENYLAMINE BY ONLINE EC/ESI-FTICR MS 121
Introduction 121
Results and Discussion 123
  ESI Parameters 123
    ES voltage 123
    ES – counter capillary distance 125
    Counter capillary voltage 126
    ES Needle Dimension 126
    Electrolyte concentration 127
    Flow Rate 128
  EC Related Parameters 130
    Working electrode (WE) area and cell configuration 130
    TPA analyte concentration 131
    EC cell voltage 132
  Reactions of TPA$^{\bullet}$ in the Gas Phase 133
    Collision-induced dissociation (CID) of TPA$^{\bullet}$ in the ICR cell 133
    Effect of Ion-accumulation time in the hexapole 134
Conclusions 135

7 OXIDATION OF POLYCYCLIC AROMATIC HYDROCARBONS AND NUCLEOPHILIC REACTIONS INVESTIGATED BY EC/ESI-FTICR MS 149
Introduction 149
Results and Discussion 150
  EC/MS of Anthracene 150
    Sensitivity in detection of anthracene 150
    Nucleophilic reactions of anthracene cation radical with pyridine 155
  EC/MS of Perylene 156
    Sensitivity in detection of perylene 156

Nucleophilic reactions of perylene cation radical with pyridine 158
EC/MS of Rubrene 159
Sensitivity in detection of rubrene 159
Nucleophilic reactions of rubrene cation radical with pyridine 160
Conclusions 161

8 CONCLUSIONS AND FUTURE WORK 178

LIST OF REFERENCES 184

BIOGRAPHICAL SKETCH 193

KEY TO ABBREVIATIONS

CI – chemical ionization

CID – collision induced dissociation

CC – chronocoulometry

CE – counter electrode

CV – cyclic voltammetry

DMAP – 4-dimethylaminopyridine

EC – electrochemistry

EC/MS – electrochemistry coupled on-line to mass spectrometry

EI – electron impact ionization

EF – enhancement factor

ES – electrospray

ESI – electrospray ionization

FIA – flow injection analysis

FTICR – Fourier transform ion cyclotron resonance

ICR – ion cyclotron resonance

LiT – lithium triflate

LOD – limit of detection

MS – mass spectrometry

MW – molecular weight

PAH – polycyclic aromatic hydrocarbon

PB – particle beam

PCI – positive chemical ionization

PEEK – polyetheretherketone

RE – reference electrode

RPG – rough pyrolytic graphite

SIM – selective ion monitoring

SS – stainless steel

TBAP – tetrabutylammonium perchlorate

TLBE – thin-layer bulk electrolysis

TPA – triphenylamine

TPB – tetraphenylbenzidine

TSP – thermospray

WE – working electrode

Abstract of Dissertation Presented to the Graduate School
of the University of Florida in Partial Fulfillment of the
Requirements for the Degree of Doctor of Philosophy

ELECTROCHEMISTRY COUPLED ON-LINE WITH MASS SPECTROMETRY AND ITS APPLICATIONS

By

Tianyi Zhang

December 2001

Chairperson: Anna Brajter-Toth
Major Department: Chemistry

Two LC/MS interfaces, particle beam (PB) and electrospray ionization (ESI) were used to couple electrochemistry (EC) to mass spectrometry (MS) EC/MS. A homebuilt thin layer EC flow cell was used in EC/PB/MS. Observation of the generation of tetraphenylbenzidine (TPB) radical monocation in the oxidation of triphenylamine (TPA) was achieved by EC/PB/MS. Significant enhancement of the TPA ion signal was observed in the presence of tetrabutylammonium perchlorate (TBAP) electrolyte. The signal enhancement was attributed to an improved PB mass transport in the presence of the electrolyte and a reduced fragmentation of the TPA ion in the EI ion source of the mass spectrometer, due to the formation of TBAP/TPA aggregates. The signal enhancement factor was ~35-fold. By keeping the TBAP/TPA concentration ratio constant at an optimum value 10/1, an enhancement in PB/MS detection sensitivity and linearity of TPA calibration curves was achieved at low concentrations.

A new electrochemical flow cell was developed and coupled to an electrospray ionization Fourier transform ion cyclotron resonance mass spectrometer (EC/ESI-FTICR MS). Identification of TPB dication in the presence of an interfering ion of the same m/z value was achieved based on the detection of isotopic ions. The MS detection sensitivity for TPB radical monocation and dication was greatly enhanced by EC/ESI-FTICR MS compared to ESI-FTICR MS detection. In ESI ionization, the oxidation of TPA was limited to the spray needle tip.

In EC/ESI-FTICR MS, the application of EC cell voltage significantly reduced the signal suppression problem from the TBAP electrolyte. This result showed that common electrolytes might be used in EC/ESI-MS. It was verified that flow rate and electrolyte concentration were the parameters that affect the MS detection sensitivity of transient electrochemical products.

Nucleophilic reactions of cation radicals with pyridine were also investigated by EC/ESI-FTICR MS. The MS detection sensitivity for anthracene-pyridine and perylene-pyridine adducts was significantly enhanced by EC/ESI-FTICR MS.

CHAPTER 1
INTRODUCTION

Electrochemistry Online with Mass Spectrometry (EC/MS)

Electrochemistry (EC) on line with mass spectrometry (MS) (EC/MS) is a powerful technique for studying complicated electrode reactions, particularly those accompanied by chemical reactions [Volk et al. 1992]. The coupling of these two techniques can provide insights into important electron transfer processes.

By using MS as a detector, structural information about reactants, short-lived intermediates and products can be derived during the electrochemical reaction. This offers a possibility to directly monitor the intermediates and products as a function of the electrode potential, in close to real time, which can help clarify pathways of the redox reactions [Hambitzer and Heitbaum 1986, Volk et al. 1990, Xu et al. 1996, Zhou and Van Berkel, 1995].

As a detector MS is universal and sensitive because all compounds, upon ionization, will show a signal at the electron multiplier [Niessen 1999]. Selectivity is achieved by monitoring characteristic ions of a species or by using tandem MS/MS methods. Thus, it is possible to perform an EC/MS experiment without a prior separation of analytes, intermediates and products, which allows the necessary time resolution to detect short-lived intermediates during an EC reaction. These features of EC/MS are of importance in the investigation of redox reactions that are complicated by follow-up chemical reactions.

The usefulness of EC/MS in probing redox chemistry was shown elegantly by Volk et al [1992] In their work, EC/MS with a thermospray interface (TSP) was used to investigate the oxidation of uric acid [Volk et al 1988 1989(a)] and thiopurines [Volk et al 1989(b)] As a result of coupling EC to MS reaction intermediates and products were identified on the basis of the m/z of the protonated or deprotonated molecular ions and from daughter mass spectra obtained with MS/MS

The online EC/MS has also been applied to the investigation of electrocatalysis [Regino and Brajter-Toth 1999] In that work, EC/MS with particle beam interface (PB) was used to investigate the catalytic oxidation of 4-dimethylaminopyridine (DMAP) by a dopamine orthoquinone The oxidant dopamine orthoquinone, was generated electrochemically by the oxidation of dopamine [Regino et al 1998] The EC/MS allowed identification of a covalent intermediate adduct of dopamine orthoquinone-DMAP, which had been postulated to explain the catalytic oxidation. In addition, the occurrence of a nucleophilic reaction between NH_3 from the NH_4Ac supporting electrolyte and the dopamine orthoquinone was observed This reaction consumed orthoquinone oxidant and was a competing reaction to the catalytic reaction

In other work, Xu and coworkers [1996] have studied the oxidation of a polycyclic aromatic hydrocarbon (PAH) compound benzo[a]pyrene (BaP), with their homebuilt electrochemical flow cell which was coupled to an electrospray ionization (ESI) mass spectrometer It was shown that a molecular radical ion can be observed without protonation in EC/ESI-MS Some hydrolysis products of the molecular ion were also detected

Other types of redox reactions such as the oxidation of metal-organic complexes [Arakawa et al. 1999] and anodic electropolymerization of aniline [Deng and Van Berkel 1999] have also been studied by EC/MS. In general, it has been established that EC/MS is an excellent tool for providing chemical information to aid the elucidation of the complex redox reactions.

Design of EC Cell for Online EC/MS

In EC/MS, the electrochemical reactions take place in an EC flow cell, which is coupled to the MS via an LC/MS liquid interface. The design of the EC cell is largely determined by the LC/MS interface used in EC/MS, which can be a TSP, PB, or ESI interface. In designing EC flow cell for EC/MS, there are two major considerations: electrolysis efficiency, which can be expressed as the percentage of the analyte electrolyzed as it flows through the EC cell, and MS response time, which is the time between the application of the voltage to the working electrode in the EC cell and the appearance of a mass spectral signal corresponding to the EC-generated ion [Volk et al. 1992]. In order to ensure sensitive detection of EC-generated species by MS, high electrolysis efficiency and a rapid MS response are necessary.

To provide chemical information in close to real time about the species formed during the reactions in the EC cell, the delay time between electrochemical generation and MS detection should be as short as possible. This is especially important for the detection of short-lived intermediates. In the development of EC/MS, a considerable effort has been made to improve the design of the EC flow cell aiming at achieving high electrolysis efficiency and rapid MS detection response. High electrolysis efficiency can be achieved by increasing the electrode area to solution volume ratio in the EC cell design A rapid MS response time can be achieved by reducing the transport path or void volume between the EC cell and the MS detector Experimental parameters such as solution flow rate also affect the electrolysis efficiency and MS response time and can be optimized to achieve the best EC/MS performance

Various commercial and homebuilt EC cells have been used for on-line EC/MS For example in their pioneering work on EC/ESP/MS Hambitzer and Heitbaum [1986] developed a three-electrode flow-through cell with a Pt-coil working electrode. An MS response time of ca. 10 s was reported Volk and coworkers used a commercial ESA coulometric cell with porous reticulated vitreous carbon working electrode and Pd counter and reference electrodes in the EC/TSP/MS studies of the oxidation of uric acid [Volk et al 1988 1989(a)] and thiopurines [Volk et al 1989(b), 1990] An MS response time of ca 500 ms was reported Recently a thin layer cell was developed [Regino and Brajter Toth 1997] and was used in EC/TSP/MS and EC/PB/MS A new feature of this thin-layer cell design is that it uses removable working, counter and reference electrodes, which allows easy access to the electrodes for cleaning or replacement Because fouling of the working electrode can be a problem during long cell operation the ease of operation of this thin-layer cell is a particular advantage over other types of cell designs

Bond and coworkers [1995] coupled a two-electrode tubular cell to ESI/MS in the investigation of the electrolysis of metal-diethyldithiocarbamate complexes The outlet of the EC cell was connected via Teflon tubing and a metal connector to a fused silica spray capillary of the ESI source of the mass spectrometer One disadvantage is that the long transport path between the EC cell and the MS may delay the MS response

Another shortcoming is the use of an extremely high EC cell voltage, 200 V, which is not desirable in typical operations.

Zhou and Van Berkel [1995] reported the use of different types of EC cells with ESI/MS, including a two-electrode tubular cell, a commercial thin-layer cell, and a commercially available porous flow-through cell. The tubular cell was operated in a floated mode. That is, the cell voltage was floated at the high ES voltage (Figure 1-1), while the thin-layer cell and porous cell were operated in a decoupled mode. That is, the cell voltage was decoupled from the high spray voltage by a grounded metal connector and a long piece of fused silica tube. A disadvantage of the decoupled EC cell is that insertion of the grounded metal connector led to a 30 cm distance between the working electrode and the ESI capillary exit, which can significantly delay the MS detection response. The floated tubular cell offers fast MS response. However, "electrochemical interference" from the electrolytic nature of the ESI may obscure the effect of the electrochemical reactions in the EC flow cell.

Cole's group developed a novel EC cell design for EC/ESI/MS constructed inside the ESI probe [Xu et al. 1996], in which a Pt wire working electrode was placed inside the ES needle and exposed out of the ES needle tip (Figure 1-2). The Pt electrode was isolated from the stainless steel ES needle by a layer of fused silica. The ES needle was used as a counter electrode, and an Ag/Ag reference electrode was placed in a PEEK cross outside of the ESI probe. A reported advantage of this cell design is that it contributes to a short MS response time, ca. 1.7 s. A shortcoming of the design is that a large-diameter ES needle must be used to hold the working electrode inside. For example, a stainless steel ES needle capillary of 350 µm i.d. and 405 µm o.d. was used which is much bigger than the 100 µm i d -200 µm o d ES needle normally used in ESI MS [Kebarle and Tang 1993] Another confusing issue is hidden in this cell design It is known that the ESI is electrolytic in nature [Blades et al 1991] In positive ion MS detection mode the ESI process requires that an oxidation reaction occur at the ES needle to maintain the charge balance [Van Berkel and Zhou 1995(a) and (b)] In Cole's EC cell design the spray needle was used as an auxiliary electrode in the online EC cell When the EC cell voltage was applied, the oxidation reaction occurred at the Pt working electrode and consequently the reduction occurred at the ES needle auxiliary electrode Thus, in the EC/ESI/MS experiment, oxidation during ESI may create complications in control of the EC voltage

Detection of Cation Radicals

Cation radicals can be created in solution by chemically or electrochemically induced electron transfer reactions which typically involve pi electrons or heteroatoms with lone electron pairs [Yoshida 1984 Adams 1969(a)] The desirable properties of conjugated polymers, such as tunable electrical conductivity charge storage capacity photoconductivity photoluminescence and electroluminescence are all tightly related to the formation, recombination and transport of cation radicals [Baumgarten and Mullen 1994] The formation of cation radicals is regarded as an initiation step in carcinogenesis [Rogan et al 1988]

The detection of cation radicals can be accomplished with electron paramagnetic resonance (EPR) [Marcoux et al 1967 Rooney and Pink 1962 Toriyama et al 1987 Erickson et al 1993] However the short lifetime of cation radicals makes the studies challenging In solution, cation radicals are susceptible to reactions with nucleophiles or can undergo other processes such as dimerization [Mann and Barnes 1970, Adams 1969(a) and (b)]. To improve the detection of cation radicals, methods to stabilize the cation radicals in solution have been developed [Marcoux et al. 1967, Knight 1986, Shiotani 1987]. The stability of cation radicals is solvent dependent and may be increased by a judicious choice of a solvent or solvent additives [Bard et al. 1976, Werst and Trifunac 1991]. As a result, cation radicals may be detected as solvent-cation radical complexes. Another way to stabilize cation radicals is to lower the temperature or to decrease the reaction rates [Werst and Trifunac 1998]. The ultimate stabilization of the cation radicals can be achieved by trapping the reactive cation radicals in an inert rigid matrix, which includes rare gas matrices and halocarbon matrices. The rare gas method involves matrix deposition on a cold surface [Knight 1986]. The typical halocarbon matrices are liquids at room temperature, and solutions can be prepared in the usual way [Symons 1984, Shida et al. 1984]. The matrix isolates the cation radicals from neutral molecules, and in the meantime, removes the excess energy from the radicals. Cation radicals can also be stabilized by adsorption on solid surfaces such as silica gel, silica-alumina and in zeolites [Werst and Trifunac 1998].

Cation radicals are often generated as intermediates in electrochemical redox reactions [Yoshida 1984]. To elucidate the mechanism of redox reactions, it is often necessary to be able to directly detect the intermediate cation radical species generated in solution. The transfer of solutions of interest to other matrices is not only laborious, but also may complicate the analysis of the final products. For this purpose, on-line techniques with fast detection capabilities are needed. Online EC/MS can provide the chemical information about the EC-generated species with excellent time resolution

[Volk et al 1992] In EC/MS cation radicals can be readily detected based on the m/z specificity of MS measurement Besides the high specificity MS detection also offers high sensitivity If desired, the sensitivity of MS measurement can be further enhanced by selected ion monitoring (SIM) [Zhang and Brajter-Toth 2000] Besides the measurement of intact cation radicals, more detailed chemical information can be derived from the fragmentation of cation radicals in an electron impact (EI) ion source, with collision induced dissociation (CID) or MS/MS Owing to the limited radical lifetimes a fast detection method is vital to the success in radical detection [Werst and Trifunac 1998] In on-line EC/MS rapid detection can be achieved via the design of the EC cell and EC cell/MS coupling [Volk et al 1992 Hambitzer et al 1998(a) and (b) Regino and Brajter-Toth 1997 Xu et al 1996 Zhou and Van Berkel 1995 Deng and Van Berkel 1999(b)] The chemical selectivity and the sensitivity provided by MS plus the good time resolution of the method is compatible with the detection of radicals and the study of their follow-up chemical reactions

Aromatic Amines

Aromatic amines with one or more phenyl rings attached to the N atom can generate cation radicals readily upon oxidation During oxidation, one electron is removed from the nitrogen lone pair, and the formed radical is stabilized as a result of the delocalization of the unpaired electron and charge throughout the conjugated phenyl rings [Adams 1969(a) and (b) Yoshida 1984 Mann and Barnes 1970] The choice of aromatic amines for EC/MS study of radicals was partly initiated to develop EC/MS as a tool to provide insight into the follow-up chemistry of dye radicals, and eventually dye fading mechanisms A sample dye was of interest in which the reactive sites were hypothesized to be the N atoms attached to the phenyl rings An EC/MS study of the aromatic amines was therefore initiated to verify the capabilities of EC/MS in radical detection and for providing insight into the reaction pathway

The cation radical of triphenylamine (TPA) shows higher stability than diphenylamine which is more stable than aniline [Mann and Barnes 1970] In fact the cation radical of aniline is so reactive that it polymerizes easily at the working electrode and causes fouling problems [Adams 1969(b) Mohilner et al 1962] The electrochemical behavior of triphenylamine is also relatively simple Based on this, triphenylamine was an ideal compound for the intended characterization of EC/MS for the investigation of the reaction pathways of N radicals

Electrochemistry of Triphenylamine (TPA)

The electrochemical oxidation of TPA has been extensively investigated [Seo et al 1966 Nelson and Feldberg 1969, Creason et al 1972 Debrodt and Heusler 1981] The reaction scheme of TPA in acetonitrile is shown in Figure 1-3 The initial step involves a loss of an electron to form the cation radical $\text{TPA}^{\bullet+}$ The $\text{TPA}^{\bullet+}$ ion radicals can couple between themselves or with neutral TPA, after a loss of hydrogen to form tetraphenylbenzidine (TPB) TPB can be more easily oxidized than TPA The oxidation of TPB undergoes two discrete one-electron transfer steps, which leads to the formation of a quinoid dication as the final product

By means of rapid sweep cyclic voltammetry, the initial oxidation of TPA was seen to be partially reversible [Oyama et al 1991] To verify that the oxidation of TPA leads to the formation of TPB the ESR spectra of the products of electrolysis of TPA and of TPB were recorded [Seo et al 1966] These spectra were complex and were not fully analyzed However they were identical and showed the evidence of splitting by two equivalent nitrogen nuclei, which indicated the presence of TPB cation radicals in both cases

Additional indication of the formation of a dimer was obtained by cyclic voltammetry [Seo et al 1966 Oyama et al 1991] The cyclic voltammogram of TPA showed a pair of smaller oxidation/reduction peaks at less positive potentials than the oxidation of TPA. These smaller peaks which occurred at the same potentials as the peaks of the TPB standard, appeared only on the second cycle, indicating that they were due to the TPB products formed in TPA oxidation

Oyama et al [1991] and coworkers used a pulse-electrolysis stopped flow method to verify the formation of TPA cation radical and TPB With this method, the TPA molecules were electrolyzed in a short time of 50 ms (current 20 mA) using a carbon-wool column electrode and the electrolyzed solution containing TPA cation radicals was immediately delivered to an optical flow cell by utilizing a stopped-flow technique By monitoring the change of absorbance at a wavelength characteristic for TPA and TPB the authors concluded that TPA cation radicals could couple to form TPB and that the TPB that was formed could be oxidized by TPA cation radicals No obvious formation of TPB dication was detected, as indicated by a lack of a characteristic absorption peak for a TPB dication in the UV absorption spectra

The rate of dimerization of TPA cation radicals in acetonitrile has been determined with rotating disk electrode [Marcoux et al 1969] and with chronoamperometry [Nelson and Feldberg 1969] By assuming a second-order ECE mechanism and a predominant formation of TPB dication from TPA oxidation, these workers reported a dimerization rate constant of ~1.2 × 10^3 $M^{-1}sec^{-1}$. Similar values of coupling rate constants, in the range of 1.1 × 10^3 to 3 × 10^3 $M^{-1}sec^{-1}$ have been reported by other researchers [Nelson and Philp 1979, Creason et al. 1972, Oyama, et al., 1991].

However, by using the pulse radiolysis method (45 MeV electron, 10 ns), Sumiyoshi proposed the formation of $(TPA)_2^{•+}$ dimer cation radical instead of a TPB cation radical in the oxidation of TPA [Sumiyoshi 1995]. This conclusion was based on the transient absorption spectra of TPA in 1,2-dichloroethane after pulse radiolysis, which exhibited new absorption bands that could not be attributed to either TPB or TPA cation radical. The $(TPA)_2^{•+}$ dimer cation radical was proposed to be produced by the reaction of TPA cation radical with the parent molecule. The rate constant for the dimer cation radical formation was determined to be 1.3 × 10^8 $M^{-1}sec^{-1}$, which was ca. 10^5 times larger than that for coupling of TPA cation radicals to TPB reported previously [Marcoux et al. 1969, Nelson and Philp 1979, Creason et al. 1972, Oyama et al. 1991].

As may be concluded from the above results, although the electrochemical behavior of TPA is relatively simple, some issues remain unresolved. The formation of TPA and TPB cation radicals has not been verified unequivocally with either ESR or absorption spectroscopy. There are still arguments about the identity of the dimer cation, i.e., whether it is $(TPA)_2^{•+}$ or $TPB^{•+}$. The coupling of TPA cation radical to form TPB is accompanied by a loss of two protons. It is still not clear whether the proton loss occurs before or after the coupling step. One limitation in the understanding of TPA oxidation behavior is the lack of a convenient and sensitive spectroscopic method that can provide chemical information about the oxidation products of TPA. MS can be used for this purpose.

Mass Spectrometry of Aromatic Amines

Aromatic amines are on the priority pollutant list of hazardous substances [Lesage 1993]. They are widely used as intermediates in the production of pesticides, dyes pharmaceuticals [Wu and Huang 1999]. Aromatic amines such as aminobiphenyl, aminoazobenzene and benzidene are carcinogenic [Wu and Huang 1999, Yoshyuki and Masakum 1995]. However, only limited MS data for aromatic amines are available [Moldovan and Bayona 2000]. Most MS investigations have been focused on heterocyclic aromatic amines and DNA adduct formation. Aromatic amines are typically analyzed by liquid/liquid or solid-phase extraction followed by HPLC [Wu and Huang 1999, Trippel-Schulte et al. 1986] or GC determinations, after derivatization with bromine or iodine [Concialini et al. 1983].

Ho and coworkers reported the use of thermospray mass spectrometry (TSP/MS) to distinguish diphenylamine (DPA) and N-nitrosodiphenylamine [Ho et al. 1990]. These two compounds cannot be distinguished by GC/MS because N-nitrosodiphenylamine can easily decompose to produce DPA at low injection port and column temperatures. However, advantage was taken of the thermal decomposition of N-nitrosodiphenylamine in TSP/MS. In the TSP interface, the thermal decomposition of N-nitrosodiphenylamine generated diphenylnitrogen radical and nitric oxide. Besides abstracting a hydrogen atom from the solvent to form DPA, the radicals could combine to form tetraphenylhydrazine which gave a new ion in the TSP mass spectrum. This too distinguished N-nitrosodiphenylamine from DPA. This work represents an example of applications of follow up radical chemistry in analytical determinations.

Hoang et al. [1996] studied adduct ion formation by aromatic amines in TSP/MS which included anilines, aminophenols, aminopyridines and hydroxypyrimidines. The protonated adduct ions with acetonitrile or methanol were observed for all compounds while water adduct ions were observed for only a few. No adduct ions with ammonia were formed when ammonium acetate was added to the LC system. It was found that the calculated hydrogen bond dissociation energy between aromatic amines and eluent constituents followed the order acetonitrile > methanol ~ water > NH_3. Based on this, the authors proposed that the incomplete evaporation of solvated and protonated molecules was responsible for the observed adduct ion formation.

Voyksner et al. [1993] determined by PB/HPLC/MS the aromatic amines originating from the chemical reduction of azo dyes. The reductive cleavage of the –N=N– bond of azo dyes by sodium hydrosulfite and tin(II) chloride led to the formation of anilines, benzidines, etc. The authors identified the products on the basis of the EI mass spectra library searches, spectral interpretation and the available aromatic amine standards. This work demonstrated the advantage of using the PB liquid interface in MS analysis, i.e., compatibility with EI ionization, which could ease data interpretation.

Moldovan and Bayona [2000] analyzed the EI mass spectra of a number of aromatic amines. Generation of molecular ion radical and a fission of a C–N bond during EI ionization of aromatic amines were reported.

Polycyclic Aromatic Hydrocarbons (PAHs)

PAHs constitute an extraordinarily large and diverse class of organic molecules. Many PAHs such as benz[a]anthracene and benzo[a]pyrene are strong carcinogens [Harvey 1991]. The formation of PAH cation radicals in biological systems through enzymatic one-electron oxidation is considered an activating step in the metabolic activation of tumor formation [Cavalieri and Rogan 1984 1988 Cavalieri et al 1990 RamaKrishna et al 1992, 1993] One-electron oxidation of PAHs has also been verified by electrochemical methods [Adams 1969(a), Peover and White 1967 Phelps et al 1967 Marcoux et al 1967] The synthesis of DNA-PAH adducts via the electrochemical oxidation and enzymatic oxidation of PAHs in the presence of DNA nucleosides has been reported [Rogan et al 1988 RamaKrishna 1992] The reactivity of PAH cation radicals varies considerably among different PAH compounds [Freeman et al 1994 Cavalieri and Rogan 1984 Pross and Moss 1990]

Electrochemistry of PAHs

The electrochemistry of PAHs has been extensively studied [Lund 1957 Neikam et al 1964 Parker 1970(a) and (b)] Because of the low solubility of PAHs in aqueous solutions the electrochemical investigations were typically carried out in nonaqueous solvents such as acetonitrile [Peover and White 1967], methylene chloride [Phelps et al 1967] or nitrobenzene [Marcoux et al 1967] The representative examples are the oxidation of anthracene, perylene and rubrene that have been investigated by cyclic voltammetry [Phelps et al 1967] In nonaqueous methylene chloride the oxidation of anthracene produced only one anodic peak in the cyclic voltammogram (with scan rate up to 5 V/s), while both anodic and cathodic peaks of equal size were observed for perylene and rubrene, with a peak separation of about 70 mV [Phelps et al 1967] These results are consistent with a one-electron reaction of PAHs, which leads to the formation of PAH cation radicals [Friend and Ohnesorge 1963] The results also suggest that the anthracene cation radical is very reactive, while the cation radicals of perylene and rubrene are stable

Coulometry and controlled-potential electrolysis of anthracene has revealed several products of follow-up chemical reactions of the cation radical [Majeski et al 1968] Hydrolysis and dimerization are the two major reactions following the production of anthracene cation radical In "dry" acetonitrile, hydrolysis (at least 4–10 mM water present in the most anhydrous solvent) occurs after the dimerization and the main product from the anodic electrolysis of anthracene is bianthrone In "wet" acetonitrile (up to 3 M water) the main electrolysis product is anthraquinone [Majeski et al 1968] The proposed reaction scheme of anthracene oxidation is shown in Figure 1-4 When pyridine was present during the electrolysis the formation of 9 10-dihydrodipyridinium salt was reported [Lund 1957]

The reactivity of PAH cation radicals can be predicted qualitatively by a simple HMO reactivity parameter ρ the unpaired electron density [Adams 1969(a) Higasi et al 1965] Table 1-1 shows the ρ values at various atomic positions for anthracene, perylene and tetracene the points of high ρ values exhibiting the greatest reactivity [Adams 1969(b)] Table 1-1 predicts that the cation radical of anthracene has two strong reactive sites, i e 9 10 positions, while that of perylene has no particularly strong reactive centers This prediction is consistent with the observed stability of anthracene and perylene cation radicals from the electrochemical experiments [Peover and White 1967] Blocking of the reactive sites can stabilize cation radicals Thus, although tetracene cation radical is very reactive, rubrene which is 5 6 11,12-tetraphenyl-tetracene gives a remarkably stable cation radical [Marcoux et al 1967, Phelps et al 1967]

MS Investigation of Nucleophilic Reactions

Besides hydrolysis and dimerization reaction, PAH cation radicals can react with other nucleophiles, including biological nucleophiles such as DNA bases and nucleosides [Rogan et al. 1988]. RamaKrishna et al. [1992] synthesized the adduct of benzo[a]pyrene-guanine nucleoside by EC and enzymatic oxidation of the PAH in the presence of the nucleoside. The adduct product was identified by both NMR and MS. The results confirmed the occurrence of a nucleophilic reaction between the PAH cation radical and the DNA nucleosides, and demonstrated the power of MS in structure elucidation of the adduct product.

MS has also been shown to be an effective tool in the investigation of gas-phase reactivity of PAH cation radicals toward biological nucleophiles. Whitehill et al. [1996(a) and (b)] studied the reaction of several different PAH cation radicals with N-methylimidazole or pyridine in the gas phase. The reactivity was investigated by admitting separately a solid PAH sample (via a heated solid probe) and a liquid nucleophile (via a heated inlet reservoir) to the EI/CI source. The results showed the adduct formation of PAH cation radicals and biological nucleophiles in the gas phase and pointed to the possible correlation of the gas-phase reactivity of the PAH cation radicals with the biological reactivity.

LC/MS Interfaces for EC/MS

In developing on-line EC/MS, a difficulty met immediately is the coupling of the liquid-environment of the EC reactions with the vacuum MS detection [Volk et al. 1992]. In order to transfer the EC reaction products present in solution to the gas phase for MS detection, an LC/MS liquid interface is needed.

Evolution of LC/MS Interfaces

Before the appearance of common LC/MS interfaces, the use of MS was limited to the analysis of nonpolar, volatile, gaseous species [Budde 2001, Niessen 1999] The development of LC/MS interfaces saw the stages between 70's and 90's of capillary inlet interface, moving belt interface (MBI) and the direct liquid introduction (DLI) Among these, MBI was the first commercial LC/MS interface, available in 1977 The actual breakthrough in the general acceptance of LC/MS as a powerful analytical technique was achieved by the introduction of the thermospray (TSP) in 1983, made possible by the research effort of Vestal and coworkers [Blakley et al 1978, 1980]

Browner and coworkers introduced MAGIC in 1984, which was short for 'monodisperse aerosol generating interface for chromatography' [Willoughby and Browner 1984] MAGIC was later developed as the particle beam interface, PB, and became commercially available after 1988 The development of the now famous electrospray interface, ESI, could date back to the late 1960s, owing to the research effort of Dole and coworkers [Dole et al 1968, Clegg and Dole 1971] However, it was not until the work of Fenn and coworkers published in 1984 [Yamashita and Fenn 1984(a) and (b)] that the ESI really caught researchers' attention A major breakthrough in ESI development was achieved in 1988 by the observation of multiply charged ions from peptides and proteins [Meng et al 1988, Covey et al 1988] This made the ESI/MS one of the most popular and powerful methods for the analysis of nonvolatile, high molecular-weight biopolymers

The development of on-line EC/MS techniques followed tightly that of the LC/MS interfaces Bruckenstein and Gadde conducted the first EC/MS experiment in the early 1970s with the use of a porous membrane interface [Brukenstein and Gadde 1974]. The early EC/MS studies were limited to the analysis of volatile species due to the difficulties in interfacing the liquid environment of EC with the gas-phase environment of MS. The breakthrough in EC/MS development came in 1986 when Hambitzer and Heitbaum [1986] first coupled a homebuilt EC cell to a MS via a TSP interface. The EC/TSP/MS methodology was further developed by Volk et al. and was demonstrated as a powerful tool for providing insight into biological redox reactions [Volk et al. 1988, 1989(a) and (b), 1990, 1992].

However, there are several limitations in the use of TSP interface for EC/MS. First, the high capillary temperature, typically above 200 °C, may cause thermal decomposition of analytes, which complicates mass spectral interpretation. Second, the production of ions in TSP largely depends on the experimental parameters that affect the vaporization and solvent-mediated chemical ionization processes, and as a result, the reproducibility can be poor. The drawback for EC/MS with TSP interface in the detection of ion radicals is that, in the positive ion detection mode, the ionic species detected by EC/TSP/MS are either protonated molecules or ammonium-adduct ions with ammonium acetate used to initiate the chemical ionization in the TSP interface. The use of TSP interface has largely been replaced by the more versatile ESI interface.

PB Interface for EC/MS

There are only a few reports depicting the use of the PB interface for EC/MS. PB interface is known to support efficient volatilization of nonaqueous solvents [Niessen 1999]. One advantage of the PB interface is that both electron impact (EI) and chemical ionization (CI) ion source can be used. The ability to generate on-line EI mass spectra in

EC/PB/MS permits the ionization and identification of neutral and nonpolar species, which are not amenable to soft ionization techniques such as TSP and ESI A disadvantage of PB is its poor sensitivity resulting from low transport efficiency of analytes through the PB momentum separator [Willoughby and Browner 1984 Bellar et al. 1990]

Regino and Brajter-Toth [1997] have used EC/PB/MS to characterize a home-built thin-layer flow cell for EC/MS The effect of solution composition on the cell conversion efficiency (percentage of the analyte reacted) was observed [Regino et al 1998] EC/PB/MS has also been used to investigate the catalytic oxidation of 4-dimethylaminopyridine (DMAP) by dopamine orthoquinone [Regino and Brajter-Toth 1999] as described earlier

Electrolytic Nature of ESI Interface

ESI is an atmospheric pressure ionization method/interface that uses an electrostatic sprayer to facilitate the transfer of ionic species initially present in solution, to the gas phase for MS detection [Kebarle 2000 Cole 1997] Since ESI involves little heating, has no volatility requirement for the analytes, and can generate multiply charged ions, the technique is suitable for analyzing thermally labile nonvolatile and polar compounds especially biopolymers of high molecular weight

During the ESI ionization the continuation of the ES current in ESI-MS necessitates a charge balancing mechanism of electrochemical nature, to compensate the selective loss of ions of one polarity ESI has been recognized as an electrolysis cell by Kebarle's group [Blades et al. 1991] and has been characterized as a controlled-current electrolytic cell by Van Berkel and coworkers [Van Berkel and Zhou 1995(a) and (b)

Kertesz and Van Berkel 2001]. The detection of cation radicals formed from neutral compounds by making use of the electrolytic nature of ESI has been reported [Van Berkel et al. 1992, Zhou and Van Berkel 1994, Xu et al. 1994, Dupont et al. 1994, Lu et al. 1995].

Use of Electrolyte in ESI-MS

Use of "spectator" electrolyte is common in ESI-MS analysis [Tang and Kebarle 1991, 1993]. The need for the electrolyte originates from the mechanism of the ES ionization process. The two main stages in the mechanism are the production of the charged droplets and the production of the gas-phase ions from the charged droplets [Kebarle and Tang 1993]. It is generally accepted that an electrophoretic separation of the ionic species in solution, i.e., a partial separation of the positive ions from the negative ions, is responsible for the first stage. To aid the electrophoretic charging, the addition of electrolyte is often needed to increase the solution conductivity and therefore the formation of charged droplets. Tang et al. have investigated the effect of solution conductivity on the ES current [Tang and Kebarle 1991]. An increase (nonlinear) of ES current with electrolyte concentration was observed.

The surface activity of electrolyte affects the second stage in the ESI process, i.e. the emission of ions from the charged droplets to the gas phase [Kebarle and Tang, 1993]. The surface-active electrolyte ions can compete strongly with the analyte ions for being emitted into the gas phase and for detection by MS. As a result of this competitive ion emission process in ESI, the analyte ion signal can be suppressed by the presence of the electrolyte. Severe signal suppression by surface-active electrolytes such as tetrabutylammonium perchlorate (TBAP) has been reported in ESI-MS [Tang and

Kebarle 1993, Xu et al. 1996, Bond et al. 1995]. For this reason, the choice of the electrolyte is important in ESI-MS detection. The use of common electrolytes such as quaternary ammonium salts is usually avoided and the concentration of electrolyte is kept as low as possible while still operational. Lithium triflate ($LiCF_3SO_3$), which causes minimal signal suppression, has been used in nonaqueous ESI-MS studies [Zhou and Van Berkel 1995, Xu et al. 1996, Lu et al. 1997].

Coupling of EC Cell to ESI-MS

Although the electrolytic nature of ESI makes possible the direct ionization and analysis of some neutral compounds by ESI-MS, its capacity has been shown to be largely limited to the detection of compounds with low oxidation potentials (below 1 V) that form stable products in solution after the ESI oxidation [Van Berkel et al. 1992, Van Berkel and Zhou 1995(a), Fernandez de la Mora et al. 2000]. The coupling of an external EC cell to the ESI-MS can facilitate the analysis of neutral compounds that are otherwise not amenable to ESI-MS. Even for those compounds that can be ionized by ESI, coupling of an EC cell to ESI-MS may enhance the analyte signal that is detected by MS [Xu et al. 1996].

Practically, it is more difficult to couple an EC cell to ESI/MS than to PB/MS or to other liquid MS interfaces, because of the use of a high voltage in the ESI [Zhou and Van Berkel 1995]. As discussed previously, in designing EC cells and coupling the EC cells to the MS, a high electrolysis efficiency and a rapid MS response time is desired. Ease of EC cell operation is another important consideration. In coupling an EC cell to ESI/MS, owing to the low flow rate operation of ESI-MS, it is necessary to place the EC cell close to the ESI needle to reduce the delay in MS response. In fact, the construction of an EC cell inside the ESI probe has been reported as described earlier [Xu et al. 1996]. However, this cell design is very complicated and has the shortcoming of the interference from the ESI in the EC cell voltage control, as discussed previously. The complicated cell design also makes it challenging for machinery/construction and difficult electrode cleaning and replacement. On the other hand, the two-electrode tubular cell design offers simplicity [Bond et al. 1995, Zhou and Van Berkel 1995]. In Bond's design, the tubular working electrode was isolated from the high-voltage ES capillary, while in Zhou's design, the stainless steel ES capillary functioned as the working electrode of the EC cell. Obviously, faster MS response can be expected from the latter. However, the latter design suffers a disadvantage of the "electrochemical interference" due to the electrolytic nature of the ESI. To distinguish the effect of reactions occurring in the EC cell from the electrochemical nature of ESI, the results from the floated EC cell design to the isolated EC cell design were compared under the same MS conditions. The EC cell designed for on-line EC/ESI/FTICR MS in this work has taken all these factors into consideration for an optimized detection, as described in Chapter 2.

Almost all the EC/MS studies that have been reported to date were carried out with a quadrupole MS, which gives only a unit mass resolution under normal conditions. However, the use of a high resolution MS such as an FTICR MS in EC/MS is desirable and sometimes necessary. High resolution MS, by providing isotopic information, can help distinguish the EC-generated multiply charged ions from the interfering ions in the sample matrix and from the fragments of the parent molecular ion. The change in charge state of the analyte due to the electron transfer reactions can be readily obtained by the measurement of the isotopic distribution [Marshall et al. 1998].

Very recently Johnson et al [2001] reported the use of a high resolution FTICR MS in the investigation of the chemical and electrochemical reduction of metalloproteins In the electrochemical reduction of cytochrome c an EC cell consisting of two 1 ml plastic syringes with the metal syringe needles as electrodes connected via a T-valve was used During electrolysis of cytochrome c in the EC cell, there was no flow to the mass spectrometer After 30 min of electrolysis, the syringe containing reduced cytochrome c solution was placed on a syringe pump and its solution was delivered to the MS Although the authors termed it as an on-line detection, this was actually an off line electrolysis combined with MS detection The high resolution FTICR MS has allowed the measurement of charge state and number of protons attached to the protein before and after the electrolysis Based on this the oxidation state of the metal was determined as Fe^{3+} in the oxidized protein and Fe^{2+} in the reduced protein

Analytical Applications

Besides providing insights into redox pathways, analytical applications of EC/MS have been pursued Xu et al [1996] reported an enhancement of signal in the investigation of PAHs by EC/ESI-MS Although not demonstrated previously, the possibility exists that this feature of signal enhancement by EC/ESI-MS may be used to pursue low level detections as shown in Chapter 7 of this dissertation

Bond and coworkers demonstrated that the signal suppression problem in ESI-MS from common electrolytes could be reduced by on-line EC/ESI-MS [Bond et al 1995] The EC results were obtained by use of a very high EC cell voltage (~200 V), which is not desirable in analytical determinations By employing a different EC cell design, it is demonstrated in this dissertation (Chapter 5) that the signal suppression from TBAP electrolyte can be greatly alleviated by the use of a low EC cell voltage i e only a few volts in the new design of EC/ESI-MS It can be concluded from these results that the choice of the electrolytes can be more flexible in EC/ESI-MS than ESI MS This may facilitate the applications of EC/ESI-MS in the determinations where the presence of surface-active electrolytes such as surfactants is unavoidable

Pretty et al [2000] showed that EC/ESI-MS is an effective approach to achieve preconcentration and matrix elimination for enhanced detection sensitivity In their work, accumulation of the targeted analytes at the working electrode of the EC cell was accomplished via a nonelectrolytic adsorption process that was controlled via the combination of the applied working electrode potential, the solvent system and the working electrode material The authors have applied this approach to the analysis of elemental species and organic analytes such as tamoxifen and 4-hydroxytamoxifen The detection level obtained was lower than that from potentiometric adsorptive stripping analysis, which is a technique that uses similar preconcentration strategy but with the use of an electrochemical detector only

In another work Deng and Van Berkel [1997] applied the EC/ESI-MS methodology to separations In that work, electrochemically modified liquid chromatography (EMLC) was coupled to MS In EMLC the retention and separation of analytes were manipulated solely through the changes in the potential applied to a conductive stationary phase One advantage of EMLC as compared to the conventional HPLC is that it minimizes complications from the changes in the mobile phase composition as typically used in chromatographic separations The authors found that the detection levels by using MS detector for EMLC were comparable to those obtained with a UV detector

In the last two applications mentioned above there was no involvement of electron transfer EC reactions The voltage applied to the working electrode was used to affect the interactions between the target analyte and the working electrode material rather than to reduce oxidation/reduction reactions

Overview of Thesis

There were several objectives for the present work. The first objective was to develop an on-line EC/MS method to characterize the EC-generated cation radicals Of interest is the direct monitoring of the generation of the cation radicals and the identification of the ion identity by EC/MS The second objective was to use EC/MS as a means to enhance the ionization efficiency of neutral compounds and thereby achieve enhanced MS detection sensitivity The third goal was to investigate the nucleophilic reactions between the EC-generated cation radicals and different nucleophiles by EC/MS Of interest is the possibility to achieve sensitive and selective determination of biological nucleophiles via attachment of cation radicals (tag) to the targeted nucleophiles

This dissertation is divided into eight chapters Chapter 1 gives a general introduction to EC/MS Chapter 2 is an experimental section Chapter 3 describes the application of EC/PB/MS in the investigation of consequent generation of cation radicals from oxidation of TPA Chapter 4 investigates the mechanism of signal enhancement due to the presence of TBAP electrolyte and its applications in enhancing the detection sensitivity and linearity of the calibration curves in PB/MS analyses In Chapter 5 a new EC cell is designed and coupled to a high resolution ESI-FTICR MS The use of high resolution FTICR MS to distinguish TPB^{2+} dication from the interfering species in TPA oxidation is exploited. A reduction of signal suppression by TBAP electrolyte in on-line EC/ESI FTICR MS is shown. Chapter 6 discusses the experimental parameters that may affect the ion formation and ion detection in EC/ESI-FTICR MS. Chapter 7 investigates the oxidation of PAHs and nucleophilic reactions between PAH cation radicals and pyridine. Strong reactivity of anthracene and perylene cation radicals toward pyridine and enhanced detection sensitivity for the nucleophilic adducts is demonstrated in EC/ESI-FTICR MS. Chapter 8 contains conclusions and recommendations for future EC/MS research.

Table 1-1 The **PAH** cation radical reactivity parameter – unpaired electron density (ρ)

Compound	Position	ρ
Anthracene	1 (4, 5, 8)	0.0967
	2 (3, 6, 7)	0.0484
	9 (10)	0.1936
Perylene	1 (6, 7, 12)	0.0835
	2 (5, 8, 11)	0.0130
	3 (4, 9, 10)	0.1076
Tetracene	1 (4, 7, 10)	0.0562
	2 (3, 8, 9)	0.0335
	12 (5, 6, 11)	0.1475

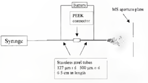

Figure 1-1 Two tubular electrode cell, with spray needle as the working electrode Adapted from [Zhou and Van Berkel 1995]

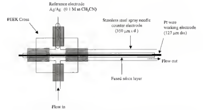

Figure 1-2 Online EC flow cell adapted from [Xu et al 1996] Pt wire working electrode was flame-sealed in a layer of fused silica. The stainless steel ES needle was used as counter electrode in the EC cell A Ag/Ag reference electrode in the PEEK cross was isolated from the sample solution by a glass tip

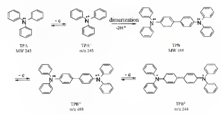

Figure 1-3 Electrochemical oxidation pathways of triphenylamine. Adapted from [Seo et al. 1966]

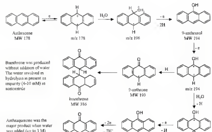

Bianthrone was produced without addition of water The water involved in hydrolysis is present as impurity (4-10 mM) in acetonitrile

Anthraquinone was the major product when water was added (up to 3 M)

Figure 1-4 Electrochemical oxidation of anthracene Adapted from [Majeski et al 1968, Parker 1970]

CHAPTER 2
EXPERIMENTAL METHODS

Methods & Instrumentation

EC Flow Cell

The thin-layer EC flow cell shown in Figure 2-1 that was used for EC/FB/MS has been detailed before [Regino and Brajter-Toth, 1997]. This home-built EC cell contains three electrodes: a rough pyrolytic graphite (RPG) working electrode (3×3 mm, Electrosynthesis, Lancaster, NY), a Pd wire (1 mm dia. Aldrich, St. Louis, MO) counter and reference electrode. The cell volume was controlled by first electrically shorting the working and counter electrodes, then loosening the threaded bolt by a fourth of a revolution (1/16"). The flow channel that was produced had a thickness of ca. 400 μm (one-fourth of 1/16 inch). The volume of the electrode compartment was determined to be ca. 4.4 μL on the basis of the RPG electrode area and channel thickness.

The EC cell shown in Figure 2-2 was designed for EC/ESI-FTICR MS. The cell incorporates stainless steel (ss) capillaries (Alfa Aesar, Ward Hill, MA) and Pd wires (Aldrich, St. Louis, MO). The dimensions for the electrodes are as described in Figure 2-2. The electrodes, ss(1), ss(2), Pd(4) and Pd(5), were placed in Teflon sleeves and held in place by ferrules on a PEEK cross (Upchurch Scientific, Oak Harbor, WA). The PEEK cross has a swept volume of ca. 1 μL. A third stainless steel capillary ss(3) was placed upstream and connected to ss(2) via a short piece of Teflon tubing. The cell can be operated in different two-electrode cell configurations, e.g. ss(1) – ss(2), ss(2) – ss(3)

Pd(4) – Pd(5) The ss(1) electrode can also function as the ES spray needle in EC/ESI-FTICR MS

Cyclic Voltammetry

A Bioanalytical Systems Electrochemical Analyzer (BAS-100, Bioanalytical Systems Inc West Lafayette, IN) was used In cyclic voltammetry, the working electrode (WE) was either a rough pyrolytic graphite (RPG 3×3 mm) or a Pt disk (1 mm diameter) The counter electrode (CE) was a Pt or Pd wire. In aqueous systems, SCE reference electrode (RE) was used In nonaqueous systems, Pd was used as a quasi reference electrode. The pyrolytic graphite WE was polished on a 600-grit silicon carbide paper (Mark V Laboratory East Granby, CT) using a metallographic polishing wheel (Ecomet 1 Buehler Evanston, IL) to produce rough pyrolytic graphite WE, followed by a 15-min ultrasonication in a water bath The metal electrodes (Pd or Pt) were polished on a felt cloth (Mark V Laboratory East Granby, CT) with a γ-alumina suspension of 1 μm particle size (Gamal Fisher Scientific, Pittsburgh, PA)

Chronocoulometry

Chronocoulometry was performed with the BAS-100 Electrochemical Analyzer The same RPG electrode as in CV was used as the WE Pt wire (1 mm dia. Aldrich, St Louis MO) was used as a counter electrode, and SCE as a reference electrode

Flow Injection/Electrochemical Detection

The setup for the flow injection with the electrochemical detection is shown in Figure 2-3 The inlet to the thin-layer flow cell (Figure 2-5) was connected to a Hewlett-Packard 1050 Series HPLC pump and the outlet to waste The analyte solution was injected through a 20 μL injector loop on the HPLC pump The thin layer-bulk-electrolysis (TLBE) method available from the BAS-100 electrochemical analyzer was used to control the EC cell voltage and monitor the faradic charge in the EC cell.

EC/PB/MS

The instrumental setup for EC/PB/MS is shown in Figure 2-4. The thin-layer EC flow cell (Figure 2-1) is positioned between a HP-1050 series HPLC pump and a HP-59980B PB interface of a HP 5989A quadrupole mass spectrometer (Palo Alto, CA). A model 173 PAR potentiostat (EG&G Princeton Applied Research, Princeton, NJ) was used for potential control of the EC cell.

EC/ESI-FTICR MS

The instrumental setup for EC/ESI/FTICR MS is illustrated in Figure 2-5. The EC cell was mounted in the ESI housing of a Bruker APEX 4.7 T FTICR mass spectrometer (Bruker Daltonics, Billerica, MA). A schematic representation of the FTICR MS instrument is shown in Figure 2-6. The ss(3) electrode in the EC cell was connected to a syringe pump (74900 series, Cole Parmer, Vernon Hills, IL) via a fused silica capillary. A continuous sample infusion mode was used, typically at a flow rate of 75 μL/h. The EC cell voltage was applied from a battery adjustable through a voltage divider. Figure 2-5 illustrates the operation of ss(1) – ss(2) EC cell configuration, in which the EC cell voltage, 7.5 V, is applied between ss(1) – ss(2) electrodes and floated at the high ES voltage (3.3 kV).

Methods Fundamentals

Cyclic voltammetry (CV)

In cyclic voltammetry, the potential of the working electrode is swept linearly with time from a potential where no electrode reaction of the analyte occurs to a potential where the redox reaction of the analyte can occur [Hamann et al 1998 Bard and Faulkner 1980] After sweeping the potential past the region where a maximum analyte current (i_p) is obtained the direction of the potential scan is reversed In the reversed scan, the electrode reactions of the products generated in the forward scan can be detected The voltammogram is characterized by several parameters the anodic (E_{pa}) and cathodic (E_{pc}) peak potentials anodic (i_{pa}) and cathodic (i_{pc}) peak currents, which can depend on the potential sweep rate. For a reversible electrode reaction, the ratio of the peak currents $i_{pc}/i_{pa} = 1$ [Bard and Faulkner 1980] Deviations of the ratio from unity are indicative of the kinetic or other complications in the electrode process The potential difference between E_{pa} and E_{pc}, ΔE_p, is also an indication of the reversibility of the electrode redox reaction For a reversible diffusion-controlled electrode reaction, the theoretical ΔE_p value is 0 059/n V at 25 °C where n is the number of electrons transferred per mole during the electrode process For a quasi reversible reaction, the ΔE_p is in the range of 0 061/n to 0 212/n V When the ΔE_p is greater than 0 212/n V the electrode reaction is considered irreversible

The theoretical peak current for a diffusion controlled reversible reaction is expressed by a Randles-Sevcik equation [Bard and Faulkner 1980]

$$i_p = (2\ 69 \times 10^5)n^{3/2}AC_o^*D_o^{1/2}v^{1/2} \qquad (2\ 1)$$

For an irreversible reaction

$$i_p = (2\ 99 \times 10^5)n(\alpha n_a)^{1/2}AC_o^*D_o^{1/2}v^{1/2} \qquad (2.2)$$

where n is the number of electrons transferred per mole A is the electrode area in cm^2 D_o is the diffusion coefficient in cm^2/sec, v is scan rate in V/s and C_o^* is the bulk concentration of the electroactive species in mol/cm^3 The α is the transfer coefficient, and n_a is the number of electrons involved in the rate determining step

The peak potentials and peak currents can be readily determined from the cyclic voltammogram obtained in a stationary solution, where the electrode reactions are diffusion-controlled However under flow conditions, the voltammograms may show a steady state response Figure 2-7 shows the cyclic voltammograms of 1×10^{-3} M $K_3Fe(CN)_6$ - 0 1 M KCl aqueous solution obtained in the thin-layer EC cell shown in Figure 2-1 When the solution is stagnant, a cyclic voltammogram with the visible peak currents (i_{pc} and i_{pa}) and peak potentials (E_{pc} and E_{pa}) is observed When the solution flows at a flow rate of 1 ml/min, a steady state current is observed indicating that the mass transport is not the rate-determining step under these conditions i e the rate of convective mass transport of the analyte to the electrode surface is greater than the rate of electron transfer so that the current does not drop after the potential is scanned past the peak potential

At steady state, the limiting current, i_L, can be described as

$$i_L = \frac{nFAD_o C_o^*}{\delta_o} \qquad (2\ 3)$$

where n is the number of electrons F is the Faraday s constant (C/eq) A is the electrode area (cm^2) D_o is the diffusion coefficient (cm^2/sec) δ_o is the diffusion distance of the analyte (cm) v is the scan rate (V/s) and C_o^* is the concentration (mol/cm^3)

The limiting current i_L also depends on flow rate as shown by Eq (2 4)

$$i_L = nF(C^* - C_f)u \qquad (2\ 4)$$

where C_f is the concentration of unreacted analyte (mol/cm^3) and u is the flow rate (ml/min) [Kissinger and Heineman 1984]

As can be seen from Eq. (2.3) and (2.4), the diffusion distance of the analyte in the cell, δ_s, is determined by flow rate ($\delta_s \propto 1/u$). At high flow rates, the analyte is quickly swapt through the thin-layer cell and cannot diffuse efficiently to the electrode surface. As a result, the fraction of the analyte that reacts at the electrode is expected to be lower at higher flow rates.

Flow Injection/EC Detection

In EC/MS, the MS ion signals of the reaction intermediates and products produced in the flow-through EC cell can be determined as a function of the WE electrode potential. The result is a MS hydrodynamic voltammogram. To correlate the MS intensity with the electrochemical currents, it is necessary to obtain the MS and the electrochemical data under the same flow conditions. Flow injection with EC detection can be used to measure the EC currents under specific flow and electrode potential conditions. Flow injection is also used to reduce the consumption of the sample and minimizes the contamination of the EC cell by the sample. By plotting the current as a function of the EC cell voltage, a hydrodynamic voltammogram is obtained, which can be compared to the MS hydrodynamic voltammogram to facilitate data interpretation.

Besides producing the hydrodynamic voltammograms, flow injection with EC detections can also be used to determine the EC cell conversion efficiency, which is a measurement of the fraction of the analyte injected that reacts in the EC cell. In this case, the EC cell voltage is set at a value past the oxidation or reduction peak potential of the analyte to ensure a complete electrode reactions of the analyte. The amount of the analyte reacted can be determined based on the Faradic charge. The total amount of the analyte injected is then calculated from the injection volume and the concentration of the analyte in the solution. The EC cell conversion efficiency is measured as the ratio of the amount of the analyte reacted to the total amount of the analyte injected. The solution flow rate may affect the cell conversion efficiency. The cell conversion efficiencies at several different flow rates in the oxidation of TPA have been determined in Chapter 3.

PB/MS

Solution-based techniques such as HPLC can be coupled to MS via liquid interfaces such as the PB interface [Niessen 1999]. The scheme of the PB interface used in this work is shown in Figure 2-8. The PB interface consists of an adjustable concentric pneumatic nebulizer, a heatable desolvation chamber, a two-stage momentum separator and a transfer tube between the momentum separator and the ion source. The nebulizer is a 100 μm i.d. fused-silica capillary, through which the liquid solution from the HPLC pump is introduced into the PB interface. The solution is nebulized pneumatically, typically with helium as the nebulizing gas, into a dissolvation chamber that is heated to 50-70 °C, which generates droplets.

The desolvation chamber is typically fabricated of an aluminum-nickel alloy and has dimensions of ca. 20 cm × 6 cm i.d. (Figure 2-8). The pressure in the desolvation chamber is between 20 and 30 kPa. In the dissolvation chamber, the solvent evaporation from the droplets leads to the formation of dry particles. Driven by the momentum gained from spraying and the reduced pressure, the dry particles are transported as a high velocity particle beam toward the momentum separator that is connected to the desolvation chamber.

The momentum separator consists of a nozzle and two skimmers, and has two differential pumping stages. The pressure is reduced from ~30 kPa in the desolvation chamber to ~10 kPa in the first pumping region, to ~30 Pa in the second pumping region, and to ~2×10^{-3} Pa in the ion-source housing. On leaving the desolvation chamber the mixture of He dispersion gas solvent vapor and analyte particles expand through a nozzle, undergoing supersonic expansion into the first low-pressure region (~10 kPa). During the expansion, the particles of high mass do not expand from the core of the expansion jet as rapidly as do the gases [Willoughby and Browner 1984]. Skimming the core of the expansion jet by the first skimmer results in substantial enrichment of the analyte relative to the gas and solvent vapor. The solvent vapor and the He gas that has been skimmed off are pumped away mechanically. This process is repeated in the second pumping stage (~30 Pa) of the momentum separator [Niessen 1999]. The analyte particles reach the ion source of the mass spectrometer through a transfer tube. In the high temperature (250 °C) MS ion source, the particles undergo flash vaporization or disintegration. The released molecules are then ionized by either electron impact ionization (EI) or chemical ionization (CI). As can be seen from the above, the mass transport processes through the PB interface preferentially transfer the high-mass analyte particles to the MS ion source and significant analyte enrichment in the gas phase is achieved before the MS detection in PB/MS analysis.

ESI/MS

The ESI process involves three major steps: production of charged droplets from the electrolyte/analyte dissolved in a solvent; shrinkage of charged droplets by solvent evaporation, followed by the repeated droplet disintegrations; gas-phase ion production from small highly charged droplets [Kebarle and Tang 1993]. A schematic illustration of the ESI process is shown in Figure 2-9.

In ESI, a high voltage (ca. 3 kV) is applied to a metal ES needle (typically 100 µm i.d. and 200 µm o.d.), which is normally located from 1 to 3 cm from a counter electrode (Figure 2-9). The counter electrode tube (500 µm i.d.) leads to the MS sampling system.

The electric field at the spray needle tip can be expressed as follows:

$$E_c = \frac{2V_c}{r_c \ln(\frac{4d}{r_c})} \qquad (2.5)$$

where E_c is the electric field (V/m), V_c is the applied voltage (V), r_c is the ES needle radius (m), d is the distance from the ES tip to the counter electrode (m). Because of the small r_c (100 µm) of the ES tip, the electric field at the ES tip is very high ($E_c \approx 10^6$ V/m). The applied electric field penetrates the liquid at the ES tip and the positive and negative electrolyte ions in the solution will move under the influence of the field. In the positive ion mode, the positive ions will migrate downfield toward the liquid surface and the negative ions drift away from the surface until the imposed field inside the liquid is essentially removed by the charge redistribution. The mutual repulsion of the positive ions at the surface destabilizes the liquid surface and the surface is drawn out so that a liquid cone (Taylor cone) forms. If the applied electric field is sufficient, emission of the charged droplets from the liquid cone occurs.

In the gas phase, the solvent evaporates from the charged droplets while charges are preserved on the droplet surface. The shrinkage of the droplet leads to an increased Coulomb charge repulsion between the positive ions on the droplet surface. The charge-preserving droplet evaporation continues until the Rayleigh limit is reached, i.e., the condition when the charge, Q, becomes sufficient to overcome the surface tension, σ that holds the droplet together As a result, a disintegration of larger charged droplets into smaller offspring droplets will occur

Two different mechanisms have been proposed to account for the gas-phase ion production from the charged droplets One of them is the charge residue model of Dole et al [Dole et al 1968 Gieniec et al 1984] which involves the formation of extremely small droplets (R ≈ 1 nm) that contain only one ion Solvent evaporation from such a droplet will convert the droplet to a gas phase ion. The other mechanism is the ion evaporation model of Iribarne and Thomson [Iribarne and Thomson 1976 Thomson et al 1982 Iribarne et al 1983] which assumes ion emission from very small and highly charged droplets Typically the droplets from which ion emission becomes competitive with Rayleigh fission have a radius of ca. 8 nm and 70 elementary charges Under these conditions the droplet does not undergo fission but emits gas-phase ions The ion evaporation model is the most widely accepted mechanism for the formation of gas-phase ions in ESI

As can be seen from Figure 2-9 ESI in the positive ion mode involves selective loss of positively charged droplets from solution As a result, a buildup of negatively charged ions will occur in solution within the metal ES needle The buildup of the negative charge inside the ES needle counteracts the externally applied electric field and will eventually stop the ESI process In order to maintain the ES current, a charge balancing mechanism has to exist Kebarle and coworkers [1991] demonstrated that the mechanism responsible for charge balance in ESI is electrochemical in nature Van Berkel's group further characterized the ESI as a controlled-current electrolytic cell [Van Berkel and Zhou 1995(a) and (b)]

The formation of charged droplets in ESI requires the initial presence of ionic species e g electrolyte ion in solution The influence of the background electrolyte on the analyte signal can be determined from the following equation [Tang and Kebarle 1991, 1993]

$$I_A \quad fp\frac{k_A[A^+]}{k_A[A^+]+k_E[E^+]}i_{ES} \qquad (2\ 6)$$

where I_A is the ion intensity of the analyte ion detected by MS i_{ES} is the spray current [A] and [E] are the concentrations of analyte and electrolyte ions in the electrosprayed solution, k_A and k_E are the rate constants expressing the rate of transfer of the respective ions from the charged droplets to the gas phase, f is the fraction of the droplet charge converted to the gas-phase ions, p is the constant expressing the efficiency of the MS for detecting the gas phase ions As can be seen from Eq (2 6) the presence of electrolyte may suppress the analyte signal in ESI/MS To minimize problems with signal suppression, it is necessary to select an electrolyte whose propensity for gas-phase ion formation, k is small relative to the analyte ion, and to use it at the lowest concentration

FTICR MS

FTICR MS is well known for its ultrahigh mass resolution, mass accuracy and temporal MS/MS measurement [Marshall 1998] The applications and development of FTICR MS have been greatly facilitated by the coupling of ESI to FTICR [Quenzer et al 2001 Krahmer et al 1999] The operation of FTICR MS is different from that of other types of mass spectrometers With FTICR, the principal functions of mass analysis and ion detection occur in the same space (the analyzer ICR cell), but are spread out in time, whereas with quadrupole and magnetic sector mass spectrometers, these events occur simultaneously and continuously in different parts of the mass spectrometer

FTICR MS is based on the principle of cyclotron motion of ions in an applied magnetic field, which can be described by the cyclotron equation

$$\omega_c = qB/m \qquad (2.7)$$

where ω_c is the angular frequency, q is charge, m is mass of the ion, B is magnetic field. All FTICR instruments have four main components: a strong magnet, an analyzer cell, an ultra-high vacuum system, and a sophisticated data system. The basic series of events that occurs in FTICR MS is referred to as a pulse sequence and consists of four events: quench, ion formation (or injection), ion excitation and ion detection. The quench event is used to empty the analyzer cell of any ions that may be present from a previous experiment. External ion injection is achieved via ESI. The ion excitation event is to excite the ions of interest into larger spatially coherent cyclotron orbits by applying an oscillating resonant phase-coherent electric field so as to generate detectable signal on the detection plates. The ion detection in FTICR MS is based on detection of the image current produced by the periodic cyclotron motion of the coherently orbiting ion packet on the two opposing detection plates. The frequency of the detected sinusoidal signal reflects the frequency of the cyclotron motion of the ions, which is related to the m/z of the ions by Eq. (2.7).

The image current detection is non-destructive, and ions can be repeatedly detected many times to improve the signal-to-noise ratio (S/N). After the time-domain image current is converted to a voltage and Fourier transformed to yield a frequency spectrum, information about frequencies and abundances of all ions trapped in the cell is obtained. Because the frequency can be measured very precisely, the mass of an ion can be determined accurately in FTICR MS. In FTICR MS, ion signals may be detected at a frequency that is an integer multiple (harmonic order) of the fundamental ICR frequency of the ions of a given m/z value [Limbach et al 1993 Grosshans and Marshall 1991] While this phenomenon has been shown to be useful for the determination of cyclotron orbital radius [Grosshans and Marshall 1992] it may interfere with the detection of multiply charged ions [Limbach et al 1991] To distinguish between a multiply charged ion and a harmonic signal, the ions of a particular m/z can be ejected from the ICR cell by applying a single-frequency resonant irradiation. The ion ejection should eliminate any harmonic signals associated with the ion, while the fundamental signal of a multiply charged ion is not affected.

Experimental Conditions

Reagents and Chemicals

HPLC grade acetonitrile (MeCN) methanol (MeOH) ACS certified methylene chloride (CH_2Cl_2), potassium chloride (KCl) potassium ferricyanide (III) ($K_3Fe(CN)_6$) were obtained from Fisher (Pittsburgh, PA) Tetrabutylammonium perchlorate (TBAP) tetraethylammonium perchlorate (TEAP) tetrabutylammonium tetrafluoroborate ($(C_4H_9)_4NBF_4$) lithium trifluoromethanesulfonate or lithium triflate ($LiCF_3SO_3$) were purchased from Alfa Aesar (Ward Hill MA) Triphenylamine (TPA, 98%) anthracene, perylene rubrene, pyridine were from Aldrich (St Louis MO) Tetrabutylammonium bromide, tetrapropylammonium bromide, tetraethylammonium bromide were from Eastman Kodak (Rochester NY) Triphenylmethane tribenzylamine tributylamine were from Chemical Service (Media, PA) All chemicals were used as received

CV Experiment

CV of TPA was performed with a BAS-100 electrochemical analyzer The solution was 1×10^{-3} M TPA, 0 1 M TBAP in acetonitrile The solution was purged with nitrogen for 5 min before the CV experiment, and a curtain of nitrogen atmosphere was maintained over the solution during the experiment A range of scan rates, from 10 mV/s to 2 V/s, has been tested Typically the potential window was +0 4 V - +1.2 V vs Pd and two scan cycles were recorded

Chronocoulometry (CC)

CC experiments were carried out in 1×10^{-3} M $K_3Fe(CN)_6$ - 0 1 M KCl aqueous solution to determine the electrode area of the RPG working electrode of the thin-layer cell A potential step from +0 40 to 0 00 V vs SCE was used The total charge Q in CC that is measured as a result of the potential step has three different sources [Anson and Osteryoung 1983] (a) double-layer charging, Q_{dl} (b) electrolysis of adsorbed species, Q_{ads}, (c) electrolysis of the diffusing species in solution, Q_{diff} The charge-time diffusion Controlled, Q_{diff}, behavior can be obtained from the integrated Cottrell equation

$$Q = Q_{diff} + Q_{dl} + Q_{ads} = 2nFAC_o^{*}D_o^{1/2}t^{1/2}\pi^{-1/2} + Q_{ads} + Q_{dl} \qquad (2\ 8)$$

The terms Q_{dl} and Q_{ads} are time independent. The area of the RPG working electrode was determined from the slope of the Q vs $t^{1/2}$ curves, which was given by $2nFAD_o^{1/2}C_o^{*}\pi^{-1/2}$ The meanings of the symbols are the same as in eq 2 1 The value of D_o for $K_3Fe(CN)_6$ in 0 1 M KCl aqueous solution was assumed to be $7\ 6 \times 10^{-6}$ cm^2/sec [Von Stackelberg et al 1953]

Flow Injection/Electrochemical Detection

The mobile phase of 0.1 M TBAP in acetonitrile was pumped continuously through the thin-layer electrochemical cell. The analyte solution, consisting of either 1 × 10^{-4} M or 1 × 10^{-3} M TPA and 0.1 M TBAP in acetonitrile, was injected into the flow stream through a 20 μL sample injection loop on the HPLC pump. To reduce the effect of the background charging current on the measured charge of TPA oxidation, the TPA injection was made 30 s after the EC cell voltage was applied. An injection of 0.1 M TBAP in acetonitrile was made before each analyte injection at each applied voltage to obtain the charge due to blank injection. The blank-subtracted charge was used to determine the EC cell conversion efficiency. With the EC cell voltage controlled at +1.2 V vs Pd, the moles of oxidized TPA were calculated from the net faradic charge following the injection of TPA solution. The total moles of TPA injected were calculated from the TPA concentration and injection volume.

The current-time (i–t) response curve was obtained by taking a derivative of the charge-time curve obtained by the BAS 100 in the calculation, $i = \delta Q/\delta t$, where $\delta t = 1$s and δQ is the difference between two successive Q values at 1 s time intervals. The average of two successive time values was used to construct the time axis of the i–t curve. Hydrodynamic voltammograms were obtained by plotting the blank-subtracted peak current from the flow injection as a function of the electrode potential.

PB and MS Conditions

The Hewlett-Packard 59980B PB interface contains a concentric, pneumatic nebulizer. The nebulizing gas was high purity helium, and its pressure was 35 kPa at the gas inlet. The PB desolvation chamber temperature was kept at 60 °C. The two-stage momentum separator rough pumps of the PB interface maintained a pressure of ~30 kPa at the first-stage and ~25 Pa at the second-stage. The mobile phase, acetonitrile, was pumped continuously through the PB interface at a flow rate of 0.4 mL/min. The differentially pumped MS diffusion pumps maintained a pressure of 2.5×10^{-3} Pa in the manifold surrounding the conventional EI ion source. The ion source temperature was 250 °C and the electron energy was 70 eV. The ion source and lens potentials were tuned automatically to optimize the ion intensity of perfluorotributylamine (PFTBA) in the range of 50 to 550 amu. Both scan and selected ion monitoring (SIM) modes were used. In the scan mode, the MS detector was repetitively scanned from 50 to 550 amu at 0.8 scan/s. In the SIM mode, multiple ions were monitored at *m/z* 488, 245, and 244. A fixed integration time of 235 μs was used in the SIM data acquisition mode, and the dwell time for sampling of a specific ion was 100 ms. All mass spectra were acquired in the positive ion mode by either EI or positive chemical ionization (PCI). The EI ionization voltage was 70 eV. In PCI, methane (CH_4) was used as the reagent gas and its pressure was ~9 kPa.

EC/PB/MS

Acetonitrile was degassed in an ultrasonic bath under reduced pressure before being used as mobile phase in EC/PB/MS. Mass spectra of TPA (1×10^{-3} M), TBAP (0.01 M), and the mixture of TPA/TBAP (1×10^{-3} M/0.01 M) in acetonitrile were first acquired in a scan mode without applying voltage to the EC flow cell. To initiate the electrooxidation of TPA, a constant voltage was applied to the EC cell with a Model 173 PAR potentiostat. Background subtraction of each ion chromatogram was performed with a blank mass spectrum obtained just prior to the foot of the first peak in the ion chromatogram. The integrated ion abundance of each ion was measured as the integrated peak area from the background-subtracted extracted-ion chromatogram.

PB/MS Analysis of TPA

In the PB/MS analysis of TPA to investigate the signal enhancement effect due to the presence of TBAP electrolyte (Chapter 4), the experimental setup was the same as in EC/PB/MS (Figure 2-4), but no voltage was applied to the EC cell. Stock solutions of 1 × 10^{-4} M TPA and 0.1 M TBAP in acetonitrile were used to prepare the required solutions just prior to analysis. The solutions with a constant concentration ratio of TBAP/TPA were prepared by diluting the 1 × 10^{-2} M TPA/0.01 M TBAP stock solution with acetonitrile.

SIM was used to obtain the TPA calibration curve data. In the absence of TBAP ions of TPA at m/z 246, 245, 244, 242 and 167 were monitored; in the presence of TBAP, m/z 77 ion was additionally monitored. In the scan mode, the data were acquired in a 50-550 amu at 0.8 scan/s.

The enhancement factor (EF) that was determined as the ratio of the integrated peak area of $TPA^{•+}$ at m/z 245 in the presence and absence of TBAP. The relative ion abundance is the ratio of the integrated peak area, or the absolute ion abundance of an ion, to that of $TPA^{•+}$ ion at m/z 245. MS sensitivity in TPA determinations was determined from the slope of the calibration curve, where the integrated area at m/z 245 (with an arbitrary unit) was plotted against TPA concentration. The limit of detection (LOD) was calculated from the statistics of the calibration curve (LOD=3σ/m, where σ is standard deviation of the slope, and m is the slope).

Solutions for EC/ESI-FTICR MS

All solutions were freshly made. In the preparation of TPA analyte solution, stock solutions of 1×10^{-3} M TPA and 2×10^{-3} M lithium triflate (LiT) in acetonitrile were made first. The typical TPA analyte solution, containing 1×10^{-4} M TPA and 2×10^{-4} M LiT electrolyte, was prepared by pipeting (microliter pipette, Rainin, Woburn, MA) 400 µl of 1×10^{-3} M TPA and 400 µl of 2×10^{-3} M LiT into a vial and diluted with acetonitrile to 4 mL. Different volumes of the stock solutions were used when different TPA analyte or LiT electrolyte concentrations were needed.

In the preparation of PAH solutions for EC/ESI-FTICR MS, a mixture of solvents (methylene chloride and acetonitrile) was used. PAHs (anthracene, perylene, rubrene) dissolve well in methylene chloride, but are sparingly soluble in acetonitrile. The reverse is true for LiT electrolyte. A stock solution of 0.01 M LiT was prepared in acetonitrile. Stock solutions of 5×10^{-3} M PAHs were prepared in methylene chloride. The typical PAH analyte solutions used in the EC/ESI-FTICR MS experiment contained 100 µM PAHs and 200 µM LiT electrolyte, and were made by first pipeting 80 µL 5×10^{-3} M PAH stock solution and 80 µL 0.1 M LiT stock solution into a vial, and then diluting the mixture with acetonitrile to 4 ml. The solutions thus made contained a mixed solvent consisting of 2% CH_2Cl_2/98% CH_3CN. Different volumes of PAH stock solutions were used when analyte solutions of different PAH concentrations were needed, but the solvent composition was maintained at 2% CH_2Cl_2/98% CH_3CN.

EC/ESI-FTICR MS Conditions

A syringe pump delivered the analyte solution continuously through the EC cell to the MS. Typically, the analyte solution contained 1×10^{-4} M analyte and 2×10^{-4} M lithium triflate electrolyte, and the solution flow rate was 75 µL/h. The high ES voltage typically 3.3 kV was applied between the ss(1) electrode of the EC cell and the counter capillary of the FTICR MS. Figure 2-5 illustrates the operation of ss(1) – ss(2) EC cell configuration, in which the cell voltage was floated at the high ES voltage. The EC cell voltage could also be applied between ss(2) – ss(3) and Pd(4) – Pd(5). In the latter two configurations the EC cell voltage was isolated from the ES voltage by the PEEK cross.

A Bruker APEX 4.7 T FTICR mass spectrometer (Figure 2-6) was used in EC/ESI-FTICR MS. An 800 L/s (N_2) and two 400 L/s cryopumps pumped the FTICR external source housing, the ion transfer region, and the high vacuum (~2×10^{-9} mbar) ICR analyzer region respectively. A dual stage ESI source (Analytica of Branford, Branford, CT) was used with a 500 L/min mechanical pump and a turbo-drag pump on the first and second stage, which reduced the pressure from atmosphere to ~5×10^{-3} mbar.

A stainless steel capillary (500 µm i.d. × 170 mm long) heated to 100°C, biased at 20 V was used for sample desolvation. The capillary - ESI needle distance was 3 mm. A skimmer, biased at 10 V, sampled the ions exiting the heated capillary. The ions were trapped in a hexapole ion transfer/storage region for 0.2 s before transfer to the ICR cell. The pressure after the hexapole was ~2.9×10^{-6} mbar. In the ion ejection experiment, ions of a particular m/z, e.g., 488, were ejected from the ICR cell by setting the pulse sequence so that it applied a single-frequency resonant irradiation at the ICR frequency corresponding to the selected m/z.

In the collision induced dissociation (CID) experiment, the ions of a particular m/z, e.g., 245, were isolated in the ICR analyzer cell by applying a pulse sequence that preserved the ions of interest while ejected all other ions from the ICR cell. The collision gas (Ar) was introduced via a pulsed valve (200 µs) to the ICR cell. The pressure in the ICR cell may reach ~1×10^{-7} mbar during CID. A delay time of 0.2 s was used before ion detection, to reduce the pressure in the ICR cell to normal operating pressure.

Regeneration of the EC Cell for EC/ESI-MS

The performance of the EC cell may deteriorate, after ca. 6-8 hours of run time, due to fouling of the electrodes by analyte and other contaminants in solution. The following procedures were found to be effective to regenerate an active working electrode surface: (1) flush the cell sequentially with 1 mL of acetonitrile, acetone, methanol, water, to dissolve salts and polar compounds; (2) pump 2 M H_2SO_4 aqueous solution through the cell at 300 µL/h for 10 min, to remove the oxide films formed on the electrode surface; (3) rinse the cell sequentially with water, methanol, acetone and acetonitrile; (4) dip the cell in an acetonitrile ultrasonic bath for 15 min.

Data Handling in FTICR MS

The Bruker Apex FTICR XMASS (ver 4.0) program was used to acquire the time-domain spectra. Broadband detection was used, with a mass range of 150 to 800 amu. Each acquired transient response signal was the average of 20 scans, unless specified otherwise, and was composed of 64K data points. A locally written program (WinICR 95) was used to facilitate handling of the time-domain XMASS spectra. After magnitude mode Fourier transformation, the ion peak heights were obtained using the line-listing command of the program, and were used to calculate the isotopic ratios of the individual ions. The program calculated the theoretical isotope distributions after the formula and charge of each ion were entered. XMASS results are shown with an absolute intensity scale determined by that program.

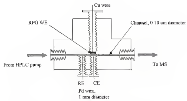

Figure 2-1 Thin-layer flow cell for on-line EC/PB/MS Adapted from [Regno and Brajter-Toth 1997] WE working electrode RE reference electrode CE counter electrode

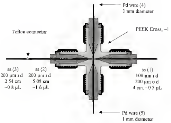

Figure 2-2 EC cell for online EC/ESI/MS

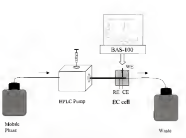

Figure 2-3 Schematic instrumental setup for flow injection with EC detection EC cell design as shown in Figure 2-1 WE working electrode, RE reference electrode, CE counter electrode BAS-100 potentiostat.

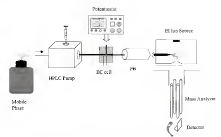

Figure 2-4 Schematic instrumental setup for online EC/PB/MS EC cell design as Figure 2-1

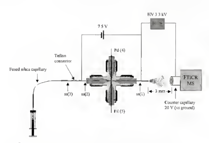

Figure 2-5 Schematic instrumental setup for online EC/ESI/MS
ss(1) ss(2) EC cell configuration, with ss(1) WE as ES needle

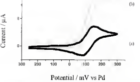

Figure 2-7 Cyclic voltammograms in the thin layer cell (a) stationary solution (b) flow at 1mL/min 1 mM $K_3Fe(CN)_6$ - 0.1 M KCl aqueous solution, scan rate 5 mV/s

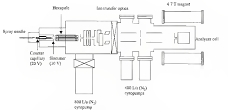

Figure 2-6 Bruker Apex 4.7 T FTICR mass spectrometer with external ESI source

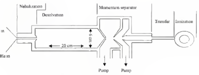

Figure 2-8 The Hewlett-Packard PB interface.

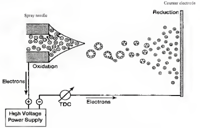

Figure 2-9 Schematic illustration of the ESI process [Kebarle and Tang 1993]

CHAPTER 3

INVESTIGATION OF THE GENERATION OF NONAQUEOUS INTERMEDIATE RADICAL CATIONS IN THE OXIDATION OF TRIPHENYLAMINE BY ELECTROCHEMISTRY/PARTICLE BEAM MASS SPECTROMETRY

Introduction

The goal of this Chapter is to investigate the nonaqueous generation of intermediate radical cations in TPA oxidation by on-line electrochemistry/mass spectrometry (EC/MS). Aothough the radical cations show better stability in nonaqueous than in aqueous environment, the use of EC/MS for the investigations of radical cation chemistry in nonaqueous systems has not received much attention. The first LC/MS interface used for EC/MS, TSP, typically used aqueous mobile phases to form protonated or ammonium-adduct ions (with ammonium acetate as supporting electrolyte) for MS detection [Hambitzer and Heitbaum 1986, Hambitzer et al. 1998(a) and (b), Volk et al. 1988, 1989(a) and (b), 1990]. More recent results indicate that nonaqueous EC/MS studies with ESI can suffer from problems arising from signal suppression by the supporting electrolyte [Xu at al. 1996, Bond et al. 1995, Zhou and Van Berkel 1995].

In this Chapter, we demonstrate the use of EC/MS with particle beam (PB) LC/MS interface in the detection of the intermediate radical cations generated during the anodic oxidation of triphenylamine (TPA) in acetonitrile, with tetrabutylammonium perchlorate (TBAP) as the supporting electrolyte. The thin-layer EC cell for the EC/PB/MS experiments has been described [Chapter 2]. TPA was chosen as a model compound because of its relatively simple electrochemical behavior and the initial interest in the oxidation of N-phenyl group containing compounds [Chapter 1] Acetonitrile was used as a solvent due to its intermediate polarity volatility and low viscosity (0 345 cp at 25 °C) [Janz and Tomkins 1972] Tetrabutylammonium perchlorate (TBAP) is commonly used as an electrolyte in organic electrochemistry due to its high solubility and electrochemical inertness in organic solvents It is preferred for its wider potential range than other quaternary ammonium salts [Janz and Tomkins 1972] In addition, it has been shown that Bu_4N^+ can be converted efficiently from solution to gas phase [Bond et al 1995 Tang and Kebarle 1993] Therefore TBAP is a reasonable electrolyte for EC/PB/MS in nonaqueous solvents

Results and Discussion

Cyclic Voltammetry of TPA

The cyclic voltammogram of TPA obtained in bulk solution is shown in Figure 3-1 During the first anodic scan only one oxidation peak at +0 883 V vs Pd is observed which is attributed to the oxidation of TPA Two reduction peaks, at +0 750 and +0 634 V respectively, are observed in the following cathodic scan During the second scan cycle two oxidation peaks and two reduction peaks are observed The cyclic voltammetric results are consistent with the proposed ECE oxidation pathway of TPA [Figure 1-3 of Chapter 1] The major oxidation peak at more positive potential is due to the oxidation of TPA, while the smaller pair of redox peaks at less positive potentials were from the oxidation/reduction of tetraphenylbenzidine (TPB), a dimer product formed by $TPA^{\bullet+}$ The electrochemical formation of $TPB^{\bullet+}$ (m/z 488) and its conversion to TPB^{2+} (m/z 244) was further investigated by EC/PB/MS as described below

Offline Flow Injection Analysis (FIA)

The electrochemical behavior of TPA under flow conditions was examined by FIA, in which the thin-layer EC cell was used [Chapter 2] Figure 3-2 shows the FIA current response curves obtained with the injection of a blank solution of 0 1 M TBAP in acetonitrile (a) followed by a mixture of 1×10^{-4} M TPA and 0 1 M TBAP in acetonitrile (b) with the EC flow-through cell voltage controlled at +1.2 V vs Pd As can be seen from Figure 3-2 the injection of the solution of 1×10^{-4} M TPA-0 1 M TBAP gives rise to a peak current, while a smooth baseline is observed after the injection of 0 1 M TBAP in acetonitrile The results verify the electrochemical oxidation of TPA in the flow cell

The EC cell conversion efficiencies in the oxidation of TPA, at several different flow rates, are summarized in Table 3-1 The contribution of the oxidation of TPB product was not considered in the calculation of the EC cell conversion efficiency Table 3-1 shows that a higher conversion efficiency is achieved at lower flow rates, which is as expected [Regino and Brajter-Toth 1997 Regino et al 1998] This observation is related to a longer residence time of analyte in the EC flow cell at lower flow rates, which increases the amount of TPA that can be converted in the electrochemical reaction during its passage through the EC cell The high conversion efficiencies in Table 3-1 may be related to the effect of the organic solvent on the EC conversion efficiency [Regino and Brajter-Toth 1997 Regino et al 1998] The presence of an organic solvent in the mobile phase has been shown to improve the EC conversion efficiency in a mixed solvent system [Regino et al 1998]

Figure 3-3 shows a hydrodynamic voltammogram that was constructed from the blank-subtracted FIA data, as described in Chapter 2 The voltage applied to the EC cell was in the range of +0 5 to +1 9 V *vs* Pd Compared to the voltammograms in Figure 3-1 the onset of the electrode reaction of TPA in the EC flow cell, which is indicated by the increase in the cell current, has been shifted to somewhat more positive potentials The current of TPA starts to increase at +0 8 V *vs* Pd, and a maximum current is observed at ~+1 1 V The positive shift of the reaction potential in the EC flow cell may be due in part to the ohmic drop in the EC cell [Regino and Brajter-Toth 1997] and may also be a result of different surface conditions at the RPG working electrode in the EC cell during the FIA experiment, under flow conditions

In Figure 3-3 the current drops to a low value at ~+1 2 V then increases to a relatively stable level, and fluctuates around this level until the potential applied to the EC cell reaches ~+1 6 V The observed current fluctuations can be attributed to the oxidation in the EC cell of TPA oxidation products such as the dimer product.

In Figure 3-3 the initial increase of the current at ~+0 8 V reflects the onset of the oxidation of TPA As the voltage that is applied to the EC cell is increased, the rate of the formation of the dimer as a result of the oxidation of TPA, and thereby the contribution of the oxidation of TPB to the current response, also increases The oxidation of TPB$^{\bullet+}$ to TPB^{2+} is a slow kinetic step [Nelson and Philp 1979 Oyama et al 1991, Sumiyoshi 1995] The current at ~+1 1 V includes mainly the contributions from the oxidation of TPA and from oxidation of TPB to TPB$^{\bullet+}$ TPB$^{\bullet+}$ can also be produced via solution chemistry i e oxidation of TPB by TPA$^{\bullet+}$ [Oyama et al 1991]

When the voltage is greater than ~+1 1 V TPB and TPB$^{\bullet+}$ predominate at the WE surface, and the current is mainly controlled by the oxidation of TPB to TPB$^{\bullet+}$ while the contribution from the oxidation of TPA to TPA$^{\bullet+}$ and of TPB by TPA$^{\bullet+}$ becomes less significant. Between ~+1.3 V and +1.6 V, the oxidation of $TPB^{\bullet+}$ to TPB^{2+} starts to be the major process contributing to the current. Above ~+1.6 V, a rapid increase in current is observed, which can be interpreted as due to further oxidation of TPB^{2+} at more positive potentials. The offline FIA results are in agreement with the EC/MS results described below.

Online FIA in EC/PB/MS

Shown in Figure 3-4 a-c are the mass spectra obtained by PB/MS following the injections of 1×10^{-3} M TPA, 0.01 M TBAP, and 1×10^{-3} M TPA/0.01 M TBAP, respectively, with the EC flow cell on-line, but without applying voltage to the cell. Figure 3-4a illustrates the mass spectrum of TPA. The ions identified following the EI ionization show significant intensities at m/z 245 ($TPA^{\bullet+}$), 167 (loss of C_6H_6 from $TPA^{\bullet+}$), 141 (loss of C_2H_2 from the fragment at m/z 167), 77 ($C_6H_5^+$), and 51 (loss of C_2H_2 from $C_6H_5^+$). Figure 3-4b shows the EI mass spectrum of TBAP, which shows ions at m/z 242 ($(C_4H_9)_4N^+$), 142 ($(C_4H_9)_2N{-}CH_2$), 100 ($(C_4H_9)(CH_3)N^+{=}CH_2$), and 57 ($(C_4H_9)^+$). The mass spectra in Figure 3-4 are in agreement with the online library spectra of TPA and TBAP [NIST 1998, 2001] and the literature [Gierlich et al. 1977, Veith 1983]. When TPA and TBAP are present together in solution, ions from the ionization of both TPA and TBAP appear in the mass spectrum, as shown in Figure 3-4c.

When voltage is applied to the EC cell in the EC/PB/MS experiment, no new ions are detected by MS in the scan mode. However, selective ion monitoring at m/z 488 ($TPB^{\bullet+}$) produces the ion chromatograms shown in Figure 3-5. When the EC cell voltage is changed from +0.6 to +2.0 V, as shown in Figure 3-5, the change in the intensity of the selected ion at m/z 488, with the potential, is clearly observed.

As can be seen in Figure 3-5 when the EC voltage is below +0.8 V only a small response is observed at m/z 488 When the voltage is increased to +1.0 V the ion intensity of m/z 488 ion increases A maximum response is observed at ~+1.2 V and above +1.2 V the ion peak due to the m/z 488 ion starts to decrease with the increase in the applied EC cell voltage The MS response at m/z 488 decreases to nearly background levels when the voltage is increased to ~+2.0 V With the voltage set back to a smaller value, e.g., +1.1 V the m/z 488 ion peak increases again, which indicates that the small response at +2.0 V is caused by the EC cell voltage and the electrochemical reactions at this voltage and is not a result of the MS response decreasing with time after multiple injections The ion chromatogram obtained at +1.1 V (Figure 3-5) also shows that the inactivation of the working electrode in the EC cell as a result of the multiple injections during a continuous operation of EC/PB/MS was not significant The results confirm the formation of $TPB^{\bullet+}$ monocation in the electrochemical oxidation of TPA.

Direct EC/PB/MS Monitoring of Radical Intermediate and Product

Figure 3-6 shows a plot of the integrated ion abundance at m/z 488 ($TPB^{\bullet+}$) as well as the ratio of ion abundance at m/z 244 (TPB^{2+}) to that at m/z 245 ($TPA^{\bullet+}$) obtained by EC/PB/MS as a function of potential As shown in Figure 3-6, an increase in the abundance of the radical cation intermediate $TPB^{\bullet+}$ is observed with the increase in the EC cell voltage between +0.8 and +1.2 V The rapid increase of the ion abundance of $TPB^{\bullet+}$ between +0.8 and +1.2 V can be attributed to a rapid formation of this radical cation as a result of the electrochemical oxidation of TPA in the flow cell The abundance of the $TPB^{\bullet+}$ intermediate decreases between +1.2 and +1.6 V vs Pd, with a rapid decrease above +1.6 V

The high rate of formation of $TPB^{\bullet+}$ between +1.2 and +1.6 V is accompanied by a high rate of formation of the dication product TPB^{2+} (m/z 244) as shown in Figure 3-6. Figure 3-6 shows that, at potentials positive of +1.2 V the latter reaction rate increases while the rate of formation of the intermediate $TPB^{\bullet+}$ decreases. Above +1.3 V the rate of conversion of $TPB^{\bullet+}$ to TPB^{2+} exceeds the rate of generation of $TPB^{\bullet+}$. Above +1.6 V the ion abundances at m/z 488 and at m/z 244 decrease rapidly with an increase in EC cell voltage, probably as a result of further oxidation of TPB^{2+} at very positive EC cell potentials. The EC/PB/MS results are in agreement with the results of off line FIA analyses illustrated in Figure 3-3. The current in Figure 3-3 at less positive potentials (of +1.2 V) is lower than that at more positive potentials (of +1.6 V), while the total ion abundance of $TPB^{\bullet+}$ and TPB^{2+} in EC/PB/MS is similar and high throughout the same potential window and this likely reflects the high sensitivity of PB/MS to the species being detected [Regino and Brajter-Toth 1999].

Ion Formation in EC/PB/MS

According to the oxidation pathway of TPA (Figure 1-3 of Chapter 1), in EC/PB/MS the electrochemical oxidation of TPA in an EC cell can be expected to produce ions at m/z 245, 488 and 244. If the ions have a long enough lifetime to enter the ion source of the mass spectrometer, and reach the MS detector, they will give rise to ion peaks in the ion chromatogram. However, in EC/PB/MS, the reverse is not true, i.e. not all ions that are observed are due to the EC oxidation of TPA. Since the EC cell conversion efficiency is rather low in the oxidation of TPA, EI ionization of TPA may generate ions in large enough quantities for them to show significant spectral overlap with the products of the electrochemical oxidation of TPA in the EC cell during

EC/PB/MS. It is therefore important to consider the possible origin of all ions, to verify the electrochemical formation of the intermediates and products.

Ion Formation by EI

Electrooxidation of TPA in the electrochemical cell generates $TPA^{\bullet+}$ (m/z 245), an intermediate radical monocation $TPB^{\bullet+}$ (m/z 488) and a dication TPB^{2+} (m/z 244). At the same time, as shown in Figure 3-4 a and c, EI ionization of TPA produces ions at m/z 245 and 244. The ion at m/z 245 is formed by EI after a loss of one electron by TPA, a reaction that is equivalent to the EC formation of the cation radical $TPA^{\bullet+}$ with the same m/z (245) in the electrochemical oxidation of TPA in the EC flow cell. However, the ion at m/z 244 formed in the ion source is not the same as the dimer TPB^{2+} (m/z 244) formed by the electrochemical oxidation of TPA in the EC flow cell. Because the EI ion source is operated under high vacuum, the residence time of ions that are formed in the ion source by EI is very short (~10^{-6} s). Combined with a relatively low reaction rate for the formation of TPB^{2+} from $TPB^{\bullet+}$ [Nelson and Philp 1979, Oyama et al. 1991], the probability of the formation of TPB^{2+} dication in the EI ion source is small. The ion intensity of the ion at m/z 244 obtained in the EI ion source is ~42% that at m/z 245 (of $TPA^{\bullet+}$), as can be seen from Figure 3-4c. Consequently, the ion abundance observed at m/z 244 as a result of the EI ionization is much too high to be due to the formation of TPB^{2+} in the EI ion source. Furthermore, the ion expected at m/z 488 of $TPB^{\bullet+}$, a dimer radical cation precursor ion of TPB^{2+} dication, is not detected after EI ionization. It can thus be concluded that the ion generated by EI at m/z 244 is not due to TPB^{2+}, but more likely results from a loss of a hydrogen from $TPA^{\bullet+}$, as a consequence of high excess internal energy during the ionization of TPA to $TPA^{\bullet+}$ in the EI ion source.

Ion Intensity Ratio for Ion Monitoring

Since the ionization of TPA by EI does not produce an ion at m/z 488, the electrochemical formation of TPB^{+} (m/z 488) monocation can be monitored directly at m/z 488 via SIM. The ion abundance at m/z 488 is in fact controlled by EC cell voltage, as can be seen from the change of the ion abundance with the change of cell voltage in Figure 3-6. The electrochemical formation of TPB^{2+} dication (m/z 244) cannot be monitored directly at m/z 244 because of the spectral interference from $[TPA-H]^{+}$ formed via a loss of hydrogen atom from TPA^{+} during EI ionization, which generates an interfering ion of high intensity at the same m/z 244. Instead, as shown in Figure 3-6, the intensity ratio of the ions at m/z 244 vs 245 can be monitored with the change in the applied EC cell voltage, to reflect the status of TPB^{2+} at m/z 244, which is only generated in the electrochemical reaction. The use of the intensity ratio also corrects the variation in the ion abundance at m/z 244 caused by injection error and/or degradation of the PB/MS performance during the EC/PB/MS experiment.

By using positive chemical ionization (PCI) in EC/PB/MS, with methane as a reagent gas, the ions generated in the MS ion source were predominantly protonated $[TPA+H^{+}]$ ions at m/z 246 with some unprotonated $TPA^{\bullet+}$ ions at m/z 245. Few m/z 244 ions were observed in the PCI mass spectrum of TPA. By applying EC cell voltage, an increase in the intensity of m/z 244 ion was observed, as shown in Figure 3-7. This indicates that the TPB dication (m/z 244) generated in the EC cell remain mostly unprotonated in the PCI ion source, as expected. In Figure 3-7, a maximum intensity of m/z 244 ions was observed at an EC cell voltage of ~1.6 V. Above 1.6 V, a decrease in the intensity of m/z 244 ions occurred. This result is consistent with the change of the intensity ratio of m/z 244 vs 245 ions shown in Figure 3-6. In Figure 3-7, the relative intensities of m/z 244 ions at less positive EC cell voltages are somewhat higher than the relative intensity ratios of m/z 244 vs 245 ions in Figure 3-6. The difference may be caused by the difference in the sensitivity of PCI vs EI, as well as the difference in direct ion monitoring versus monitoring of the intensity ratio. The results demonstrate that the spectral interference at m/z 244 from the EI ionization can be minimized by use of PCI ionization in EC/PB/MS.

Concentrations of TPA and TBAP

Both TPA and TBAP are nonvolatile and when their concentrations are high, PB/MS analysis of TPA-TBAP mixtures causes plugging of the PB interface, degradation of the PB interface performance, and contamination of the EI ion source. To alleviate these problems, low concentrations of TPA and TBAP are preferred. But at low concentrations (e.g., 1×10^{-4} M TPA and 1×10^{-3} M TBAP) the $TPB^{\bullet+}$ intermediate is not detected via either scan or SIM mode. When the concentrations of TPA and TBAP are higher, e.g., 1×10^{-3} M and 0.01 M, respectively, $TPB^{\bullet+}$ can be detected via SIM. High concentrations of TBAP also improve electrical conductivity in the EC flow cell, which improves the control of the EC cell voltage and reduces the ohmic drop.

When the concentrations of TPA and TBAP are high, a decrease in the ion intensity of TPA ions is observed at m/z 244 and 245 after each injection. Nevertheless, monitoring of the intensity ratio at m/z 244/245 allows detection of the TPB^{2+} dication (m/z 244) formed in the electrochemical reaction.

The ion peak at m/z 488 of $TPB^{\bullet+}$, of the radical intermediate formed in the electrochemical oxidation reaction of TPB in the EC cell, is less sensitive to the deteriorating performance of the PB interface and the EI ion source, which is observed at high concentrations of TPA and TBAP. This is consistent with a higher mass and higher momentum of TPB^{+}, which favors transfer of the ion into the MS ion source [Regino and Brajter-Toth 1999]. An apparent carrier effect, which contributes to improved ion transfer in the presence of TBAP, which is discussed in the following section, additionally contributes to the increase in the transmission efficiency of $TPB^{\bullet+}$. When the concentrations of TPA and TBAP are lower, e.g., to 1×10^{-4} M TPA and 1×10^{-3} M TBAP, the contamination of the PB interface and the ion source is reduced, and good sensitivity is observed after repeated sample injections.

Signal Enhancement with TBAP

A comparison of the abundance scales of the mass spectra in Figure 3-4 a and c shows that in the presence of TBAP a significant increase in the ion signal is obtained in EI ionization of TPA. Figure 3-8 compares the extracted-ion chromatogram of $TPA^{\bullet+}$ at m/z 245 in the absence and presence of TBAP. The apparent enhancement in the presence of TBAP, quantified as a peak area, is estimated at ~35-fold. As a result, MS detection sensitivity is improved, and the detectable concentration of TPA is reduced from about 1×10^{-4} to 1×10^{-6} M, or the mass detection limit is reduced from about 490 to 4.9 ng. The observed enhancement of the ion signal in the presence of TBAP is similar to the signal enhancement observed previously in LC/PB/MS analysis of different classes of compounds in the presence of ammonium acetate [Bellar et al. 1990, Ho et al. 1992], neutral analogues of analytes [Incorvia Mattina 1991(a) and (b)], and in the presence of isotope-labeled compounds [Apffel and Perry 1991]. A similar effect was found previously to influence sensitivity in water containing organic mobile phases.

Unlike ammonium acetate, whose volatility and decomposition were believed to play a role in the signal enhancement observed previously [Li and Koropchak 1998], TBAP is nonvolatile and is relatively stable under mild temperature conditions of the PB interface. TBAP is also different from neutral analyte analogues and/or isotope-labeled compounds that were observed previously to contribute to the signal enhancement in PB detection in that it contains an ionic charge. Here, we report for the first time that in a nonaqueous solvent, acetonitrile, ion signal enhancement can be achieved in PB/MS via addition of a nonvolatile electrolyte, TBAP. The effect of TBAP on the sensitivity enhancement in EC/PB/MS may play an important role in enabling the direct monitoring of the formation of the intermediate radical cation TPB$^{\bullet+}$ by EC/PB/MS.

Conclusions

Anodic oxidation of TPA was investigated by on-line EC/PB/MS with EI ionization. Direct detection of an intermediate radical ion, TPB$^{\bullet+}$, in the electrochemical oxidation of TPA was achieved. The electrochemical formation of TPB$^{\bullet+}$ and its subsequent electrochemical oxidation to TPB^{2+} was verified by EC/PB/MS, and the rate of the formation of each ion was shown to be a function of the electrode potential.

In conventional cyclic voltammetry, TPA showed an oxidation peak at +0.88 V vs Pd, while hydrodynamic voltammograms obtained by FIA indicated a small positive shift of the reaction potential in the EC flow cell. EC/PB/MS allowed the identification of the EC cell potentials at which the rate of generation of the radical intermediate was the highest. The results confirmed a slower rate of the electrochemical formation of the final dication product. The EC/PB/MS results showed that the oxidation of the dimer TPB to a monocation TPB$^{\bullet+}$ and then to the dication TPB^{2+}, following the initial electrooxidation of TPA to TPA$^{+\cdot}$ in the EC flow cell occurs at highest rates at different potentials that are more positive than the potentials of the voltammetric oxidation of TPA

We also report, for the first time, a significant signal enhancement in FB/MS in the presence of TBAP The observed signal enhancement may facilitate other EC/MS studies including in nonaqueous solvents The EC/PB/MS results show the advantages of the PB interface in EC/MS studies such as the ease of coupling of EC with MS via the PB interface, flow rate compatibility, and the advantage of the EI ionization, which generates mass spectra that can be library searched Mainly the compatibility of PB/MS with EC/MS stems from the ability to use an electrolyte at high concentrations The resulting signal enhancement observed in the presence of a nonvolatile electrolyte TBAP may facilitate other applications of LC/MS

Table 3-1 Cell conversion efficiency for the oxidation of TPA[a]

Flow rate (mL/min)	TPA injected (mol)	Charge detected (C)	Conversion effic. (%)[b]
0.4	2.0×10^{-8}	3.38×10^{-4}	17.5
1.0	2.0×10^{-8}	1.76×10^{-4}	9.1
2.0	2.0×10^{-8}	8.34×10^{-5}	4.3

[a] Conditions: 1×10^{-3} M TPA/0.1 M TBAP in acetonitrile, injection volume 20 µl, mobile phase 0.1 M TBAP in acetonitrile and voltage applied +1.2 V vs Pd.

[b] Oxidation of chemical follow-up reaction product was not considered. Fluctuations of the EC cell conversion efficiency were estimated to be 30–40%.

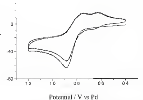

Figure 3-1 Cyclic voltammetry of TPA in acetonitrile Conditions 1×10^{-3} M TPA/0.1 M TBAP RPG (0.093 cm^2) working electrode Pd reference and counter electrodes and scan rate 100 mV/s

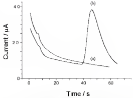

Figure 3-2 Electrochemical detection in off-line FIA (a) 0.1 M TBAP (b) 1×10^{-6} M TPA/0.1 M TBAP in acetonitrile Conditions injection volume 20 µL mobile phase 0.1 M TBAP-acetonitrile, flow rate 0.4 mL/min Voltage applied +1.2 V vs Pd and injections 30 s after cell voltage was applied

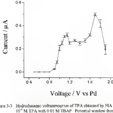

Figure 3-3 Hydrodynamic voltammogram of TPA obtained by FIA. Conditions: 1 × 10^{-4} M TPA with 0.01 M TBAP. Potential window from +0.5 to +1.9 V. Other experimental conditions as in Figure 3-2. Voltammogram of TPA was constructed by plotting the blank-subtracted peak current response.

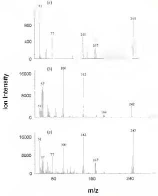

Figure 3-4 EI mass spectra of TPA, TBAP and TPA/TBAP obtained by PB/MS (a) 1×10^{-5} M TPA (b) 0 01 M TBAP (c) 1×10^{-5} M TPA/0 01 M TBAP in acetonitrile Conditions injection 20 μL mobile phase acetonitrile flow rate 0 4 mL/min EI electron energy 70 eV and source temperature 250 °C

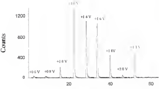

Figure 3-5 Mass spectrometric ion chromatogram at m/z 488 with change of cell voltage in EC/PB/MS. 1×10^{-3} M TPA-0.01 M TBAP in acetonitrile, injection 20 µL, Acetonitrile mobile phase, flow rate 0.4 mL/min. Injection at 30 s after cell voltage was applied. Selective ion monitoring at m/z 488.

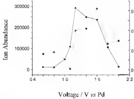

Figure 3-6 Effect of cell voltage on $TPB^{\bullet+}$ ion abundance at m/z 488 and on ion intensity ratio of ions at m/z 244 (TPB^{2+} to 245 ($TPA^{\bullet+}$) in EC/FB/MS ● ion abundance at m/z 488 solid line left Y-axis ♦ ratio of ion abundance at m/z 244 to that at m/z 245 dashed line right Y axis The ion abundance was measured as the integrated peak area of the corresponding ion peaks

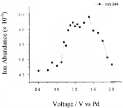

Figure 3-7 Direct monitoring of TPB^{2+} (m/z 244) generation in EC/PB/MS with positive chemical ionization (PCI). CH_4 as the reagent gas, 1.3 torr at inlet. SIM

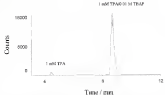

Figure 3-8 Mass spectrometric extracted-ion chromatogram at m/z 245 obtained by PB/MS with the EI ionization. Conditions: 1 × 10^{-3} M TPA, followed by 1 × 10^{-3} M TPA/0.01 M TBAP in acetonitrile. Same conditions as Figure 3-4.

CHAPTER 4
HIGH SENSITIVITY IN PARTICLE BEAM MASS SPECTROMETRY WITH A NONVOLATILE ELECTROLYTE

Introduction

Particle beam (PB) liquid interface has been used extensively to couple liquid delivery systems (LC) to mass spectrometers in LC/MS [Willoughby and Browner 1984, Winkler et al 1988, Kim et al 1990, Voyksner et al 1990, Ho et al. 1992, Caren et al 1996, Cappiello 1996]. Problems in analysis with PB/MS include a nonlinear response and relatively poor sensitivity at low concentrations [Young and Lafontaine 1993, Cappiello et al 1997, Bellar et al 1990, Caren et al. 1999, Klemtop et al. 1993], which is due to low mass transport efficiency of analyte through the PB interface, where the PB momentum separator acts as a high-pass particle size filter [Bellar et al 1990, Brown and Draper 1991, Apffel and Perry 1991, Li and Koropchak 1998].

Willoughby and Browner [1984], the PB inventors, predicted that the PB mass transport efficiency would be greatest for involatile analytes because of the use of the momentum separator in the PB interface. The involatile compounds can readily form high-mass particles, which can be more efficiently transported through the momentum separator of the PB interface than the solvent and analyte vapors [Chapter 2].

It has been reported that the addition of semi volatile salts to the mobile phase, such as ammonium acetate [Cappiello 1996, Bellar et al 1994, Caren et al 1996, Caren et al. 1999] and compounds structurally related to the analyte [Kim et al. 1990, Incorvia Mattina 1991(a) and (b), Young and Lafontaine 1993] as well as the isotope-labeled internal standards [Bellar et al 1990, Ho et al 1992], can enhance the analyte signal and improve the linearity of the calibration curves in LC/PB/MS analysis. The signal enhancement has generally been accepted as due to the improved mass transport of the analyte through the PB interface, despite the existence of some discrepancies as to the mechanism of this process [Bellar et al. 1994, Wilkes 1995(a) and (b), Li and Koropchak 1998]. However, it has been argued that the addition of the mobile phase additives such as ammonium acetate [Apffel and Perry 1991, Bellar et al. 1992, Young and Lafontaine 1993, Razzazi-Fazeli and Schmid 1998] or the isotope-labeled internal standards [Brown and Draper 1991] is ineffective at linearizing the detector response in PB/LC/MS, although the analyte signal can be improved. A constant level of the mobile phase additives was used in all of these studies.

In Chapter 2, a thin layer electrochemical flow cell was coupled to a particle beam mass spectrometer (EC/PB/MS), with an electron impact (EI) ionization MS ion source, to detect the radical cations generated in the electrochemical oxidation of triphenylamine (TPA). It was found that the presence of a nonvolatile organic electrolyte, tetrabutylammonium perchlorate (TBAP), caused a significant enhancement of the TPA$^{\bullet+}$ signal, which facilitated the detection of the radical products formed in TPA oxidation.

While the mobile phase additives have been used frequently in PB/LC/MS analysis to enhance the analyte signal [Li and Koropchak 1998, Doerge et al. 1992], the use of a nonvolatile salt such as TBAP as the mobile phase additive to enhance the signal of a neutral analyte has not been reported.

In this Chapter, the enhancement of TPA MS signal, in PB/LC/MS, in the presence of TBAP is investigated, without the EC oxidation. The goal is to enhance the analytical capabilities of PB/LC/MS in the determination of TPA.

The present work demonstrates that in addition to the well-known improved mass transport of the analyte through the PB interface, reduced fragmentation of the analyte molecular ion, $TPA^{+\cdot}$, during the EI ionization in the presence of TBAP contributes to the observed signal enhancement. In addition, the results indicate that in the signal enhancement process the concentration ratio of TBAP/TPA is important; linear response, and best sensitivity and reproducibility of the calibration curves are obtained when a constant ratio, near an optimum value, is maintained during the calibrations rather than using a constant concentration of TBAP.

Results and Discussion

Change in the EI Mass Spectrum of TPA

EI PB/LC mass spectra of acetonitrile solutions of TPA (1 mM) in the absence and presence of TBAP (0.01 M) are shown in Figure 4-1 a and b, respectively. Figure 4-1b was obtained by subtracting the mass spectrum of 0.01 M TBAP from that of 1 × 10^{-3} M TPA/0.1 M TBAP mixture. The EI ionization of TPA in PB/LC/MS generates $TPA^{+\cdot}$ molecular ion at m/z 245 with major fragment ions at m/z 167, 141, 77, 51. The ion identities and the corresponding ion abundances (i.e., ion peak areas) are illustrated in Table 4-1.

A comparison of the intensity scales in Figure 4-1a and b shows the significant signal enhancement that was observed for TPA in the presence of TBAP [Chapter 3]. The integrated ion abundance at m/z 245 is 7.6 × 10^{3} in the absence and 2.6 × 10^{5} in the presence of TBAP. The enhancement factor (EF), defined as the ratio of the ion abundance at m/z 245 in the presence and absence of TBAP, is ca. 35-fold.

Table 4-1 compares the absolute and relative ion abundance values of major fragment ions of TPA that are observed in PB/LC/MS in the absence and presence of TBAP. As can be seen from Table 4-1, in the presence of TBAP the absolute ion abundance of all fragment ions is enhanced. This indicates that the sensitivity in the MS detection of TPA is significantly improved in the presence of TBAP. The sensitivity is determined by the efficiency of TPA mass transport through the PB/LC/MS interface and by the efficiency of the EI ionization process, after the analyte is delivered to the MS ion source from the PB/LC interface. The enhanced abundance of all ions of TPA in the presence of TBAP, shown in Table 4-1, indicates that the mass transport of TPA through the PB interface into the EI ion source and/or the ionization efficiency of TPA are improved.

Although in the presence of TBAP the absolute ion abundance of all fragment ions of TPA increases, the change in the relative ion abundance is not the same for all ions. As can be seen from Table 4-1, the relative abundances of ions at m/z 244 and 167 (defined as the ratio of the ion abundance of the ion, to that of the parent ion at m/z 245) increase in the presence of TBAP, but those of the lower mass ions at m/z 166, 141, 77 and 51 decrease. The observed change in the relative ion abundance of the fragment ions indicates a change in the ionization pattern of TPA in the presence of TBAP.

The change in the ionization pattern of TPA can also be observed from Figure 4-1. In Figure 4-1a, the low mass fragment ion at m/z 51 is the base ion, while in Figure 4-1b, the base ion is the $\text{TPA}^{+\bullet}$ molecular ion at m/z 245. Apparently, the presence of TBAP electrolyte has contributed to the reduced fragmentation of $\text{TPA}^{+\bullet}$. Thus, we report for the first time that the mobile phase additive in PB/LC/MS may contribute to a change in the EI ionization pattern of an analyte. Since the ion intensity of the $\text{TPA}^{+\bullet}$ ion was used to calculate the signal enhancement factor (EF), the reduced fragmentation and the increased intensity of $\text{TPA}^{+\bullet}$ ion in the presence of TBAP contribute to the calculated signal enhancement.

Formation of TPA/TBAP Aggregates

The change in the EI ionization of TPA in presence of TBAP can be rationalized by considering ion fragmentation pathways. TPA ions at m/z 245 and 244 are formed without breaking C-N bonds and the phenyl groups stabilize the charge on the N atom [Nelson and Adams 1968, Zhang and Brajter-Toth 2000]. On the other hand formation of the ions at m/z 167 involves a loss of C_6H_6 from TPA by breaking a C-N and a C-H bond. Additional fragmentation generates ions at m/z 166, 142 and 141. The ion at m/z 77 is a (C_6H_5) fragment formed via charge relocation (from N to phenyl) and breaking of C-N bond; the ion at m/z 51 forms after a loss of a neutral C_2H_2 group from (C_6H_5). Because fewer bonds are broken when the fragmentation is less extensive, less energy is required to form higher mass ions such as m/z 245 and 244 than the highly fragmented lower mass ions. An increase in the relative ion abundance of the high-mass ions, relative to a decrease in the relative ion abundance of the low-mass fragment ions, indicates a limited fragmentation of TPA^{+}, which in turn indicates "softer" or lower-energy ionization of TPA in the presence of TBAP.

Based on these results it can be postulated that during the EI ionization, TBAP can absorb some energy from the high energy electrons, and as a result, effectively shields TPA molecule ion from extensive fragmentation. Aggregation of TBAP and TPA in the PB interface can facilitate this process. An alternative explanation is that TBAP aggregates can generate an ionization buffer, which limits fragmentation of TPA during the EI ionization. The formation of TBAP/TPA aggregates is consistent with the observed improvement in mass transport efficiency of TPA, which caused an enhancement of the absolute ion abundance for all of the ions in the presence of TBAP.

Effect of TBAP Concentration

The effect of TBAP concentration on the magnitude of the signal enhancement is illustrated in Figure 4-2. In Figure 4-2, the signal enhancement factor EF is plotted as a function of TBAP concentration, at a fixed concentration of TPA (1×10^{-4} M). As can be seen from Figure 4-2, the EF increases rapidly with the increasing concentration of TBAP, reaches a maximum at TBAP/TPA concentration ratio of ca.10/1, and slowly decreases at higher concentrations of TBAP. The observed change in the EF with the concentration of TBAP is in agreement with earlier results, where the signal enhancement in the analysis of caffeine has been achieved by post-column addition of ammonium acetate [Bellar et al. 1990, Ho et al. 1992, Young and Lafontaine 1993]. The previous results have shown that too low or high concentrations of ammonium acetate resulted in a decrease of the signal.

The low value of the EF that is observed (Figure 4-2) at low concentrations of TBAP is likely due to the lower transport efficiency, through the PB interface, of smaller aggregates of TPA and TBAP that are expected to form at lower concentrations of TBAP. The low sensitivity in TPA detection at low concentrations of TBAP is also consistent with the more extensive fragmentation of TPA, during the EI ionization at low concentrations of TBAP. The decrease in the EF at high concentrations of TBAP is likely a result of increased material losses (due to gravity) during transport through the PB interface, of a large number of large particles of TPA and TBAP, which are expected to form at high concentrations of TBAP [Willoughby and Browner 1984, Li and Koropchak 1998].

In the PB interface, which acts as a momentum separator, small particles are pumped away and increased mass of aggregates improves the transport efficiency. Since TBAP is less volatile than TPA, formation of TBAP-TPA aggregates can also reduce the evaporation losses of TPA, which can contribute to signal enhancement. As shown in Figure 4-2, a maximum TPA signal is reached for TPA/TBAP concentration ratio of ca. 10/1. Assuming that the aggregates form, and this results in a uniform composition of aggregates, an optimum aggregate mass will result in efficient transport [Young and Lafontaine 1993, Incorvia Mattina 1991]. To achieve such an optimum mass of particles, it is essential to maintain an optimum concentration ratio of TPA/TBAP. Figure 4-2 shows that the optimum concentration ratio of TPA/TBAP is ~10, indicating that in the optimum-mass particles one TPA is surrounded by ca. 10 TBAP molecules. It can be inferred from these results that in constructing calibration curves, keeping the concentration ratio of TPA/TBAP constant at an optimum value may help to enhance the linearity and the sensitivity of the calibration curves. This hypothesis has been verified experimentally as discussed below.

TPA Calibration Curves

The low sensitivity and the nonlinear behavior at low concentrations limit applications of PB/LC/MS in analysis. Figure 4-3 shows an example of a calibration curve that is obtained for TPA in PB/LC/MS. The curve shows a linear response of TPA at high concentrations (500 μM ~ 5 mM). The sensitivity at lower concentrations (10 ~ 200 μM) is independent of the concentration of TPA. This results in nonlinear calibration response. The lowest detectable concentration of TPA is 10 μM. The limit of detection (LOD) calculated from the calibration curve is 0.55 μM.

To achieve the linearity and increase the sensitivity at low concentrations in the determination of TPA, the calibration curves of TPA were constructed in the presence of TBAP, as shown by Figure 4-4. Figure 4-4a was obtained in the presence of a fixed concentration of TBAP (1×10^{-3} M). Figure 4-4b was obtained by maintaining a constant concentration ratio of TBAP/TPA (10/1) to achieve the highest sensitivity.

At a fixed concentration of TBAP, the calibration curve (Figure 4-4a) shows improved linearity (R=0.998) at low concentrations (5 μM – 250 μM) as compared to the results in Figure 4-3 in the absence of TBAP. The calibration curve in Figure 4-4b shows excellent linearity (0.999) at lower concentration levels (0.5 μM – 200 μM), high sensitivity (6.6×10^{5} counts/μM) and good reproducibility (RSD 3~5%). The LOD obtained from the calibration curve is 0.07 μM, significantly below the 0.55 μM LOD in the absence of TBAP.

The results in Figure 4-3 and Figure 4-4 were obtained in SIM signal acquisition mode. In the presence of TBAP more ions were monitored by SIM and as a result these determinations are less sensitive. However, the results in Figure 4-4 still show significantly enhanced sensitivity in the determination of TPA as compared to the results in Figure 4-3.

The results in Figure 4-4 demonstrate that in the determination of TPA^{+} (parent ion), the presence of TBAP improves the sensitivity, linearity, and the linear response range. The results show that the limitations of PB/LC/MS in analysis can be overcome when a nonvolatile electrolyte, such as TBAP, is present in the sample. The best linearity, sensitivity, and reproducibility are obtained when the concentration ratio of the electrolyte/analyte is maintained near a value, which produces a maximum enhancement of the analyte signal.

To apply this method to analysis of unknowns, a calibration curve for the analyte standard has to be obtained without the electrolyte, to identify the nonlinear region of the curve. The electrolyte can then be added to a series of standard solutions to obtain the optimum ratio of the analyte/electrolyte, for a maximum response. The optimized ratio can be used to construct a calibration curve and can be used in standard addition experiments. Although this procedure is complicated, as compared to the typical standard addition method, and requires that the differences in the composition between the sample solution and standard solutions have no effect on the optimum ratio of the electrolyte/analyte, it provides a way to significantly enhance the analyte signal and linearity of response at low concentrations.

In constructing the FB/LC/MS calibration curves, the signal that was obtained in the first injection was significantly higher than the signals that were obtained in subsequent injections at the same concentrations. Because of the high reproducibility that was achieved in consecutive injections, it is not likely that the higher signal in the first injection was due to poor reproducibility of the method. In constructing the calibration curves, four consecutive injections were made at each concentration. The results from the first injection were not used in the calculations of precision.

Effect of Different Electrolyte Additives on TPA Signal

Table 4-2 summarizes the EF values, which were defined as the ion abundance ratio of ions at m/z 245 (EI) or 246 (PCI) in the presence and absence of different electrolytes and other compounds. The comparison of the values in Table 4-2 indicates that the electrolyte cation and anion have an effect on the value of the EF. For example, with TBA cation, only ClO_4 but not Br, I or BF_4 induce a significant enhancement of TPA signal. As shown in Table 4-2, in the presence of ClO_4 change of a cation from $(C_4H_9)_4N$ to $(C_2H_5)_4N$ or Na causes a decrease in the EF value.

The electrolyte cation and anion can control aggregate formation and can determine the interactions within and between the aggregate particles, which, accordingly, determine the properties of the aggregates. The EF values reflect the combined contributions of the cation and anion to these properties. For example, $(C_5H_{11})_4N^+$ cation produces a small signal increase when Br^- is the anion. However when Br^- is the anion, $(C_3H_7)_4N^+$ gives rise to a more significant signal enhancement. The relatively small values of the EF for TPA^+ signal in the presence of $(C_2H_5)_4N\ ClO_4^-$ (TEAP) and $NaClO_4$ are in agreement with the overall efficiency of conversion of solution ions into the gas phase ions which follows the order $(C_4H_9)_4N^+ > (C_2H_5)_4N^+ >$ alkali metal cation [Kebarle and Tang 1993, Bond et al. 1995]. The absence of TPA signal enhancement in the presence of $NaClO_4$ likely suggests the importance of the hydrophobic interactions as well as the cation size to signal enhancement.

Effect of Neutral Additives

Neutral compounds $(C_6H_5)_3CH$, $(C_6H_5CH_2)_3N$, $(C_4H_9)_3N$ and $(HOC_2H_5)_3N$ which are structurally related to TBAP were also tested (Table 4-2) to verify the role of the hydrophobic interactions of the added compounds with TPA in TPA signal enhancement. Phenyl groups of $(C_6H_5)_3CH$ and $(C_6H_5CH_2)_3N$ facilitate intermolecular hydrophobic and pi-pi interactions with TPA. The results in Table 4-2 demonstrate that $(C_6H_5)_3CH$ and $(C_6H_5CH_2)_3N$ produce greater signal enhancement than $(C_4H_9)_3N$ and $(HOC_2H_5)_3N$.

The results in Table 4-2 also show that the neutral additives enhance TPA signal less than the electrolytes such as TBAP and TEAP. Therefore electrolytes are advantageous as additives, because they allow larger signal enhancement than is possible when the analyte or analyte analogues are used. The observation that the EF with neutral compounds is smaller than with electrolytes indicates that the charge may be important in determining the intermolecular interactions and may aid in the signal enhancement [Bellar et al. 1994]. Electrolyte charge can reduce undesired spontaneous electrostatic charging of aerosol drops during sample nebulization [Wilkes et al 1995(a) and (b)] Another function of charge may be to limit aggregate mass As shown in Figure 4-1 the maximum enhancement factor for TPA signal is observed when TBAP/TPA concentration ratio is ca. 10/1 In TPA-TBAP aggregates, the size of the aggregates is determined not only by the size of the tetrabutyl group, but also by the electrostatic interactions (charge-charge repulsions and attractions) between TBA$^+$ and ClO_4^- ions, and by the ion-dipole interactions between the electrolyte ion and the analyte

Effect of TBAP on Signals of Different Analytes

To further exploit signal enhancement owing to the use of electrolyte additives the enhancement factor for different analytes that are structurally related to TPA was examined in the presence of TBAP electrolyte (Table 4-3) As can be seen from Table 4-3 the EF for $(C_6H_5)_3CH$ in the presence of TBAP in both EI and PCI mode is close to that for TPA and is much bigger than the EF for $(C_6H_5CH_2)_3N$ This is consistant with different interactions between the analytes and the TBAP

TPA and $(C_6H_5)_3CH$ are structurally similar except for the central atom. Their steric and hydrophobic interactions with TBAP can be expected to be similar In addition, the molecular size and mass of $(C_6H_5)_3CH$ is similar to that of TPA On the other hand, $(C_6H_5CH_2)_3N$ structure is significantly different from TPA, because of the CH_2 spacer between the benzyl groups and the central N Consequently the structure of $(C_6H_5CH_2)_3N$ is not as rigid as that of TPA, which may lead to different interactions with TBAP The molecular size and mass of $(C_6H_5CH_2)_3N$ is also higher than that of TPA. Based on the above results, it can be expected that the aggregate formation between $(C_6H_5)_3CH$ and TBAP is similar to that of TPA/TBAP while different from that of $(C_6H_5CH_2)_3N$/TBAP in terms of size and mass As a result, as shown by Table 4-3, the EF in the presence of TBAP is similar for $(C_6H_5)_3CH$ and TPA, and is much smaller for $(C_6H_5CH_2)_3N$

Effect of Ionization Mode on Signal Enhancement

Table 4-2 and 4-3 list signal EF values that were determined from EI and PCI mass spectra. The EF values are generally higher in EI than PCI ionization. This confirms that both mass transport and reduced analyte fragmentation in the EI ion source contribute to signal enhancement in PB/MS in the presence of carriers. The contribution to signal enhancement from reduced fragmentation of the analyte, or its softer ionization, are limited in PCI ionization. Consequently, only the contributions from improved mass transport can be observed in PCI. As a result, smaller EF values are determined in PCI than EI. Since the EF values from the PCI and EI ionization are close, it can be inferred that the contribution of the reduced fragmentation of analyte molecular ion (softer ionization) to the observed signal enhancement must be less significant than the improved mass transport.

Conclusions

The presence of TBAP in the sample produces a significant enhancement of the $TPA^{+•}$ ion signal in PB/LC/MS. The mass spectral analysis indicates that the EI fragmentation of TPA is influenced by the presence of TBAP. The enhancement of TPA^{+} signal is a result of improved mass transport efficiency of TPA through the PB/LC interface and less extensive fragmentation of TPA during the EI ionization. An enhancement of MS ion signal has been observed for other compounds in the presence of TBAP. The highest sensitivity is obtained in the TPA calibrations when TBAP/TPA concentration ratio is maintained at a value, which produces a maximum signal enhancement. The TPA calibration curves constructed under these conditions show good linearity, high sensitivity, and good reproducibility over a wider range of TPA concentrations.

Comparison of TPA signal enhancement in the presence of different electrolytes and neutral compounds shows that neutral compounds produce lower signal enhancement than the electrolytes that were studied. This may suggest a role of ionic charge in facilitate aggregate formation, which affects signal enhancement and is consistent with the observations that both electrolyte cation and anion affect the magnitude of the signal enhancement. The importance of the hydrophobic interactions is indicated from studies with different analytes, with TBAP as the electrolyte. However, the present results do not allow a generalization about the properties that are most significant to the signal enhancement in FB/MS.

Table 4-1 Absolute and relative ion abundances of major fragment ions of TPA (1×10^{-3} M) in the presence and absence of TBAP (0.01 M)

m/z	Ion identity	TPA		TPA-TBAP	
		Absolute ion abundance ($\times10^{4}$)	Relative ion abundance	Absolute ion abundance ($\times10^{6}$)	Relative ion abundance
245	$(C_6H_5)_3N^{\bullet+}$	7.6	1	2.7	1
244	$(C_6H_5)_2N^+(C_6H_4)$	2.5	0.33	1.1	0.43
167	$(C_6H_5)N^+(C_6H_4)$	1.8	0.24	0.8	0.32
166	$(C_6H_5)N^+(C_6H_3)$	3.6	0.47	0.7	0.26
142	$(C_4H_3)N^+(C_6H_5)$	1.0	0.13	9.7	3.59[a]
141	$(C_4H_2)N^+(C_6H_5)$	1.9	0.25	0.6	0.22
77	$(C_6H_5^+)$	6.3	0.83	1.4	0.52
51	$(C_4H_3^+)$	13.2	1.74	4.2	1.55[b]

[a] From the uncorrected absolute ion abundance values. The ion abundance at m/z 142 in 1×10^{-3} M TPA-0.01 M TBAP and 0.01 M TBAP is 9.7×10^{6} and 10.1×10^{6} respectively.

[b] From the corrected absolute ion abundance values. The correction was made by subtraction of m/z 51 ion abundance in 0.01 M TBAP from that in 1×10^{-3} M TPA-0.01 M TBAP.

Table 4-2 EF of TPA molecular ion in EI and PCI ionization mode in the presence of different electrolyte and neutral compounds [a]

Additive	EF	
	EI[b]	PCI[c]
$(C_4H_9)_4N^+ClO_4^-$	43	36
$(C_2H_5)_4N^+ClO_4^-$	14.0	9.1
$Na^+ClO_4^-$	0.85	0.32
$(C_4H_9)_4N^+(BF_4)^-$	2.0	2.3
$(C_4H_9)_4N^+I^-$	2.9	4.0
$(C_4H_9)_4N^+Br^-$	4.5	3.4
$(C_3H_7)_4N^+Br^-$	23	18
$(C_2H_5)_4N^+Br$	2.9	2.2
$(C_6H_5)_3CH$	6.7	4.6
$(C_6H_5CH_2)_3N$	7.5	4.4
$(C_4H_9)_3N$	0.93	1.0
$(HOC_2H_4)_3N$	0.19	0.12

[a] 1 × 10^{-4} M TPA, 1 × 10^{-3} M compound added in acetonitrile. Acetonitrile mobile phase 0.4 ml/min, scan 50-550 Da. Source 250 °C

[b] 70 eV. m/z 245 as quantitative ion in the calculation of EF

[c] methane as reagent gas (1.3 torr). m/z 246 as quantitative ion in the calculation of EF

Table 4-3 EF with TBAP for different analytes [a]

Analyte (MW)	EF	
	EI	PCI
$(C_6H_5)_3N$ (245)	43	36
$(C_6H_5)_3CH$ (244)	31	27
$(C_6H_5CH_2)_3N$ (288)	4.3	4.7

[a] 1×10^{-4} M analyte, 1×10^{-3} M TBAP in acetonitrile. Conditions as Table 4-1

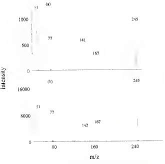

Figure 4-1 EI mass spectra of TPA (a) no TBAP (b) with 0.01 M TBAP Spectrum (a) was obtained from 1×10^{-3} M TPA in acetonitrile. spectrum (b) was derived by subtracting the EI spectrum of 0.01 M TBAP in acetonitrile from that of 1×10^{-3} M TPA/0.01 M TBAP in acetonitrile Conditions injection volume 20 µL, mobile phase acetonitrile, flow rate 0.4 ml/min EI 70 eV source 250 °C

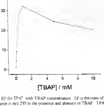

Figure 4-2 Change of EF for TPA^+ with TBAP concentration. EF is the ratio of TPA^+ ion abundance at m/z 245 in the presence and absence of TBAP. TPA concentration was fixed at 1×10^{-5} M. Scan mode, 50~550 Da. Other conditions as in Figure 4-1

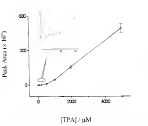

Figure 4-3 Calibration curve of TPA (SIM, 245) in the absence of TBAP. Triplicate injections. Other conditions as Figure 4-1

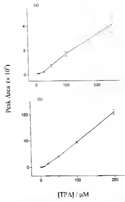

Figure 4-4 Calibration curve of TPA (SIM, 245) in the presence of TBAP (a) 1×10^{-3} M TPA (b) [TBAP]/[TPA] = 10/1 Other conditions as Figure 4-1

CHAPTER 5
ENHANCEMENT OF THE IONIZATION EFFICIENCY BY ELECTROCHEMICAL REACTION PRODUCTS IN ELECTROCHEMISTRY/ELECTROSPRAY FOURIER TRANSFORM ION CYCLOTRON RESONANCE MASS SPECTROMETRY

Introduction

In most recent developments in EC/MS several research groups have reported the use of an electrospray ionization (ESI) interface for coupling of electrochemistry to mass spectrometry [Bond et al. 1995, Xu et al. 1996, Zhou and Van Berkel 1995, Arakawa et al. 1999, Jurva et al. 2000, Johnson et al. 2001]. ESI operates at atmospheric pressure, involves little heating and has no volatility requirement for the analytes. Multiply charged ions can be readily generated in ESI-MS. Therefore, ESI-MS is often a method of choice for analyzing polar, nonvolatile and thermally labile compounds. Unique problems encountered in coupling of an EC cell to the ES ion source include high voltage hazard from the use of high voltage in ESI-MS and possible interference with the EC cell voltage. Signal suppression from electrolytes in ESI-MS is another problem that has to be considered in the development of new EC/ESI/MS methods. As introduced in Chapter 1, surface-active electrolytes such as tetrabutylammonium perchlorate (TBAP) and tetrabutylammonium hexafluorophosphate (Bu_4NPF_6) are commonly used in organic electrochemistry, but they can suppress analyte signal in ESI-MS [Tang and Kebarle 1993, Fenn 1993]. The successful and practical use of electrolytes for EC/ESI-MS in nonaqueous systems has been limited to less surface active lithium triflate ($LiCF_3SO_3$) [Arakawa et al. 1999, Bond et al. 1995, Xu et al. 1996, Zhou and Van Berkel 1995].

In Chapter 3, EC/MS with PB liquid interface was used to investigate the anodic oxidation of triphenylamine (TPA). In EC/PB/MS, a molecular ion, $\mathrm{TPA}^{\bullet +}$, at m/z 245 and an ion at m/z 244 were detected. While the ion at m/z 245 was easily assigned to the $\mathrm{TPA}^{\bullet +}$ radical cation, the identity of the ion at m/z 244 was more ambiguous. The m/z 244 ion could be detected as a result of a loss of a hydrogen atom from the $\mathrm{TPA}^{\bullet +}$ radical cation of m/z 245 or may be due to the formation of a dication of tetraphenylbenzidine (TPB), TPB^{2+}, which is an EC reaction product from the initial oxidation of TPA.

The goal of this work was three-fold. The first aim was to design an EC cell to allow the distinction of the effect of the reactions occurring in the EC cell from the electrolytic ESI process without changing the ESI-MS conditions. The second aim was to exploit the high mass resolving power of FTICR MS, to resolve the problems arising from interfering species in EC/ESI-MS. The third aim was to examine the possibility to overcome the signal suppression problem from surface active electrolytes in EC/ESI-MS.

The EC cell that has been designed was shown as Figure 2-2 in Chapter 2, and the use of EC/ESI-FTICR MS is described in that Chapter. The EC/ESI-FTICR MS results have revealed two identities of the m/z 244 ion that were due to TPB^{2+} dications when the EC cell voltage was applied in the oxidation of TPA, and to $[\mathrm{TPA}^{\bullet +}\text{-}\mathrm{H}^{+}]^{+}$ ions in the absence of the EC cell voltage. The two types of ions were distinguished by their m/z values and the relative abundances of their isotopic ions as determined by FTICR MS. In addition, TPB^{2+} was distinguished from the second harmonic signal of the $\mathrm{TPB}^{\bullet +}$ ion at the same frequency in separate experiments in which selective ion ejection from the ICR cell was employed. The present work demonstrates that the signal suppression problem by TBAP electrolyte in ESI-MS can be reduced in EC/ESI-MS. The EC/ESI-FTICR MS results also point to an uneven distribution of interfacial potentials along the axial position of the ES needle that has been predicted by Van Berkel and coworkers [1999] by computer simulations of the ESI process The present work demonstrates the advantages of coupling of an EC cell to ESI-MS for enhancement of the sensitivity in ESI-MS signal detection The processes that lead to the formation of transient radicals and dications during the oxidation of TPA are verified by EC/ESI-FTICR MS

Results and Discussion

EC Cell.

The design and construction of the EC cell for EC/ESI-FTICR MS experiments has been described in Chapter 2 One advantage of the EC cell design is that it allows testing of different electrode configurations under the same MS conditions For example, for a fast MS response the ES needle ss(1) and ss(2) can be used as the working and counter electrode respectively In this cell operation, the EC cell voltage is floated at the high ES spray voltage (Figure 2-5 of Chapter 2) The EC cell voltage can also be isolated from the high ES voltage by using ss(2) as the working electrode and ss(3) as the counter electrode The comparison of the results from the use of different electrode configurations, with the cell voltage isolated from or floated at the high ES voltage, may permit determination of the effect of EC cell voltage on the ESI process

ESI and EC/ESI-MS of TPA

Figure 5-1a shows an ESI-FTICR MS mass spectrum of TPA The m/z 245 412 and 488 ions are due to $TPA^{\bullet+}$ $[TPA+(TPA-C_6H_4)]^{\bullet+}$ and $TPB^{\bullet+}$ respectively The ion assignments are confirmed by the isotope distributions and the abundance ratios of the isotopic M and (M+1) ions illustrated in Table 5-1 These ions form during the ESI of neutral TPA by electrolytic ESI processes [Blades et al. 1991 Van Berkel and Zhou 1995(a) and (b)] which favor oxidation of compounds with low oxidation potentials. The high $TPA^{\bullet+}$ signal relative to $TPB^{\bullet+}$ signal confirms fast formation of $TPA^{\bullet+}$ in ESI MS

Figure 5-1b shows the EC/ESI-MS mass spectrum after the EC cell voltage is applied with ss(1) and ss(2) as the electrodes with the oxidation occurring at the ss(1) electrode As can be seen from the results in Figure 5-1a and b a significant enhancement of the $TPB^{\bullet+}$ ion signal is observed relative to the $TPA^{\bullet+}$ ion signal after the EC cell voltage is applied The oxidation of TPA occurs in the EC cell and the TPB dimer is the product of the electrochemical oxidation of TPA [Zhang and Brajter-Toth 2000 Seo et al 1966] The dimer yield is affected by flow rate, as discussed below

The EC/ESI-MS and ESI-MS results, which shows enhancement of TPA oxidation after application of the EC cell voltage support previous predictions, from computer simulations, of a decrease in the ES interfacial potential along the ES needle [Van Berkel et al 1999], which is consistent with lower oxidation efficiency in the ES needle in the absence of the applied EC cell voltage In ESI-MS therefore the formation of $TPA^{\bullet+}$ is limited to the ES tip which limits dimer formation

Ion Assignments

The insets of Figure 5-1a and b show formation of m/z 244 09 ions in ESI-MS and EC/ESI-MS An isotopic ion at m/z 244 59 is only observed in the EC/ESI-FTICR MS mass spectrum (Figure 5-1b inset) The half integral m/z separation that is observed between the isotopic ions strongly suggests that a doubly charged TPB^{2+} ion forms in EC/ESI-MS [Zhang and Brajter-Toth 2000] As shown in Table 5-1 the abundance ratio of the isotopic ions of 36 6% matches closely that calculated for the 244 09 and 244 59 ions of TPB^{2+} from the known isotopic abundances The final assignment of the 244 09 and 244 59 ions was made after the harmonic ion contribution was excluded, as described below

The m/z 244 09 ion, which is detected without the isotopic 244 59 ion when the EC cell voltage is not applied in ESI-MS (Figure 5-1a, inset), was assigned to $[TPA^{\bullet+}-H^{\bullet}]^{+}$ The isotopic (M+1) ion of $[TPA^{\bullet+}-H^{\bullet}]^{+}$ has the same m/z as $TPA^{\bullet+}$ (m/z 245 10) The presence of the (M+1) ion of $[TPA^{\bullet+}-H^{\bullet}]^{+}$ is not apparent from the (M+1)/M ratio because of interferences

Harmonic signals can be detected in FTICR MS at multiples of the fundamental ICR frequencies [Grosshans and Marshall 1991 Limbach et al 1991] This can interfere with the proper assignments of multiply charged ions because the harmonic signals and those of multiply charged ions have the same isotopic distributions For example, when the m/z 488 15 $TPB^{\bullet+}$ ion was detected by EC/ESI-FTICR MS the third harmonic signal at m/z 162 75 and 163 09 was detected As a result, the assignment of TPB^{3+} ions required further verification

Selective ion ejection from the ICR cell of ions of a particular m/z can eliminate the associated harmonic signals [Grosshans and Marshall 1991 Limbach et al 1991] $TPB^{\bullet+}$ was expected to be present in the ICR cell, because the signal of this ion is enhanced in EC/ESI-FTICR MS To determine if the peaks at m/z 244 09 and 244 59 ions were due to the second harmonic signal of $TPB^{\bullet+}$ m/z 488 15 ions were ejected from the ICR cell The results are shown in Figure 5-2 As can be seen from Figure 5-2, after the ejection of the ions at m/z 488 15, the signals at m/z 488 15, 162 75, and 163 09 disappeared, as expected for TPB$^{\bullet+}$ generated signals. At the same time, the m/z 244.09 and 244.59 ions maintained their intensity, which verified formation of TPB$^{\bullet+}$.

Ion Formation in the EC Cell

The change of ion intensities of TPA$^{\bullet+}$, TPB$^{\bullet+}$, TPB^{2+} and the corresponding isotopic intensity ratios with time after EC cell voltage was applied is shown in Figure 5-3. As can be seen from Figure 5-3a, after the EC cell voltage is applied to the ss(1) and ss(2) electrodes, oxidation at the ss(1) electrode leads to an increase in TPA$^{\bullet+}$ signal first, which then decreases while the signal of TPB$^{\bullet+}$ increases. The steady state signals are reached rapidly. When the EC cell voltage is disconnected the signals return to their background level. An increase of the m/z 244.09 TPB^{2+} ion signal is also observed after the EC cell voltage is applied (Figure 5-3a); the steady state signal of this ion is reached more slowly. The results show that the oxidation of TPA and formation of TPB$^{\bullet+}$ in the EC cell is rapid after the EC cell voltage is applied, while TPB^{2+} formation is slow. The slow oxidation of TPB$^{\bullet+}$ to TPB^{2+} has been reported previously [Seo et al. 1966; Nelson and Philp 1979; Oyama et al. 1991; Sumiyoshi 1995].

The slow increase of the m/z 244.09 ion signal after the EC cell voltage is applied can be a result of the formation of TPB^{2+} or can result from a slow formation of $[\mathrm{TPA}^{\bullet+}-\mathrm{H}^{+}]^{\bullet}$, since both ions have the same m/z. The close value of the isotopic ratio of m/z 244.59/244.09 and the TPB$^{\bullet+}$ m/z 489.14/488.15 ions shown in Figure 5-3b, which can be expected to be similar, indicates that the m/z 244.09 ion is due to TPB^{2+}. The small initial value of the ratio shown in Figure 5-3b indicates that $[\mathrm{TPA}^{\bullet+}-\mathrm{H}^{+}]^{\bullet}$ ions initially contribute to the signal at m/z 244.09. The $[\mathrm{TPA}^{\bullet+}-\mathrm{H}^{+}]^{\bullet}$ ion isotopic signal is at m/z of 245.10, thus ion is not monitored in Figure 5-3b ratio.

Protonation of TPA in EC/ESI-MS

The increase of the m/z 246.11/245.10 ion ratio with time after the EC cell voltage is applied shown in Figure 5-3b is consistent with the protonation of TPA to $[TPA+H^+]^+$ (m/z 246.11). The $[TPA+H^+]^+$ ions are observed when the ES needle functions as the ss(1) working electrode in the ss(1)/ss(2) on-line EC cell (Figure 5-3b). The results in Table 5-1 verify that the formation of the $[TPA+H^+]^+$ ions is not significant in ESI-MS in the absence of the EC cell voltage, as indicated by the intensity ratio of m/z 246.11 to 245.10 ions in ESI-MS of 23.0%, which is close to that expected from TPA isotopic abundance ratio (20.7%). The m/z 246.11 to 245.10 ion ratio increases to 31.1% in EC/ESI-MS, supporting formation of $[TPA+H^+]$ when the EC cell voltage is applied.

In a stable ES process, based on charge balance considerations, the ES current at the ES metal/solution interface has to be equal in magnitude to the faradic electrolysis current [Blades et al. 1991, Van Berkel and Zhou 1995(a) and (b)]. The actual redox reactions during the electrolysis and the extent to which they occur during the ES ionization are determined by the redox potentials and the relative concentrations of species, which can include capillary metal, analytes, water and the solution impurities [Van Berkel and Zhou 1995(b)]. It is possible that after the EC cell voltage is applied the increase in ESI current is a result of higher ion concentrations because of the electrochemical reactions in the on-line EC cell. The higher ESI current can lead to water oxidation present in acetonitrile (at least 4-10 mM [Majeski et al. 1968]), decreasing the pH [Van Berkel et al. 1997].

The basicity of an aromatic amine depends on the availability of the lone pair of electrons on N for protonation. The availability of the lone pair is reduced by resonance stabilization, which arises due to the interactions of the lone pair of electrons with the delocalized π orbitals of the aromatic ring [Barton and Ollis 1979]. As a result, aromatic amines are weak bases when compared with ammonia or aliphatic amines. For example aniline has a pK_a of 4.58. TPA has even greater opportunity for resonance stabilization. As a result, TPA cannot be considered as basic [Barton and Ollis 1979].

However, water oxidation in EC/ESI-MS, with the oxidation occurring at the ss(1) ES capillary working electrode in the ss(1) –ss(2) EC cell configuration, may cause a decrease in solution pH, which facilitates the protonation of TPA in EC/ESI-MS. Possibly as a result of the larger current more stable ES current is observed when the EC cell voltage is applied. The intensity ratio of m/z 246.11 to 245.10 ion in ESI-MS is close to the expected isotopic abundance ratio of TPA, indicating that the oxidation of water is limited in ESI-MS without the EC cell voltage.

EC/ESI-MS with the ss(2) - ss(3) Electrodes

The ss(2) – ss(3) EC cell configuration was tested in EC/ESI-MS, with ss(2) and ss(3) as the working and counter electrode, respectively (refer to Figure 2-5, Chapter 2). In this configuration, the EC cell voltage is isolated from the ESI voltage by the PEEK cross. The changes in ion signals of $TPA^{\bullet+}$, $TPB^{\bullet+}$ and TPB^{2+} ions in this electrode configuration (Figure 5-3c and d) are similar to the changes in ion signals that were detected with ES ss(1) as the working electrode where the oxidation occurred (Figure 5-3a and b). Detection of the ions that are formed is slower (ca. 2.5 min) with the ss(2) ss(3) EC cell because of the greater distance of the EC cell to the ESI ion source. No obvious protonation of TPA was observed during use of the ss(2) - ss(3) EC cell configuration as evidenced by the constant intensity ratio of m/z 246.11 vs 245.10 ions (~

23 0%) in Figure 5-3d, which is consistent with lower ESI currents in this electrode configuration

Effect of Flow Rate

Figure 5-4 shows the effect of flow rate on the relative signal intensities of $TPA^{+\bullet}$, $TPB^{+\bullet}$ and TPB^{2+} ions The results in Figure 5-4 show that the detection sensitivity can be improved by optimizing the flow rate For example, in EC/ESI-MS (open symbols) at higher flow rates, above 100 µL/h, the $TPA^{+\bullet}$ ion signal is high At flow rates between 75 and 150 µL/h, the $TPB^{+\bullet}$ ion signal is high This signal is significantly higher in EC/ESI-MS than in ESI-MS TPB^{2+} signal can be detected in EC/ESI-MS at low flow rates below 45 µL/h

In addition, it is interesting to note that at very low flow rates, new ions at m/z 487 14 486 13 485 12, and 484 12 were observed, as shown in Figure 5-5 The ion at m/z 487 14 can be attributed to a loss of H from the $TPB^{+\bullet}$ ion at m/z 488 15 The ions at m/z 486 13 485 12, and 484 12 may be due to a repetitive loss of either H or H_2 from the ion at m/z 487 14 or 488 15 No attempt has been made to further identify the mechanism of this hydrogen loss The loss of hydrogen from the cations in the gas phase has been previously reported [Guo and Sievers 1999]

Limited Signal Suppression by TBAP in EC/ESI-FTICR MS

Electrolytes are required in the electrochemical experiments to sustain the EC cell current but their presence can contribute to the suppression of the ESI-MS signal of analytes of interest [Bond et al 1995, Xu et al 1996 Tang and Kebarle 1993, Kebarle and Tang 1993 Fenn 1993] In the presence of electrolytes such as TBAP and Bu_4NPF_6, analyte signal suppression is a result of a competitive emission of the electrolyte ions in the presence of the analyte ions TBAP and Bu_4NPF_6 are surface-active electrolytes and formation of their ions is efficient in ESI even at low electrolyte concentrations [Xu, et al 1996 Bond et al 1995] Lithium triflate, which is less surface active than TBAP and Bu_4NPF_6, has been found to cause minimal signal suppression in EC/ESI-MS [Xu et al 1996 Bond et al 1995 Lu et al 1997 Zhou and Van Berkel 1995 Arakawa et al 1999] In order to enhance electrolysis efficiency in EC/ESI-MS in the presence of Bu_4NPF_6, off-line bulk electrolysis was investigated by Bond and coworkers [1995] With an EC cell which was operated at ~200 V the electrochemical reaction products were detected in the presence of Bu_4NPF_6 Fused silica ES capillary was used in these experiments

When a stainless steel ES capillary is used in ESI MS TBA^+ electrolyte signal is also observed, and the analyte signal of TPA is not detected (Figure 5-6a) After the EC cell voltage is applied $TPA^{\bullet+}$ and $TPB^{\bullet+}$ signal can be detected and the electrolyte signal (of TBA^+) decreases (Figure 5-6b) Similar results are observed in the ss(1) and ss(2) and the ss(2) and ss(3) EC cell configurations (Figure 5-6c)

The results in Figure 5-5 indicate that in the new EC/ESI-MS cell design the apparent high efficiency of ion formation contributes to the high MS sensitivity and this can limit the analyte signal suppression by TBAP electrolyte As a result the EC/ESI-MS results with TBAP and lithium triflate are similar (Figure 5-4 and 5-5) The EC cell configuration with the ES stainless steel needle ss(1) as the working electrode (Figure 5-5 b) produces the highest MS sensitivity

Conclusions

A new EC cell was designed and coupled to an ESI-FTICR MS The high mass resolving power and ion ejection capability of FTICR MS revealed different identities of the m/z 244 ions in the oxidation of TPA, i e TPB^{2+} with cell-on and $[TPA^{\bullet+} H^{+}]^{+}$ with cell-off The results show that the coupling of the new EC cell to the ESI FTICR MS can significantly enhance the ion signals of $TPA^{\bullet+}$ $TPB^{\bullet+}$ and TPB^{2+} The results indicate that the electrochemical generation of $TPB^{\bullet+}$ ons is fast while the oxidation of $TPB^{\bullet+}$ to TPB^{2+} is slow The results also suggest that in ESI-MS the oxidation of TPA may be confined to the ES tip which results in an uneven voltage distribution along the ES capillary in the absence of the applied EC cell voltage The occurrence of protonation of TPA in EC/ESI MS in the ss(1) ss(2) cell configuration with the ES needle as the working electrode has also been observed This has been interpreted as due to water oxidation, which decreased the solution pH as a result of the increased ES current after the EC cell voltage is applied Together the ESI-MS and EC/ESI-MS results provide the experimental evidence for the uneven distribution of the interfacial potentials along the ES needle in ESI-MS

It is shown that the relative signal enhancement of $TPA^{\bullet+}$ $TPB^{\bullet+}$ and TPB^{2+} ions depends on flow rate The increased EC reaction time at low flow rates produces more TPB^{2+} ions, and the detection of a loss of up to four hydrogen atoms from $TPB^{\bullet+}$ ions is observed The comparison of the results from different EC cell configurations shows that the use of the ES needle as working electrode in ss(1) – ss(2) EC cell configuration is advantageous in terms of fast response and high MS sensitivity It is demonstrated that the signal suppression problem from TBAP electrolyte can be alleviated in EC/ESI-MS at low EC cell voltage (i e several volts) The cell configuration that employs the ES needle as working electrode is again found to be advantageous for this purpose. This finding is of significance to the future development and applications of EC/ESI-MS

Table 5-1 Calculated and measured m/z values for the proposed ions and corresponding isotopic distributions

Ion identity	Calculation			Measured			
	m/z		Isotopic ratio %	m/z		Isotopic ratio %	
	M	M+1	(M+1)/M	M	M+1	(M+1)/M ESI	(M+1)/M EC/ESI[a]
$[TPA-H]^+$	244.11	245.12	20.6	244.09	245.10	1500[b]	450[b]
TPB^{2+}	244.11	244.61	41.2	244.09	244.59	nd[c]	36.6
$TPB^{\bullet+}$	488.22	489.23	41.2	488.15	489.14	38.6	38.6
$TPA^{\bullet+}$	245.12	246.12	20.7	245.10	246.11	23.0	31.1
$(TPB-C_6H_4)^{\bullet+}$	412.19	413.20	34.4	412.14	413.15	33.0	33.4
TBA^{+}	242.28	243.29	18.7	242.26	243.28	17.5	16.9

[a] EC cell on, with the nd(1) – ss(2) configuration as shown in Figure 1

[b] unreasonably high value due to spectral overlap of the peaks due to isotopic (M+1) ion of $[TPA^{\bullet+} - H^+]^+$ and $TPA^{\bullet+}$ at m/z 245.10

nd = not detected

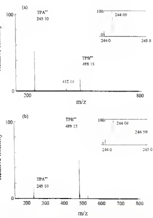

Figure 5-1 ESI (a) and EC/ESI (b) mass spectra of TPA 1 × 10^{-4} M TPA and 2 × 10^{-4} M lithium triflate in acetonitrile Continuous flow at 75 µL/h, ES voltage 3 3 kV, scan range 150 – 800 amu, 20 scans EC/ESI-MS EC cell voltage 7 5 V, ss(1) – ss(2) configuration

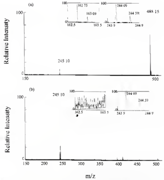

Figure 5-2 EC/ESI MS spectra of TPA. (a) before ejection of m/z 488 ion, (b) after ejection of m/z 488 ion from the ICR cell. Insets in (a) show the presence of ions at m/z 162.75 and 163.09, m/z 244.09 and 244.59 before the ion injection. Insets in (b) show the disappearance of ions at m/z 162.75 and 163.09 (only background noise was shown). The ions at m/z 244.09 and 244.59 are still observed.

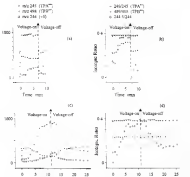

Figure 5-3 EC/ESI-MS ion intensities (a, c) and isotopic intensity ratios (b, d) as a function of time. Cell configuration: ss(1) - ss(2) for (a) and (b), ss(2) - ss(3) for (c) and (d). Other conditions as Figure 5-1.

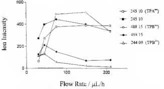

Figure 5-4 Effect of flow rate on ESI-MS (solid) and EC/ESI-MS (open) $TPA^{\bullet+}$ (square), $TPB^{\bullet+}$ (circle) and TPB^{2+} (triangle) ion intensities. EC/ESI-MS data were collected at ~5 min after the EC cell voltage was applied. Other conditions as Figure 5.1

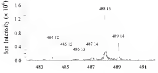

Figure 5-5 Loss of hydrogen atoms from $TPB^{\bullet+}$ in EC/ESI-MS at a flow rate of 30 µL/h Bruker XMASS intensity scale. Other conditions as Figure 5-3

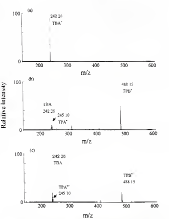

Figure 5-6 ESI-MS (a) and EC/ESI-MS (b, c) mass spectra of TPA in the presence of TBAP electrolyte (a) ESI (b) ss(1) – ss(2) (c) ss(2) - ss(3) Spray voltage 3.0 kV, scan range 150-800 amu, 5 scans Other conditions as Figure 5-1

CHAPTER 6
EXPERIMENTAL FACTORS CONTROLLING DETECTION SENSITIVITY IN THE OXIDATION OF TRIPHENYLAMINE BY ON-LINE EC/ESI-FTICR MS

Introduction

Electrospray ionization (ESI) is electrochemical in nature [Blades et al. 1991; Van Berkel and Zhou 1995(a) and (b)] and, as a result, the ions detected in ESI-MS, which result from the ionization of neutral compounds, can form during the ESI electrochemical processes. In Chapter 5, it has been demonstrated that the oxidation of triphenylamine (TPA) to $TPA^{\bullet+}$ can occur during the ESI, which is accompanied by the generation of a tetraphenylbenzidine (TPB) monocation, $TPB^{\bullet+}$, of low relative intensity. By coupling an EC cell to ESI-MS, the detection sensitivity for TPB radical monocation is significantly increased, indicating increased formation of the TPB dimer product in the EC flow cell.

In on-line EC/ESI-MS, the detection sensitivity for the electrochemical reaction products is determined by the efficiency of ion generation in the EC cell and the efficiency of the ESI process in ESI-MS, and the MS detection sensitivity. The major parameters that affect ion formation efficiency in the EC cell include working electrode area, EC cell voltage and cell configuration, and analyte concentration. The controlling ESI parameters include ES voltage, ES-counter capillary distance and voltage, ES needle dimensions, and electrolyte concentration and flow rate.

As introduced in Chapter 2, the ES voltage, ES needle dimension and the ES tip-counter capillary distance affect the electric field in ESI [Eq. (2.5) of Chapter 2]. The electrolyte concentration affects solution conductivity, and the solution flow rate affects the mass input to the MS ion source. The electric field, solution conductivity and the solution flow rate determine directly the ES current produced in the ESI process [Tang and Kebarle 1993, Ikonomou et al. 1991], which can be described as,

$$i_{ES} = H V_f^{\,v} \sigma_S^{\,n} E_{ES}^{\,e} \quad \{\sigma_S = \lambda_m^{\circ} C_E\} \qquad (6.1)$$

where H is a constant, which depends on the dielectric constant and surface tension of the solvent. V_f is the volumetric flow rate, σ_S is the solution conductivity, E_{ES} is the imposed electric field at the ES tip. The value of the σ_S can be expressed in terms of the limiting molar conductivity of the electrolyte, λ_m°, and the concentration of the electrolyte, C_E. The values of the exponents in the equation are estimated to be $v \approx 0.5$, $e \approx 0.5$, and $n \approx 0.2$-0.3 [Tang and Kebarle 1993]. The analyte ion signal detected in ESI-MS is related to the ES current, electrolyte concentration and analyte concentration by Eq. (2.6) of Chapter 2.

Other factors that may affect the detection sensitivity of ESI-MS for the ions formed in the electrochemical flow cell and/or ESI are the secondary gas-phase processes. In the relatively high-pressure region (~2x10^{-4} mbar) between the counter capillary exit and the skimmer (refer to Figure 2-6 in Chapter 2) the counter capillary voltage bias gives the ions emerging from the counter capillary sufficient kinetic energy to undergo gas phase processes such as declustering of the residual solvent molecules. Increasing the bias and thus energizing the ions further can induce fragmentation from collision of the molecular ions with nitrogen/oxygen that is present in air between the exit of the counter capillary and the skimmer, which is a region of relatively high pressure (~2x10^{-4} mbar). This may lead to the formation of ions different from those initially generated from the ESI process.

In this Chapter, the effect of the experimental parameters on the detection sensitivity of the reaction products produced in the on-line electrochemical oxidation of TPA is investigated by EC/ESI-MS. The experimental setup is as shown in Figure 2-5 of Chapter 2. The experimental parameters investigated are grouped into two categories, i.e., ESI parameters and EC-related parameters. The ESI parameters that are investigated include ES voltage, ES needle dimension, ES – counter capillary distance, ES counter capillary voltage, flow rate and electrolyte concentration. In these investigations, EC cell voltage is not applied and TPA is ionized by the ESI processes. The EC-related parameters that are investigated include electrode configurations and electrode area, analyte concentration, and cell voltage. These parameters are investigated when the EC cell voltage is applied. Additionally, the effect of ion accumulation time in the hexapole of the FTICR mass spectrometer on the ion signals generated from ESI is investigated. The selective collision induced dissociation (CID) of TPA molecular ion in the ICR analyzer cell is performed to provide an insight into the gas-phase ion chemistry of TPA TPA ions.

Results and Discussion

ESI Parameters

ES voltage

As shown by Eq. (2.5) (Chapter 2), ES voltage affects the electric field at the ES tip, and therefore, the ES current (Eq. (6.1)). Typically, the ES voltage in ESI-MS is in the range of 2 – 5 kV. The actual ES voltage needed to maintain a stable ES current depends on the needle dimension, flow rate, ES – counter capillary distance, concentrations of electrolyte and analyte. Due to the limited ES voltage range and small value of ∈ exponent (–0.5) in Eq. (6.1), it is expected that the effect of ES voltage on the analyte signal is limited. When a stable ESI process is reached, an increase in ES voltage may cause only a slow increase in ES current and therefore the analyte ion signal.

Figure 6-1 shows the ion signals obtained in ESI ionization of TPA as a function of the ES voltage. The ES needle tested has an i.d. of 200 µm. The distance between the ES tip and counter capillary is 3 mm. The solution flow rate is 75 µl/h. The lithium triflate electrolyte concentration is 2×10^{-4} M and the TPA analyte concentration is 1×10^{-4} M. The ES voltage range investigated is from 3.0 to 4.3 kV. Below 3.0 kV, a stable ES current was not maintained. Above 4.3 kV, corona discharge was observed. As can be seen from Figure 6-1, the effect of the ES voltage on the ion signals of $TPA^{\bullet+}$ at m/z 245 and $TPB^{\bullet+}$ at m/z 488 is small. It should be mentioned that equations 2.5, 6.1 and 2.6 are valid for the transfer of stable ions initially present in solution to the gas phase by ESI. In this work, TPA is a neutral analyte and the situation is further complicated by the follow-up chemical reactions after the ESI oxidation of TPA, which produces TPB, and the subsequent oxidation of TPB to $TPB^{\bullet+}$. In Figure 6-1, a small decrease of $TPB^{\bullet+}$ vs a continuous increase of the ion signal at m/z 244.09 with the increase in ES voltage is observed. The m/z 244.09 ion is due to $[TPA^{\bullet+}-H^{\bullet}]$. This is presumably a result of the increased kinetic energy of $TPA^{\bullet+}$ at higher ES voltages, which may facilitate hydrogen loss and disfavor coupling of $TPA^{\bullet+}$. Besides the hydrogen loss, high ES voltage also facilitates a loss of $C_6H_5^{\bullet}$ or C_6H_6 group from $TPA^{\bullet+}$ or $[TPA^{\bullet+}-H^{\bullet}]$, as shown in Figure

6-2. It should be noted that no hydrogen loss from TPB^{-} was detected as the ES voltage was increased. This is probably because TPB^{-} ion is more energetic and the change in the ES voltage does not cause a substantial energy change to TPB^{-} to induce the hydrogen loss or ion fragmentation.

ES – counter capillary distance

The distance between the ES and the counter capillary (z distance) affects the electric field (Eq. (2.5) of Chapter 2) and therefore the ES current and the analyte ion signal. Figure 6-3 shows the effect of the ES – counter capillary distance on the signals of TPA^{+}, TPB^{-} and [TPA^{+} – H^{+}] ions formed in the ESI-MS of TPA. As shown in Figure 6-3, the optimum z distance for TPA^{+} signal detection is 4-4.5 mm. Shorter z distance (below 4 mm) facilitates loss of hydrogen from TPA^{+} and produces greater [TPA^{+} – H^{+}] signal. The observation of the higher [TPA^{+} – H^{+}] signal at reduced z distance is consistent with a stronger electric field at the ES, with a resulting greater ion energy facilitating hydrogen loss from TPA^{+}.

The results above were obtained with a centered ES needle, which was on-axis with the center of the counter capillary (500 µm i.d.). The ES needle formed a part of the EC cell that was mounted on a X, Y, Z-scaled movable platform. The position of the ES needle was controlled by first placing the needle in contact with and in the center of the counter capillary, then withdrawing it in z direction. The z distance could be read from the z scale of the mounting platform. With the z distance of 3 mm, it was found that the adjustment of the ES needle up off axis (< 1.7 mm) did not cause a significant change in the relative yield of $TPA^{\bullet+}$ ions in ESI-MS. In all subsequent experiments, an on-axis position of the ES needle was used, with a fixed z distance of 3 mm.

Counter capillary voltage

The counter capillary biased at voltage versus ground (Figure 2-6 in Chapter 2) may add kinetic energy to ions in the capillary. The counter capillary voltage accelerates the ions into the skimmer and then to the hexapole. Figure 6-4 shows the signals of TPA ions in ESI-MS as a function of the counter capillary voltage. As shown in Figure 6-4, an initial increase of $TPA^{\bullet+}$ signal is observed at low capillary voltage (0–10 V), presumably due to an increased transport rate of ions with the applied capillary voltage. A plateau is reached at a capillary voltage in the range of 10-25 V. A further increase of the capillary voltage caused a small decrease of $TPA^{\bullet+}$ signal, which corresponds to an increase of $TPB^{\bullet+}$ signal. This indicates that the formation of TPB from $TPA^{\bullet+}$ can occur in the gas phase. A rapid decrease of $TPA^{\bullet+}$ signal seen at capillary voltages from 60 to 80 V is accompanied by a rise of $[TPA - H]^+$ signal at m/z 244.09, which is consistent with the increased fragmentation of $TPA^{\bullet+}$, including through loss of a phenyl group (C_6H_5 or C_6H_6). To limit fragmentation and gas-phase reactions, a capillary voltage of 20 V was used in other experiments.

ES needle dimension

The ES needle dimensions affect the electric field at the ES needle tip in ESI-MS (Eq. (2.5) in Chapter 2). In this work, two stainless steel ES needles of 200 μm and 100 μm i.d., respectively, were used. Similar relative intensities for $TPA^{\bullet+}$ and $TPB^{\bullet+}$ in ESI-MS of TPA were detected. However, the smaller ES needle offered a better ES stability, and the lower end of useful ES voltages could be extended down to 2.1 kV while with the bigger ES needle, an ES voltage of 3.0 kV or higher had to be used in order to maintain a stable ESI process.

Electrolyte concentration

Electrolyte concentration affects the solution conductivity, and therefore, the ES current (Eq. (6.1)). On the basis of Eq. (6.1) an increase in ES current is expected when the electrolyte concentration is increased. However, Eq. (2.6) shows that the analyte ion signal is not only determined by the ES current, but also affected by the concentrations and the rates of transfer of the ions from electrolytes and analytes in solution to the gas phase. Since the electrolyte concentration and the transfer rate constant of electrolyte ion to the gas phase are in the denominator of the Eq. (2.6), a suppression of analyte ion signal is expected when the electrolyte concentration is increased. Thus, the ultimate effect of an increase in electrolyte concentration on analyte signal is a balance between the increased ES current and the increased signal suppression from the electrolyte.

Van Berkel and coworkers [1995(a)] reported that electrolyte concentration has a more significant effect on the ES current than expressed in eq 6.1 where a value of ~0.2 for the *n* exponent was assumed by Kebarle et al [Tang and Kebarle 1993]. A higher exponent value, $n \approx 0.7$ was suggested for the solution conductivity term in the equation 6.1. These workers also reported an increase in analyte (~10^{-5} M) signal with an increase in electrolyte concentration up to 10^{-4} M and a decrease in analyte signal at higher electrolyte concentrations [Van Berkel and Zhou 1995(b)].

In the present work, the effect of LiT electrolyte concentration on signals of TPA^- and TPB^- ions was investigated in ESI-MS, and the results were shown in Figure 6-5. The ES voltage was 3.3 kV and the concentration of TPA analyte was 100 μM. As shown in Figure 6-5, an increase in both TPA^- and TPB^- signals with LiT electrolyte concentration was observed initially. When the electrolyte concentration was above 200 μM, a decrease in TPA^- signal was observed. When the concentration of electrolyte was above 500 μM, a drop in TPB^- signal was also detected. These results can be rationalized by considering the balance between signal suppression effect of electrolyte and increased solution conductivity when the electrolyte concentration is increased. The data shown in Figure 6-5 indicate that the suppression of TPA^- signal occurred at lower electrolyte concentration than that of TPB^- signal. Similar effect of LiT electrolyte concentration on TPA^- and TPB^- ion signals has been observed in EC/ESI-MS. As shown in Figure 6-5, an electrolyte concentration of 200 μM produced a maximum TPA^- signal. Therefore, the LiT electrolyte concentration was typically controlled at 200 μM in this dissertation work.

Flow rate

Flow rate affects the mass input to the MS ion source. The dependence of ES current on flow rate is depicted by Eq. (6.1), in which the exponent v is ~0.5 [Tang and Kebarle 1993]. Interestingly, researchers in the same group have reported that although ES current increased with solution flow rate, the gas phase ion current due to analyte remained constant and even decreased at high flow rates [Ikonomou et al. 1991]. This phenomenon was interpreted as due to an increase in the droplet size during the ESI processes when the flow rate was increased [Fernandez de la Mora and Locertales 1994]. The yield of gas-phase ions from the charged droplets may decrease as the droplet size increases [Cole 1997]. In contrast, Van Berkel et al. [1995(a)] reported that solution flow rate had little effect on the ES current and the value of the exponent v for the flow rate term in eq 6.1 was estimated to be ~0.03. An increase in flow rate also caused a decrease in the electrolysis efficiency of nickel(II) octaethylporphyrin (Ni^{II}-OEP) during ESI ionization, which was interpreted as due to a reduction in the residence time of analyte in the ES needle when the flow rate was increased [Van Berkel and Zhou 1995(a)].

In this work, the effect of flow rate on the ion intensities of $TPA^{•+}$ and $TPB^{•+}$ was investigated by ESI-MS (Figure 6-6). The ion signals of $TPA^{•+}$ and $TPB^{•+}$ initially increase with flow rate. Figure 6-6 shows that a decrease in $TPB^{•+}$ signal is observed when the flow rate exceeds 45 μL/h. The signal of $TPA^{•+}$ also decreases when the flow rate is above 75 μL/h. The observed effect of flow rate on analyte signals in ESI-MS is similar to those reported in the literature [Ikonomou et al. 1991; Van Berkel and Zhou 1995(a)]. It is interesting to note that when the flow rate is increased, the drop in $TPB^{•+}$ signal occurs earlier, i.e., at lower flow rate, than $TPA^{•+}$ signal. This can be rationalized by considering that $TPB^{•+}$ is the follow-up reaction product of $TPA^{•+}$ and its formation requires more time. At increased flow rate, the proportion of the $TPA^{•+}$ ions that undergo dimerization during ESI ionization is decreased. As a result, a drop in $TPB^{•+}$ signal was observed. However, while $TPB^{•+}$ signal decreases, the ion signal of $TPA^{•+}$ may continue to increase with flow rate as long as the effect of reduced electrolysis efficiency at increased flow rate can be cancelled out by the gain from increased mass input to the MS ion source and decreased dimerization rate of $TPA^{\bullet+}$ ions. As shown in Figure 6-6, $TPA^{\bullet+}$ signal shows a maximum value at a flow rate of 75 μL/h. Therefore, this flow rate has been typically used in the ESI-MS and EC/ESI-MS experiments. The effect of flow rate on the electrochemical reaction products in TPA oxidation in EC/ESI-MS has been discussed previously (Chapter 5).

EC related Parameters

Working electrode (WE) area and EC cell configuration

The EC flow cell used in this work was described in Chapter 2 (Figure 2-2). Figure 6-7 illustrates the mass spectra of TPA from ESI-MS and EC/ESI-MS with different two-electrode configurations. As can be seen from Figure 6-7a, the ESI mass spectrum of TPA shows ion signals at m/z 245.10, 488.15 and 412.15, which can be assigned to $TPA^{\bullet+}$, $TPB^{\bullet+}$ and $[TPB^{\bullet+}-C_4H_4]^{+}$, respectively [Zhang et al. 2001]. Figure 6-7a shows a high relative intensity of $TPA^{\bullet+}$ and a low relative intensity of $TPB^{\bullet+}$. By applying EC cell voltage in EC/ESI-MS, an increase in the relative intensity of $TPB^{\bullet+}$ is observed (Figure 6-7 b-d).

Results in Figures 6-7 b-d demonstrate that the relative intensity enhancement of $TPB^{\bullet+}$ ion in EC/ESI-MS varies with the electrode configurations in the EC cell. In the on-line EC cell, the area of the working electrode corresponding to EC cell in Figures 6-7b-d is ~0.8 mm² for Pd(4), 12.5 mm² for ss(1), and 31.9 mm² for ss(2). The areas were calculated from the diameter of Pd(4) or internal diameter plus the length of the capillary (for ss(1) and ss(2)). A correlation exists between the relative intensity of $TPB^{\bullet+}$ and the working electrode area, since the higher relative intensity of $TPB^{\bullet+}$ is observed at larger electrodes It is conceivable that greater efficiency of TPA oxidation produces more $\mathrm{TPB}^{\bullet+}$ It is interesting to note that although the area of Pd(4) WE is very small, the enhancement in the $\mathrm{TPB}^{\bullet+}$ relative intensity in Pd(4) – Pd(5) EC cell configuration is high. The relative ion intensity at m/z 412 15 is also higher than in other EC cell configurations. This ion at m/z 412.15 may be due to a loss of C_4H_9 group from $\mathrm{TPB}^{\bullet+}$ The results from Pd(4) – Pd(5) EC cell configuration may be due to the thin-layer EC cell design, which may contribute to good electrolysis efficiency The low flow rate can contribute to the enhanced ionization efficiency [Zhang et al 2001]

A change in MS response time with the electrode configurations of the on-line EC cell was observed. After the EC cell voltage was applied the increase of the TPB ion signal was observed at ca. 45 s in Pd(4) – Pd(5), 10 s in ss(1) - ss(2) and 2 5 min in ss(2) - ss(3) EC cell configurations This trend of delay in MS response time is expected based on the distance of the WE to the MS detector in each of the electrode configurations Due to the rapid MS response time and good electrochemical ionization efficiency of TPA observed in ss(1) – ss(2) EC cell configuration, where the ES needle functions as the WE, this setup was employed to obtain EC/ESI MS data

TPA analyte concentration

With an increase in TPA concentration the MS signal is expected to increase However, because the TPA molecular ion radicals can rapidly dimerize the dimerization rate can increase with TPA concentration This can be verified by plotting the intensity ratio of $\mathrm{TPB}^{\bullet+}/\mathrm{TPA}^{\bullet+}$ ions as a function of TPA concentration, as shown in Figure 6 8 An increase in $\mathrm{TPB}^{\bullet+}/\mathrm{TPA}^{\bullet+}$ ratio with TPA concentration is observed, verifying an increase in the dimerization rate of TPA$^{\bullet+}$ with TPA concentration. Higher TPB$^{\bullet+}$/TPA$^{\bullet+}$ intensity ratio is observed in EC/ESI MS compared to ESI MS consistent with the enhanced generation of TPB in EC/ESI-MS At low TPA concentrations because of the limited dimerization, it was found that the enhancement in the ionization efficiency of TPA by EC/ESI-MS is displayed as an enhancement of TPA$^{\bullet+}$ signal, as illustrated in Figure 6-9 In Figure 6-9 the magnitude of the TPA$^{\bullet+}$ signal obtained from EC/ESI MS with TPA concentration at 1 µM is ~3 times that from ESI-MS

EC cell voltage

To determine the EC cell voltage needed to initiate the oxidation of TPA in the on-line EC/ESI-MS in the ss(1) ss(2) EC cell configuration, the ion intensity of the reaction product TPB was determined as a function of the EC cell voltage and the results are shown in Figure 6-10 As shown by Figure 6-10a, when the cell voltage is below 1 7 V no effect of the EC cell voltage on the TPB signal is observed Above 1 7 V the ion intensity of TPB increased with the EC cell voltage and reached a plateau at ca 3 V A small increase in the ion signal at m/z 244 with the EC cell voltage is observed, which can be interpreted as due to the increased generation of TPB^{2+} This is supported by Figure 6-10b which displays the isotopic intensity ratio for TPB (m/z 489 15/488 14) and TPB^{2+} (m/z 244 59/244 09) with the EC cell voltage The intensity ratio of m/z 489 15/488 14 does not change with EC cell voltage, indicating that TPB$^{\bullet+}$ is the sole ion at m/z 488 which is as expected However, a change in the intensity ratio of m/z 244 59/244 09 with EC cell voltage is observed which indicates a change in the ion identity at m/z 244 with the EC cell voltage Based on the previous discussion (Chapter

5), at low EC cell voltage the ion signal at m/z 244 can be attributed to [TPA$^{\bullet+}$-H]$^{+}$ which has an isotopic ion at m/z 245 but not at m/z 244.5. It is expected that TPB$^{\bullet+}$ and TPB^{+} have the same isotopic ratio. However, the intensity ratio of m/z 244.59/244.09 approaches that of m/z 489/488 only when the EC cell voltage is above 3 V. These results indicate that only at higher EC cell voltage (> 3 V) the ions at m/z 244 are predominantly due to TPB^{2+}.

The effective cell voltage (> 3 V) for the generation of TPB^{2+} is higher than the electrochemical oxidation potential of TPA, which is ~0.9 V vs SCE [Zhang and Brajter-Toth 2000, Seo et al. 1966, Nelson and Philp 1979, Oyama, et al. 1991]. This may be caused by possibly low ionization efficiency under the experimental conditions.

Reactions of TPA$^{\bullet+}$ Ions in the Gas Phase

Collision induced dissociation (CID) of TPA$^{\bullet+}$ in the ICR cell

The gas-phase ion chemistry may affect the detection of ions generated in solution in ESI-MS. An evidence of the occurrence of gas phase reaction of TPA$^{\bullet+}$ ions was obtained from CID experiments. The results are shown in Figure 6-11. The TPA$^{\bullet+}$ ions were first selectively isolated in the ICR analyzer cell (Figure 6-11a). Fragmentation of the TPA$^{\bullet+}$ ions was initiated by introducing argon collision gas via a pulsed valve and by applying an ion activation pulse. The results are shown in Figure 6-11b. Two fragments were observed at m/z 167 and 139, which were due to a loss of C_6H_6 from TPA$^{\bullet+}$ and a further loss of C_2H_4 from [TPA-C_6H_6]$^{\bullet+}$, respectively. The loss of hydrogen atoms from TPA$^{\bullet+}$ was also detected, as shown by the ions at m/z 244, 243, 242, 241 and 240 in the inset of Figure 6-11b. One surprising result is the observation of an ion signal at m/z

488, which is likely due to TPB$^{\bullet+}$. This assignment has been confirmed by the measured isotope intensity ratio of m/z 489 vs 488. It was found that an increase in the ion activation energy pulse diminished TPA$^{\bullet+}$ ion at m/z 245, which caused an increase in the ion intensity of TPB$^{\bullet+}$ and two fragments at m/z 167 and 139 (Figure 6-11c).

Based on the above CID data of TPA$^{\bullet+}$ ion, it can be concluded that TPA$^{\bullet+}$ can dimerize to form TPB in the gas phase. The coupling of TPA$^{\bullet+}$ ions would produce neutral TPB with a loss of two protons, as shown by Figure 1-3 of Chapter 1. The observation of TPB$^{\bullet+}$ ion signal in the CID of TPA$^{\bullet+}$ indicates that the charge can be transferred from TPA$^{\bullet+}$ to TPB in the gas phase, i.e., oxidation of TPB by TPA$^{\bullet+}$ may occur. Thus, the present work indicates the formation of TPB via TPA$^{\bullet+}$ coupling and the oxidation of TPB by TPA$^{\bullet+}$ ion in the gas phase.

Effect of ion accumulation time in the hexapole

Accumulation of the ions in the hexapole may improve MS detection sensitivity [Belov et al. 2001]. However, the increase in the ion concentration in the hexapole may cause gas phase reactions and complicate MS data interpretation.

Figure 6-12 shows several ion signals from ESI ionization of TPA as a function of ion accumulation time (D1). As can be seen from Figure 6-12, the TPA$^{\bullet+}$ signal initially increases with D1 up to 0.75 s, due to the increased ion concentration. A further increase of D1 caused a decrease of TPA$^{\bullet+}$ signal. TPA$^{\bullet+}$ signal disappeared when D1 was above 2 s, which is due to the increased ion collision and gas-phase reactions under this condition. This interpretation is consistent with the detection of [TPA$^{\bullet+}$-H]$^+$ ions at m/z 244.09 when D1 was at 2.5 s, and the increase of TPB$^{\bullet+}$ signal at m/z 488 and [TPB$^{\bullet+}$

$C_6H_4]^{+\cdot}$ signal at m/z 412. New ions at m/z 579 and 502 were observed when D1 was above 0.5 s. The ion at m/z 579 is likely due to (412 + 167), viz. [(TPB-C_6H_4) + (TPA-$C_6H_4)^{+\cdot}]^{+\cdot}$, and the ion at m/z 502 is likely due to a loss of C_6H_5 group from the ion at m/z 579. The fragmentation of $TPB^{+\cdot}$ becomes significant when D1 is above 7.5 s, which causes a decrease of $TPB^{+\cdot}$ signal and an increase of the ion signal at m/z 579.

Conclusions

A variety of experimental parameters in EC/ESI-MS that may affect the detection sensitivity for the electrochemically generated species in TPA oxidation have been investigated. Among them, the effect of flow rate, electrolyte concentration and analyte concentration is significant. The parameters such as ES needle dimension, ES voltage and ES tip – counter capillary distance, while showing some effect, are relatively insignificant. Comparison of the results from different EC cell configurations has suggested a correlation between MS detected signal and WE area, MS response time and distance of the WE to the MS detector. In on-line EC/ESI-MS, the EC cell voltage needed to effectively oxidize TPA is higher than the oxidation potential of TPA, which is attributed to a relatively high solution resistance with the use of low electrolyte concentrations.

The present work also demonstrates that gas-phase reactions may be a factor that controls the MS detection sensitivity for the ions initially generated in the liquid solution. The CID of $TPA^{+\cdot}$ ions in the ICR cell provides avidances for the coupling of $TPA^{+\cdot}$ ions to form TPB and the oxidation of TPB by $TPA^{+\cdot}$ in the gas phase. The occurrence of gas-phase fragmentation, ion-molecule or ion-ion reactions has also been found in the investigation of the effect of capillary voltage and ion accumulation time in the hexapole. New ions have been produced from fragmentation or unwanted gas-phase reactions by collision with other molecules or ions. To minimize the complication from TPA fragmentation and/or gas-phase reaction, the capillary voltage and the ion accumulation time in the hexapole have been set at a low value, i.e., 20 V and 0.2 s, respectively, in the previously performed experiments.

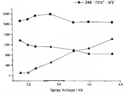

Figure 6.1 Effect of ES voltage on ESI signal of $TPA^{\bullet+}$ (square), $TPB^{\bullet+}$ (circle), $[TPA^{\bullet+} - H^+]^+$ (triangle). 1×10^{-4} M TPA + 2×10^{-4} M LiT in acetonitrile, 75 µL/h. ES needle 200 µm i.d. ES – counter capillary distance 3 mm, counter capillary voltage 20 V. 150 – 800 Da, 50 scans. One measurement is included for each date point. The variation error between different runs is below 10%.

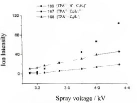

Figure 6-2 Ion signal at m/z 168 (triangle) 167 (circle), and 166 (square) with ES voltage. Conditions as Figure 6-1

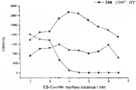

Figure 6-3 ES -counter capillary distance (z distance) with TPA$^{\bullet+}$, TPB$^{\bullet+}$ and [TPA$^{\bullet+}$ - H^{+}]$^{+}$ on signal. ES voltage 3.3 kV. Other conditions as Figure 6-1

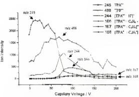

Figure 6-4 Ion intensity vs counter capillary voltage. ES voltage 3.3 kV. ES tip-counter capillary distance 3.0 mm. Other conditions as Figure 6-1.

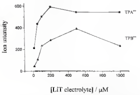

Figure 6-5 Ion intensity of TPA^{++} and TPB^{++} with electrolyte concentration in ESI-MS ES needle 100 μm i d 150 – 1000 Da, 20 scans Other conditions as Figure 6-1

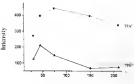

Figure 6-6 Ion intensities of $TPA^{\bullet+}$ and $TPB^{\bullet+}$ with flow rate Conditions as Figure 6-5

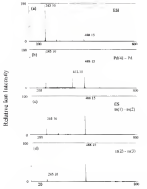

Figure 6-7 ESI (a) and EC/ESI (b-d) mass spectra of TPA. Electrode configurations (b) Pd (4) – Pd(5) (c) ss(1)-ss(2) (d) ss(2)-ss(3). Solution 1×10^{-4} M TPA – 2×10^{-4} M LiT in acetonitrile, 75 µl/h, ES voltage 3.3 kV. EC cell voltage 7.5 V. ES needle 100 µm i.d. 150-800 Da, 20 scans.

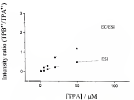

Figure 6.8 Effect of TPA concentration on the intensity ratio of $TPB^{\bullet+}/TPA^{\bullet+}$ (m/z 488/245) in ESI-MS (square) and EC/ESI-MS (circle) ss(1) – ss(2) configuration. Other conditions as Figure 6.7

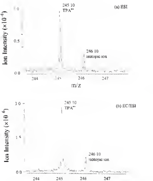

Figure 6-9 TPA$^{•+}$ signal at low TPA concentration (1×10^{-6} M). (a) ESI-MS. (b) EC/ESI-MS. ss(1) – ss(2) configuration. Conditions: 1×10^{-6} M TPA – 2×10^{-4} M LiT in acetonitrile, 75 µL/h. EC cell voltage 7.5 V. ES needle 100 µm i.d. ES voltage 3.3 kV. 150 – 800 Da, 20 scans.

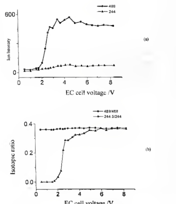

Figure 6-10 EC cell voltage and (a) intensity of $TPB^{\bullet+}$ (m/z 488) and TPB^{2+} (m/z 244), (b) isotopic intensity ratio of m/z 489/488 and m/z 244.59/244.09 ss(1) – ss(2) cell configuration. 1×10^{-4} M TPA – 2×10^{-4} M LiT in acetonitrile, 75 μL/h ES 3.3 kV ES needle 100 μm i.d. 150-800 Da, 20 scans Other conditions as Figure 6-7

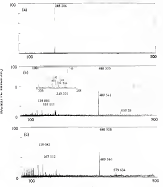

Figure 6-11 CID of TPA molecular ion (a) isolation of m/z 245 in the ICR cell, (b) CID ion activation 22 db (c) CID ion activation 20 db Smaller db value represents increased activation energy Solution 1×10⁻⁴ M TPA - 2×10⁻⁴ M LiT in acetonitrile 75 μL/h, ES voltage 3 3 kV EC cell voltage 7 5 V, ES needle 100 μm i d. 150-800 Da, 20 scans ICR pressure 1×10⁻⁷ mbar during CID

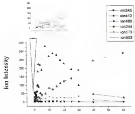

Figure 6.12. Ion intensities with accumulation time in the hexapole of FTICR MS Inset shows the change of ion intensities with accumulation time 0.1-3 s.

CHAPTER 7
OXIDATION OF POLYCYCLIC AROMATIC HYDROCARBONS AND NUCLEOPHILIC REACTIONS INVESTIGATED BY EC/ESI-FTICR MS

Introduction

In the oxidation of neutral compounds, the follow-up chemical reactions after the initial electron transfer can be (1) the dimerization of the ion radical, (2) reaction of the ion radical with solvent, (3) hydrolysis reaction of the ion radical, (4) reaction of the ion radical with solvent impurities [Adams 1969, Mann 1970]. Except for reaction (1), reactions (2)-(4) can be considered as nucleophilic reactions. As described in Chapter 5, EC/ESI MS can provide high detection sensitivity for monitoring products of dimerization [Zhang et al. 2001]. In this Chapter, the use of EC/ESI-FTICR MS in the investigation of nucleophilic reactions is exploited.

Nucleophilic reactions between cation radicals and biological nucleophiles are of widespread occurrence in biological systems [Pryor 1984]. For example, in chemical carcinogenesis, polycyclic aromatic hydrocarbon (PAH) carcinogens can form PAH-DNA adducts, which has been shown to contribute to tumor initiation [Harvey 1985, RamaKrishna et al. 1992]. Formation of PAH cation radicals, via one electron transfer reactions, has been shown to be enzymatically catalyzed by enzymes such as horseradish peroxidase [Rogan et al. 1988] or cytochrome P-450 [Cavalieri et al. 1988, Burka et al. 1985]. The enzymatic formation of the radicals can be simulated electrochemically, which can facilitate EC/MS real-time investigations of the reactions between the electrochemically-generated cation radicals and nucleophiles of interest. The formation of cation radical nucleophile reaction adducts may facilitate the detection of the nucleophiles by ESI MS in positive ion detection mode which will avoid the discharging problem associated with negative ion detection in ESI MS

In this Chapter PAH cation radicals were generated via electrochemical oxidation in an EC flow cell and the nucleophilic reactions of the radicals were investigated by EC/ESI-MS using the instrumental setup shown in Figure 2-5 of Chapter 2 In this setup, the EC cell was coupled to an ESI FTICR MS and the ES needle, ss(1), formed a part of the EC cell. ESI-FTICR MS can provide high resolution and high sensitivity for the detection of cation radicals [Zhang et al. 2001] A rapid MS response time and high electrolysis efficiency can be provided by employing the ss(1) – ss(2) EC cell configuration, in which the ss(1) needle is used as the working electrode of the EC cell [Chapter 5] In this work the oxidation of three PAHs, i e anthracene perylene and rubrene was studied by EC/ESI-FTICR MS The anthracene radical cation is reactive, with a lifetime of a few milliseconds [Peover and White 1967 Majeski et al 1968], while the perylene and rubrene cation radicals are stable [Phelps et al 1967 Adams 1969(a); Mann and Barnes 1970] The principal goal of this Chapter is to examine the reactivity of the different PAH cation radicals and provide some preliminary results on the ESI-MS detection sensitivity of the cation-tagged adduct ions

Results and Discussion

EC/MS of Anthracene

Sensitivity in detection of anthracene

It has been reported that the oxidation of anthracene (MW 178) is a one-electron reaction, which leads to the formation of the anthracene cation radical [Marcoux et al

1967, Phelps et al. 1967]. However, the anthracene cation radical is very reactive and did not produce a cathodic peak in cyclic voltammogram (with scan rates up to 5 V/s) in methylene chloride [Phelps et al. 1967]. In controlled potential electrolysis of anthracene in acetonitrile, the major product is bianthrone (MW 386), produced via coupling of 9-anthrone radical (MW 193) produced via hydrolysis of anthracene cation radical [Majeski et al. 1968], as shown in Figure 1-4 of Chapter 1. The water involved in hydrolysis was present as trace impurity in acetonitrile (at least 4-10 mM water is present in most anhydrous solvent [Adams 1969(a), Majeski et al. 1968]).

In the present work, the detection of anthracene radical cation was readily achieved by EC/ESI FTICR MS, as shown by the ion peak at m/z 178 in Figure 7-1. This result supports one-electron oxidation of anthracene and confirms that a direct two-electron anodic oxidation process proposed in earlier studies [Lund 1957] is not favored. The generation of 9-anthrone (MW 193) in the EC oxidation of anthracene, due to the hydrolysis of anthracene radical cation, was also detected, as shown by the ion signal at m/z 193 in Figure 7-2a. The ions at m/z 195 and 194 were identified as the intermediates that precede the formation of 9-anthrone, i.e., 9-anthrone is a result of further EC oxidation of these ions in the EC flow cell. The corresponding ion identities are illustrated in Figure 7-2a. In this work, the acetonitrile solvent used was of an HPLC grade, and was used as received. The labeled water content from the manufacturer is 0.002%, which is ~0.9 mM. The moisture level may be increased during solution preparation and during the atmosphere ESI ionization process. It is reasonable to assume that the concentration of water impurity in anthracene-acetonitrile solution is at the literature-reported level, ~4-10 mM [Adams 1969(a)]. Majeski et al. have reported that when the water concentration was below 50 mM, the primary product from the electrolysis of anthracene in acetonitrile was bianthrone (MW 386). The formation of anthraquinone (MW 208) was only favored at higher water concentrations [Majeski et al. 1968]. In our EC/ESI-FTICR MS, no anthraquinone (MW 208) product ion was detected. However, an ion signal at m/z 211, which may be due to 9,10-dihydroxy-anthracene, was sometimes (not always) detected in EC/ESI-FTICR MS (Figure 7-2b). This intermediate product, 9,10-dihydroxy-anthracene, can be oxidized easily to form anthraquinone [Majeski et al. 1968].

Bianthrone (MW 386) has been reported to be the major product of anthracene oxidation in acetonitrile [Majeski et al. 1968]. Therefore, the detection of a high relative intensity of bianthrone ion was expected in EC/ESI-MS. Figure 7-3 shows the results obtained from oxidation of anthracene in ESI-MS and EC/ESI-MS. Indeed, an ion signal at m/z 385 was detected in EC/ESI-MS, as shown in Figure 7-3b, which can be attributed to the bianthrone ion, after a loss of hydrogen. However, the relative ion intensity of this ion is very small, indicating that the formation of bianthrone is not favored under these conditions. Instead, an ion at m/z 355, which is the base ion in the mass spectrum shown in Figure 7-3b, was detected. This ion was assigned as due to the coupling (dimerization) of anthracene cation radical, after a loss of hydrogen. This result indicates that anthracene cation radicals, once generated, can dimerize without undergoing extensive reactions. The relative yield of the dimer product is affected by anthracene concentration. When the concentration of antharacene was 100 μM, as was used in Figure 7-3, the intensity ratio of the dimer ion vs the anthracene cation radical in EC/ES-FTICR MS was ~30. When the anthracene concentration was reduced to 10 μM, the intensity ratio of the dimer ion vs anthracene cation radical in EC/ESI-MS decreased to ~7. This effect of anthracene concentration on the dimer product is as expected [Chapter 6]. The dimer product ion at m/z 355 does not hydrolyze readily, as can be seen from the small signals due to the hydrolyzed ions at m/z 370 and 385 shown in Figure 7-3b. A reaction scheme for the formation of these ions is illustrated in Figure 7-4.

In Figure 7-3, several ions such as those at m/z 321 and 349 were not identified. The EC/ESI-MS experiments were performed when the best vacuum pressure of the instrumental system was higher (~ 8×10^{-9} mbar in the ICR cell) than normal (~2×10^{-9} mbar), which may contribute to noise and impurities. A CID experiment of the m/z 321 ion gave rise to the fragments at m/z 149, 105, 77 and 51. A possible structure that can be proposed for this ion is $[(CF_3SO_3)(C_6H_5)_2H_2O]$, which may be due to adduction of triflate (CF_3SO_3, from electrolyte, MW 149) and positively charged biphenyl ($((C_6H_5)_2$, source unknown, MW 77 × 2), with one water molecule attached. The ion at m/z 269 may be due to a phenyl adduct of 9-anthrone, as shown in Figure 7-3a.

In EC/ESI-MS, the solvent used consisted of 98% acetonitrile/2% methylene chloride (v/v). PAHs dissolve well in methylene chloride but are sparingly soluble in acetonitrile, while the reverse is true for lithium triflate [Xu et al. 1996]. The use of such a mixed solvent system ensures sufficient solubility for both PAHs and lithium triflate electrolyte in solution. In our experiment, acetonitrile was used as a major solvent (98% v/v) because it provides better ES stability than methylene chloride [Blades et al. 1991]. Under this condition, anthracene could be ionized in ESI-MS (Figure 7-3a). Since the $E_{1/2}$ of anthracene is ~1.09 V vs SCE [Xu et al. 1996], this result indicates that the neutral compounds that can be ionized by electrolytic ESI ionization may not be limited to those with oxidation potentials below 1 V, as reported previously [Van Berkel et al. 1992. Xu et al. 1994]. It was also found that the solvent affects strongly ESI ionization of anthracene. When methylene chloride was used as a major solvent (98% acetonitrile/2% methylene chloride, v/v) it was difficult to get a stable ES current and the anthracene cation radical was not detected.

Xu et al. [1996] has reported not being able to detect anthracene ions by ESI-MS. The solvent used in their experiments was 95% CH_2Cl_2/5% CH_3CN (v/v). Several PAHs with different $E_{1/2}$ values were tested. It is interesting to note that their results indicated no correlation between the $E_{1/2}$ values of the neutral compounds and the ESI electrolytic ionization feasibility. For example, no ion signals of 9-methylanthracene and 9,10-dimethylanthracene, which have a low $E_{1/2}$ of 0.96 and 0.87 V vs SCE, respectively, were detected in ESI-MS. On the other hand, 9,10-diphenylanthracene, with its $E_{1/2}$ at 1.22 V vs SCE, was readily ionized in ESI-MS. In their work, only the ion abundances of PAH molecular ions were provided, and no dimerization or hydrolysis products were reported.

In our work, anthracene could be ionized in ESI-MS. However, it was found that the use of EC/ESI-MS significantly enhanced the MS detection sensitivity of the dimerization and hydrolysis products (Figure 7-3b). As a result of this, EC/ESI-FTICR MS can be used to pursue low-level detection of anthracene. A solution containing 100 μM anthracene was used to obtain the results shown in Figure 7-3. It was found that when the concentration of anthracene was reduced to 1 μM, the anthracene ion signal, either at m/z 178 or 355, could not be detected by ESI MS (Figure 7-5a). By applying the EC cell voltage in EC/ESI-FTICR MS, the ion signals of anthracene radical cation at m/z 178 and its dimer product at m/z 355 were detected (Figure 7-5b). This indicates that

EC/ESI-MS will likely be a useful tool for pursuing low level detections of PAHs such as anthracene.

Nucleophilic reactions of anthracene cation radical with pyridine

When a strong nucleophile, pyridine, was present (0.5% v/v) in anthracene solution containing 100 μM anthracene-200 μM LiT electrolyte in a mixed solvent of 98% acetonitrile/2% methylene chloride (v/v), the oxidation of anthracene in ESI-MS gave rise to a new ion at m/z 256 (Figure 7-6a). The relatively intensity of this new ion was significantly enhanced in EC/ESI-MS (Figure 7-6b). Figure 7-6b shows that this ion at m/z 256 is the base ion in the EC/ESI-MS spectrum. While the presence of pyridine nucleophile resulted in the ion at m/z 256, it also caused the disappearance of the dimer product of anthracene radical coupling that was observed at m/z 355 as shown in Figure 7-3. The ion at m/z 256 can be attributed to 9-anthrylpyridinium, which is an anthracene-pyridine adduct formed via the nucleophilic reaction shown in Figure 7-6c. The formation of the anthracene-pyridine adduct ion at m/z 256 and the disappearance of the dimer ion of anthracene at m/z 355 indicates that the nucleophilic reaction of pyridine with anthracene radical cation is more efficient than the dimerization reaction under the experimental conditions. In EC/ESI-MS, the high MS detection sensitivity of the adduct ion reduced the interference of ions at m/z 321 and 349.

Lund [1957] reported the generation of 9,10-dihydroanthraquinyldipyridinium diperchlorate from the bulk electrolysis of anthracene (~0.037 M) in acetonitrile in the presence of pyridine (~0.34 M), with sodium perchlorate (~0.82 M) as electrolyte. Our EC/ESI-FTICR MS results show that under the present experimental conditions, which employed 100 μM anthracene, 200 μM LiT electrolyte and 0.5% (v/v) pyridine (~0.063

M), the product detected is 9-anthrylpyridinium, which is a 1:1 anthracene pyridine adduct. Whitehill and coworkers have reported similar results in the gas-phase reactivity study of anthracene cation radical with pyridine [Whitehill et al. 1996(b)].

EC/MS of Perylene

Sensitivity in detection of perylene

Perylene, with an $E_{1/2}$ of 0.85V vs SCE [Mann and Barnes 1970], can lose one electron to form the perylene cation radical [Xu et al. 1996]. Xu et al. [1996] reported the ESI-MS and EC/ESI-MS results of perylene in methylene chloride, and demonstrated that the signal of perylene cation radical can be improved by EC/ESI-MS. In that work, only the detection of perylene molecular ion radical was reported. In the present work, a molecular ion radical of perylene was observed at m/z 252 in ESI-MS (Figure 7-7a), which was obtained in a mixed solvent of 98% CH_3CN/2% CH_2Cl_2 (v/v). The application of EC cell voltage in EC/ESI-MS increased the ion signal of perylene radical cation, as shown in Figure 7-7b. The intensity of the perylene cation radical in EC/ESI-MS is ~6 times that in ESI-MS, indicating enhanced detection sensitivity for perylene in EC/ESI-MS. This result is in agreement with that reported by Cole and coworkers [Xu et al. 1996]. Unlike anthracene, which could not be ionized by ESI-MS in 98% CH_2Cl_2/2% CH_3CN (v/v), a stable ES current was observed in ESI ionization of perylene in the same solvent. This difference in ESI-MS results is probably caused by the difference in oxidation potentials between perylene and anthracene, i.e., perylene has much lower $E_{1/2}$ (0.85 V vs SCE) than anthracene (1.09 V vs SCE). However, it was found that a higher ES voltage (3.5 kV) is needed to ionize perylene in 98% CH_2Cl_2/2% CH_3CN (v/v) than in

2% CH_2Cl_2/98% CH_3CN (v/v). In the latter solvent, an ES voltage of 2.8 kV is sufficient to maintain the ES current.

Perylene ion radical is stable [Adams 1969(b), Ristagno and Shine 1971]. Accordingly, no product ions from hydrolysis or dimerization were detected in EC/ESI-MS. Addition of 5% (v/v) water to 100 μM perylene solution caused the appearance of ions of small relative intensity at m/z 267, 287, 285 and 283 (Figure 7-8). The reactive sites in perylene ion radical are at 3- and 10- position, as shown in Table 1.1 (Chapter 1). The proposed ion identities for the ions from hydrolysis reactions of perylene ion radical in the presence of water are illustrated in Figure 7-8. In the electrochemical oxidation of perylene, 3-hydroxyperylene (MW 268) has been regarded as a short-lived intermediate and the final products isolated from the electrolysis mixture were 3,10-perylenequinone (MW 282) besides the perylene cation radical (m/z 252) [Ristagno and Shine 1971]. In the EC/ESI-FTICR MS experiments, the intermediate 3-hydroxyperylene (MW 268), which would produce an ion at m/z 268, was not detected. Instead, the appearance of an ion at m/z 267 was observed, which can be attributed to the oxidation of 3-hydroxyperylene to 3-perylenone (MW 267). The product ion of 3,10-perylenequinone (MW 282) was not detected in EC/ESI-MS. However, the ions at m/z 287, 285 and 283 can be considered as intermediate ions preceding the formation of 3,10-perylenequinone. The small relative intensities of these ions indicate that the formation of 3,10-perylenequinone was not favored under the present experimental conditions, which employed a solution of 100 μM perylene-200 μM LiT electrolyte in 98% CH_3CN/2% CH_2Cl_2 (v/v) mixed solvent.

Nucleophilic reactions of perylene cation radical with pyridine

As discussed above, perylene cation radical is stable and the addition of water (5% v/v) caused only limited formation of hydrolysis products of the perylene cation radical, indicating that water was a poor nucleophile in the reaction with the perylene cation radical. A different EC/ESI-MS result was obtained when the oxidation of perylene was performed in the presence of pyridine nucleophile (Figure 7-10). The spectrum shown in Figure 7-10a was obtained in ESI-MS, with the addition of 0.5% (v/v) pyridine to the perylene (100 µM)-LiT (200 µM) solution in 98% CH_3CN/2% CH_2Cl_2 (v/v). The ions at m/z 321, 349 and 365 were due to impurities present in the system, as discussed previously. However, the ion at m/z 330 was newly produced. When the EC cell voltage was applied in EC/ESI-MS, the relative intensity of this ion was significantly increased and became the base ion in the spectrum (Figure 7-10b). This ion can be attributed to the formation of perylene-pyridine adduct, 3-pyridiniumperylene (Figure 7-10c). The results shown in Figure 7-10 indicate that the nucleophilic reaction of pyridine with perylene radical cation is efficient.

The difference between the pyridine and water reactions may be attributed to the difference in nucleophilicity, i.e., pyridine is a stronger nucleophile than water. The formation of the perylene-pyridine adduct ion was further verified by a CID experiment, in which the ion at m/z 330 was isolated in the ICR analyzer cell (Figure 7-11a), and fragmentation was initiated by introducing argon collision gas and applying an ion activation energy pulse, which produced a fragment at m/z 250 (Figure 7-11b). This fragment ion at m/z 250 can be attributed to a loss of C_5H_4N generated from the ion at m/z 330.

EC/MS of Rubrene

Sensitivity in detection of rubrene

Rubrene, with an $E_{1/2}$ of 0.82 V [Mann and Barnes 1970], can also be ionized directly in ESI-MS. Cole et al. have reported a 4-fold signal enhancement of rubrene ion radical by EC/ESI-MS over ESI-MS in methylene chloride [Xu et al. 1996]. In their work, the rubrene molecular ion radical was the only ion that has been detected in either ESI-MS or EC/ESI-MS.

In the present work, a molecular ion signal of rubrene was observed at m/z 532 in ESI-MS (Figure 7-12a). In addition, an ion at m/z 547, which is of small relative intensity, was detected. By applying EC cell voltage (7.5 V) in EC/ESI-FTICR MS, the relative ion intensity of the ion at m/z 547 was significantly enhanced so that this ion became the base ion in the spectrum (Figure 7-12b). Rubrene can be considered as substituted tetracene, 5,6,11,12-tetraphenyl-tetracene. By referring to table 1.1 (Chapter 1), it can be seen that the most reactive sites in tetracene cation radical are at 5-, 6-, 11-, 12- atomic positions since these positions give the highest values of unpaired electron density. However, in rubrene, these sites are blocked by phenyl groups, and therefore are not available for further reactions. The reactions such as hydrolysis of the rubrene cation radical must occur in the next most reactive sites, 1-, 4-, 7-, 10- atomic positions. Based on this rationale, a reaction scheme that accounts for the formation of the ion at m/z 547 is proposed, as shown in Figure 7-13.

It should be noted that during the experiments, the instrumental parameters were tuned so as to optimize the detection sensitivity of rubrene cation radical at m/z 532. It was found that, in order to obtain the ESI-MS results shown in Figure 7-12, which shows a predominant ion peak of rubrene ion radical at m/z 532, a high counter capillary voltage, e g. 150 V, has to be used At lower counter capillary voltage, in addition to the ions at m/z 532 and 547 which are due to rubrene cation radical and 1-rubrenone, respectively, another ion peak at m/z 565 was observed (Figure 7-14a) This ion can be rationalized as due to the water adduct of 1-rubrenone at m/z 547 as illustrated in Figure 7-13 The best detection sensitivity of this water adduct ion was obtained when the counter capillary voltage was around 50 V When the counter capillary voltage was increased loss of water molecule from the adduct ion took place which reduced the adduct ion signal At a counter capillary voltage of 150 V no water-adduct ion at m/z 565 was detected in either ESI MS or EC/ESI-MS as shown in Figure 7-12. A further increase of counter capillary voltage, e g. to 200 V, caused fragmentation of the rubrene cation radical (Figure 7-14b) which produced two fragment ions at m/z 455 and 377 These two fragments were produced through a stepwise loss of C_6H_5 and C_6H_6 group

Nucleophilic reactions of rubrene cation radical with pyridine

Unlike anthracene and perylene the cation radical of rubrene is stable toward the pyridine nucleophile In the presence of pyridine (0 5% v/v) no rubrene-pyridine adduct ion (expected m/z 610) was detected in ESI-MS (Figure 7-15a) Figure 7-14a shows an ion of small relative intensity at m/z 708 By applying EC cell voltage in EC/ESI-FTICR MS the relative ion intensity of this ion was improved (Figure 7-15b) A possible composition of this ion is (rubrene + water + 2 pyridine) However no attempt was made to further identify this ion

Conclusions

Molecular ion radicals have been detected for anthracene, perylene and rubrene by EC/ESI-FTICR MS, which verified the initial one-electron transfer in the oxidation of the PAHs. The results show that anthracene cation radical is very reactive and can rapidly undergo dimerization and hydrolysis reactions. The high MS detection sensitivity for the dimer product, which was formed via coupling of anthracene cation radical without hydrolysis, indicates that dimerization reaction has faster kinetics than the hydrolysis reaction. It has been demonstrated that EC/ESI-MS can be used to pursue low level detection of anthracene as a result of enhanced detection sensitivity demonstrated for the products generated in anthracene oxidation. The nucleophilic reaction between anthracene cation radical and pyridine produces high yield of anthracene-pyridine adduct. Enhanced MS detection sensitivity for the anthracene-pyridine adduct has been obtained in EC/ESI-MS.

Perylene cation radical is stable and shows only limited hydrolysis reaction in EC/ESI-MS. However, the reaction between perylene cation radical and pyridine nucleophile is efficient, which generated perylene pyridine adduct with high MS detection sensitivity in EC/ESI-MS. No obvious reaction of pyridine with rubrene cation radical has been detected in EC/ESI-MS.

The intermediate ions and products generated in the oxidation of anthracene, perylene and rubrene were identified in EC/ESI-FTICR MS, which have either confirmed or provided new insights into the oxidation pathways of the corresponding PAH compound.

The present work demonstrates that significantly high MS detection sensitivity for the PAH-pyridine adduct ion can be achieved by use of EC/ESI-MS. The attachment of PAH "cation tag" to the nucleophiles may enhance the detection sensitivity and reduce the interference from sample matrix in EC/ESI-MS. This represents a new strategy for the application of EC/ESI-MS in the sensitive determination of nucleophiles especially those of biological interest.

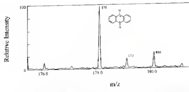

Figure 7-1 Anthracene in EC/ESI-FTICR MS. Conditions: 100 μM anthracene-200 μM lithium triflate in 98% acetonitrile/2% methylene chloride (v/v); continuous infusion: 75 μL/h; ES voltage 3.0 kV; EC cell voltage 7.5 V; counter capillary voltage 50 V; ss(1)-ss(2) EC cell configuration as Figure 2-5 in Chapter 2

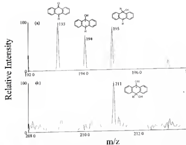

Figure 7.2 Hydrolysis products of anthracene radical cation detected in EC/ESI MS (a) monooxygenation (b) dioxygenation. Same conditions as in Figure 7.1

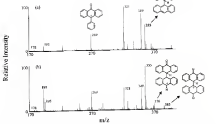

Figure 7-3 Product ions observed in anthracene oxidation (a) ESI-MS (b) EC/ESI-MS Conditions as Figure 7-1

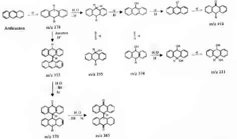

Figure 7-4 Reaction scheme for the ions detected in the oxidation of anthracene by EC/ESI-FTICR MS

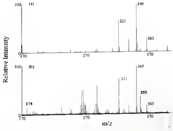

Figure 7-5 Detection of anthracene at low concentration (a) ESI-MS (b) EC/ESI-MS Solution 1 μM anthracene-200 μM LiT electrolyte same other conditions as Figure 7-1

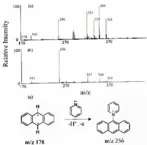

Figure 7-6 Reaction of pyridine with anthracene cation radicals (a) ESI MS (b) EC/ESI MS, (c) Nucleophilic formation of anthracene pyridine adduct 0.5% (v/v) pyridine, 100 μM anthracene-200 μM LiT electrolyte in 98% acetonitrile/2% methylene chloride (v/v) Other conditions as Figure 7-1

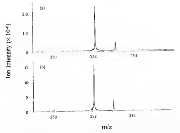

Figure 7-7 Ion intensity of perylene ion radical detected by (a) ESI MS (b) EC/ESI-MS 100 µM perylene 200 µM LiT in 98% acetonitrile/2% methylene chloride Same other conditions as Figure 7-1

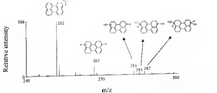

Figure 7.8 Hydrolysis of perylene cation radical in EC/ESI-MS. 5% water was added to a solution consisting of 100 µM perylene + 200 µM LiT in 98% acetonitrile/2% methylene chloride. Same other conditions as Figure 7.7

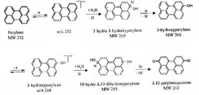

Figure 7-9 Oxidation pathway of perylene in acetonitrile [Ristagno and Shine 1971]

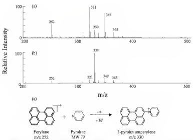

Figure 7.10 Pyridine with perylene in (a) ESI/MS (b) EC/ESI/MS, (c) proposed formation of perylene-pyridine adduct. 0.5% (v/v) pyridine, 100 μM perylene-200 μM LiT electrolyte. Other conditions as Figure 7-7

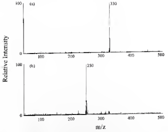

Figure 7-11 CID of m/z 330 ion of 3-pyridiniumperylene (a) ion isolation (b) loss of (pyridine + H) group

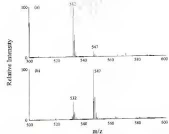

Figure 7-12 (a) Rubrene in ESI-MS (b) Rubrene production in EC/ESI-MS 100 μM rubrene 200 μM LiTf counter capillary voltage 50 V Other conditions as Figure 7-1

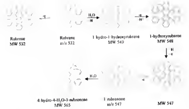

Figure 7 13 A proposed reaction scheme for the EC/ESI-MS oxidation of rubrene

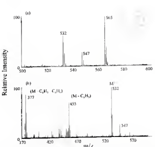

Figure 7-14 Effect of counter capillary voltage on EC/ESI-MS (a) water adduct of 1-rubrenone at a counter capillary voltage of 50 V (b) fragmentation of rubrene radical cation at a counter capillary voltage of 200 V Other conditions as Figure 7-11

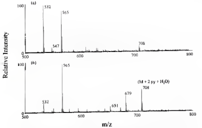

Figure 7-15 Rubrene cation with pyridine (a) ESI-MS (b) EC/ESI MS 0.5% (v/v) pyridine 1 × 10^{-4} M rubrene-2 × 10^{-4} M LiT electrolyte in 98% acetonitrile/2% methylene chloride (v/v) Counter capillary voltage 50 V Other conditions as Figure 7.12

CHAPTER 8
CONCLUSIONS AND FUTURE WORK

This dissertation work was focused on coupling electrochemistry (EC) on-line with mass spectrometry (MS), EC/MS. The driving force for this work originates from the need to gain chemical information about the intermediates and products in electrochemical reactions, in close to real time. The topics in this research range from the use of different LC/MS interfaces for EC/MS, design of electrochemical flow cell, use of electrolyte, enhancement of ionization efficiency and signal suppression from electrolytes, etc.

It was demonstrated first that particle beam (PB) LC/MS interface is a suitable liquid interface for EC/MS investigation of generation of intermediate radical cations, in a nonaqueous solvent. In this work, a homebuilt thin-layer electrochemical flow cell was conveniently inserted between a HPLC pump and the PB interface of a quadrupole mass spectrometer. The advantages for using PB interface include gas-phase analyte enrichment due to the PB transport characteristics, ability to acquire library-searchable EI mass spectrum, high flow rate that enables fast MS detection response. Most of all, the use of electrolyte is not a problem in EC/MS with a PB interface. EC/PB/MS has been used to investigate the nonaqueous generation of the intermediate radical cations in the electrochemical oxidation of triphenylamine (TPA). The MS hydrodynamic voltammogram obtained, in which the intensity of the MS-detected ionic species is plotted as a function of the electrode potential, has explained the change of current with cell voltage in off line flow injection analysis (FIA)

In the EC/PB/MS investigation of TPA oxidation, the intermediate monocation of tetraphenylbenzidine (TPB) was readily detected. However the detection of TPB dication was hampered by an interfering ion produced from EI ionization This problem was circumvented by monitoring the intensity ratio of the ion of interest vs the TPA molecular ion against the EC cell voltage It was also shown that the use of chemical ionization (CI) could alleviate the spectral overlap problem. The ultimate solution came from the use of electrospray ionization (ESI) combined with a high-resolution Fourier transform ion cyclotron resonance mass spectrometer (FTICR MS)

One additional finding from the EC/PB/MS study was that the use of a nonvolatile electrolyte, tetrabutylammonium perchlorate (TBAP), could significantly enhance the signal of TPA molecular ion The mechanism of this signal enhancement process has been investigated by changing the TBAP concentration, using different electrolyte and neutral additives, employing different ionization modes and different analytes. It was concluded that the types of electrolyte cation and anion as well as the charge were influential factors The signal enhancement was attributed to an improved mass transport of analyte through the PB interface as well as a reduced fragmentation of TPA molecular ion in the EI ion source The formation of TPA/TBAP aggregates was considered responsible for these results It was found that the optimum mass transport efficiency was obtained when the concentration ratio of TBAP/TPA was ~10/1 It was further concluded that by maintaining the concentration ratio at this value during the calibrations, an enhanced detection sensitivity and linearity of calibration curves could be obtained. This hypothesis has been verified experimentally. This finding also explained why in many cases, the addition of mobile phase additives in PB/MS analysis could not enhance the linearity of calibration curves, when a constant concentration of additives were used.

The use of ESI interface and high resolution FTICR MS for EC/MS has been exploited, to distinguish the TPB dication from the interfering ionic species at the same m/z. In this work, a new EC flow cell was developed and coupled to the ESI-FTICR MS. A novel feature of this cell design is that it allows testing different electrode configurations without interrupting MS conditions. In one configuration, the working electrode functioned as spray needle, which greatly minimized the MS detection response time. Significant enhancement of TPB radical monocation in the EC/ESI-FTICR MS was achieved. The generation of TPB dication was detected, and was distinguished from the interfering ions based on the isotopic ions and isotopic abundance ratios. The EC/ESI FTICR MS results have verified the generation and conversion of TPA radical ion, TPB radical monocation and TPB dication during TPA oxidation. Comparison of the results from EC/ESI-MS and ESI/MS suggested that the electrospray ionization of TPA was limited to the spray tip region.

Signal suppression from electrolytes is a known phenomenon in ESI-MS analysis. The choice of electrolytes for EC/ESI-MS in nonaqueous system was limited to the use of lithium triflate, a less common electrolyte. This lack of general applicability of EC/ESI-MS to common electrolytes such as quaternary ammonium salts has greatly hindered the development of EC/ESI-MS. In EC/ESI-FTICR MS, it was found that the application of EC cell voltage could significantly reduce the signal suppression problem arising from a surface-active electrolyte, TBAP. In fact, it was shown that by using the EC cell configuration that employed the spray needle as working electrode, the EC/ESI MS results obtained with TBAP as electrolyte were similar to those with lithium triflate electrolyte. This finding is of great significance because it demonstrated that the signal suppression problem from electrolytes could be easily overcome by applying a few volts of voltage to the ES spray needle, which was a part of the EC cell.

The effect of experimental parameters on the MS detection sensitivity for the electrochemical reaction products in EC/ESI-FTICR MS was also investigated. It was demonstrated that the solution flow rate, electrolyte concentration and analyte concentration were influential parameters. The relative intensity of TPA ion radical, TPB monocation and dication can be easily adjusted by changing these parameters. These parameters played their functions by affecting the reaction time, analyte oxidation potential and dimerization rate of the radical cations in the electrochemical cell. The effect of ESI parameters such as spray voltage and spray tip – counter capillary distance is relatively insignificant. However, the parameters related to the gas-phase processes might have significant impact on the MS detection sensitivity for the ions initially generated in solution by electrochemical reactions. The collision induced dissociation (CID) of TPA molecular ion in the ICR analyzer cell indicated that the TPA ion could undergo fragmentation and dimerization to form TPB product in the gas phase. The results showed that TPA ion radical could oxidize TPB in the gas phase, which led to the formation of TPB ion radical. As a result of gas-phase ion molecule or ion-ion reactions, it was found that a change in capillary voltage and ion accumulation time in the hexapole caused a change in the relative intensities of the electrochemically-generated ion intermediates and products. These results suggest that the experimental parameters in EC/ESI-FTICR MS should be carefully set so that they won't affect the MS detection of the ions originated in solution due to electrochemical reactions.

The reaction of cation radicals, generated from electrochemical oxidation of polycyclic aromatic hydrocarbons (PAHs), with pyridine was investigated by EC/ESI-FTICR MS. It was proposed that the nucleophilic reactions of the cation radicals with biological nucleophiles might be used to determine the concentrations of the nucleophiles. Among the three PAHs investigated, i.e., anthracene, perylene and rubrene, the anthracene and perylene cation radicals reacted readily with pyridine nucleophile. Significantly high MS detection sensitivity was observed for the anthracene-pyridine and perylene-pyridine adduct ions in EC/ESI-FTICR MS. It was demonstrated that the strong nucleophilic reaction with pyridine could greatly reduce the yield of hydrolysis products and dimerization products of the anthracene and perylene cation radicals.

One future direction of this work is to use EC/ESI-MS to pursue low-level detection of biological nucleophiles such as DNA bases, nucleosides and proteins, by attaching the cation radical "tag" to the targeted nucleophile and monitoring the adduction products. Another application that may be worth pursuing is the use of dual EC cells in EC/MS, in which two EC cells are in-line, with one used for reduction, another for oxidation. This dual cell setup can be particularly useful for the MS study of nitro-containing compounds. MS detection of nitro compounds is usually performed in the negative ion mode. With the use of dual cell in EC/MS, it may be possible to determine the nitro compounds in positive ion mode.

Suppression of analyte signal by surface-active electrolytes is of big concern in ESI-MS analysis. We have demonstrated that this problem can be overcome by using EC/ESI-MS in the oxidation of TPA. It would be of interest to extend this work to other systems. If this methodology is generally applicable, it may facilitate the development and application of HPLC/EC/MS and CE/MS since surfactant electrolytes are often involved in the separations.

Some improvements of the current EC/ESI-FTICR MS setup can also be made. The biggest problem with the current setup is the EC cell voltage control. In the performed EC/ESI-MS experiments, the EC cell voltage was applied from a battery source and was floated at the high ES spray voltage. As a result, accurate cell voltage control is impossible. If we can modify the electric configuration of the ESI MS and ground the spray needle, the high voltage hazard will be removed and more sophisticated electrochemical equipment can be used for cell voltage control. The grounding of the spray needle, which is a part of the EC cell in our setup, will not only make the EC/ESI-MS easier to perform, but also reduce the "electrochemical interference" from the ESI process. Under this condition, a three electrode cell operation can be employed for fine cell voltage control.

LIST OF REFERENCES

Adams R. N *Acc. Chem Res* **1969(a)** *2* 175

Adams R N *Electrochemistry at Solid Electrodes* Marcel Dekker New York, **1969(b)**

Amatore C Brown A R *J Am Chem Soc* **1996** *118* 1482

Anson C F Osteryoung A R *J Chem Edu* **1983** *60* 293

Apffel A Perry M L *J Chromatogr* **1991** *554* 103

Arakawa, R. Akura T Fukuo T Horiguchi, H. Matsubayashi, G *Bull Chem Soc Jpn* **1999** *72* 1519

Bard, A. J Faulkner L R *Electrochemical Methods* Wiley New York 1980

Bard A J Ledwith A Shine, H. J In *Advances in Physical Organic Chemistry* Gold, V Bethell D Eds. Academic Press New York, 1976 Vol 13 pp 155

Barton, D Ollis, W D *Comprehensive Organic Chemistry the Synthesis and Reactions of Organic Compounds* Oxford Pergamon Press New York, 1979

Baumgarten, M Mullen K *Top Curr Chem* **1994** *169* 1

Bellar T A Behymer T D Budde W L *J Am Soc. Mass Spectrom* **1990** *1* 92

Bellar T A Budde, W L Kryak D D *J Am Soc Mass Spectrom* **1994** *5* 908

Belov M E Nikolaev E N Anderson G A Auberry K J Harkewicz, R Smith R D *J Am. Soc Mass Spectrom* **2001** *12* 38

Bennett, J Gillen, G *J Am Soc. Mass Spectrom* **1993,** *4* 930

Beverbach A, Sabbioni G *Biomarkers* 1999 *4* 229

Bittins-Cattaneo B Cattaneo E Konigshoven, P Vielstich, W in *Electroanalytical Chemistry* Bard, A. J Ed Marcel Dekker Inc New York 1991 pp 181

Blades, A. T Ikonomou, M G Kebarle, P *Anal. Chem* **1991** *63* 2109

Blakley, C R., Carmody J J, Vestal, M L *Anal Chem* **1980** *52*, 1636

Blakley C R, McAdams, M J, Vestal, M L *J Chromatogr* **1978**, *158* 261

Bond, A M, Colton, R, Dagnostino A, Downard, A J, Traeger, J C *Anal Chem* **1995** *67* 1691

Brown, F R., Draper W M *Biol. Mass Spectrom.* **1991** *20* 515

Bruckenstein, S , Gadde, R R *J Electroanal Chem* **1974**, *50*, 163

Budde W L *Analytical Mass Spectrometry–Strategies for Environmental and Related Applications* Oxford University Press New York, 2001

Burka, L T, Guengerich, F P , Willard R J, MacDonald T L *J Am. Chem. Soc* **1985** *107* 2549

Cappiello A. Mass Spec Reviews, **1996** *15* 283

Cappiello A, Famiglini G, Rossi L, Magnani, M *Anal Chem* **1997** *69*, 5136

Careri M, Lombardi P, Mucchino, C, Cantoni, E *Rapid Commun. Mass Spectrom* **1999** *13* 118

Careri M, Mangia, A., Musci M *J Chromatogr A* **1996** *727* 153

Cavalieri, E. L, Rogan E G *Xenobiotica* **1995** *25*, 677

Cavalieri, E L, Rogan, E G *Free Radicals in Biology* Academic New York, 1984

Cavalieri E L, Rogan, E, Cremonesi, P, Devanesan, P *Biochem Pharmacol* **1988** *37*, 2173

Cavalieri E L, Rogan, E. G., Devanesan, P D, Cremonesi P, Cerny R L, Gross M L, Bodell W J *Biochemistry* **1990** *29* 4820

Clegg, G A, Dole, M *Biopolymers* **1971** *10* 821

Cole R. B Ed., *Electrospray Ionization Mass Spectrometry – Fundamentals Instrumentation and Applications* John Wiley&Sons, Inc New York 1997

Concialini V , Chiavari G, Vitali F *J Chromatogr* **1983**, *258* 244

Covey, T R, Bonner R. F, Shushan, B I, Henion, J D *Rapid Commun Mass Spectrom* **1988** *2* 249

Creaser C S Stygall, J W *Analyst* **1993** *118* 1467

Creason, S C Wheeler J Nelson, R. E. J *Org Chem* **1972** *37* 4440

Davoli, E Cerny R L, Gross, M L *Adv Mass Spectrom* **1989** *11A* 268

Debrodt, H Heusler K E *Z Phys. Chem* **1981** *125* 35

Deng, H T , Van Berkel G J *Anal Chem* **1999(a),** *71* 4284

Deng H. T Van Berkel G J *Electroanal* **1999(b),** *11* 857

Doerge, D R Burger M W Bajic S *Anal. Chem* **1992** *64* 1212-1216

Dole M Hines, R L Mack L L Mobley R C Ferguson, L D Alice M B *J Chem Phys.* **1968** *49* 2240

Dolnikowski G G., Gross, M L Cavalieri E L *J Am Soc Mass Spectrom* **1991** *2* 256

Dryhurst G *Electrochemistry of Biological Molecules* Academic Press New York, 1977

Eberson, L Nyberg, K *J Am Chem. Soc.* **1966** *88* 1686

Erickson R Lindgren, M Lund, A Sjoqvist, L *Colloids Surf A* **1993**, *72* 207

Fenn, J B *J Am. Soc. Mass Spectrom* **1993** *4* 524

Fernandez de la Mora, J Locertales I G *J Fluid Mech* **1994** *243* 561

Fernandez de la Mora, J Van Berkel G J Enke C G Cole, R B Martinez-Sanchez, M. M. Fenn, J B *J Mass Spectrom* **2000** *35* 939

Freeman, J A., Johnson J V Yost, R A., kuehl, D W *Anal Chem* **1994** *66* 1902

Friend, K. E. Ohnesorge W E *J Org Chem* **1963** *28* 2435

Gieniec, J Mack L L Nakamae, K Gupta, C Kumar V Dole, M *Biomed. Mass Spectrom.* **1984** *11* 259

Gierlich, H H. Rollgen, F W Borchers F Levsen, K *Org Mass Spectrom* **1977**, *12*, 387

Gold, A., Jayaraj K Ball L M *J mol Catal A-Chem* **1997** *125* 23

Grosshans, P. B., Marshall, A. G. *Int. J. Mass Spectrom.* **1991**, *107*, 49

Grosshans, P. B., Marshall, A. G. *Int. J. Mass Spectrom. Ion Processes* **1992**, *115*, 1

Guo, X., Sievers, H. L., Grutzmacher, H. F. *Int. J. Mass Spectrom.* **1999**, *185*, 1

Hamann, C. H., Hamnett, A., Vielstich, W. *Electrochemistry*, Wiley-VCH, Weinheim, Germany, 1998

Hambitzer, G., Heitbaum, J. *Anal. Chem.* **1986**, *58*, 1067

Hambitzer, G., Heitbaum, J., Stassen, I. *Anal. Chem.* **1998(a)**, *70*, 838

Hambitzer, G., Heitbaum, J., Stassen, I. *J. Electroanal. Chem.* **1998(b)**, *447*, 117

Hammerich, O., Parker, V. D. *J. Am. Chem. Soc.* **1974**, *96*, 4289

Hammerich, O., Parker, V. D. *Acta Chem. Scand. B* **1982**, *36*, 519

Harvey, R. G., Ed. *Polycyclic Aromatic Hydrocarbons: Chemistry and Carcinogenicity*, Cambridge University Press, Cambridge, 1991

Higasi, K., Baba, H., Rembaum, A. *Quantum Organic Chemistry*, Wiley (Interscience), New York, 1965

Ho, J. S., Behymer, T. D., Budde, W. L., Bellar, T. A. *J. Am. Soc. Mass Spectrom.* **1992**, *3*, 662

Ho, J. S., Bellar, T. A., Eichelberger, J. W., Budde, W. L. *Environ. Sci. Technol.* **1990**, *24*, 1748

Honing, M., Barcelo, D., van Baar, B. L. M., Brinkman, U. A. T. *J. Mass Spectrom.* **1996**, *31*, 527

Ikonomou, M. G., Blades, A. T., Kebarle, P. *Anal. Chem.* **1991**, *63*, 1989

Incorvia Mattina, M. J. *J. Chromatogr.* **1991(a)**, *549*, 237

Incorvia Mattina, M. J. *J. Chromatogr.* **1991(b)**, *542*, 385

IriBarne, J. V., Dziedzic, P. J., Thomson, B. A. *Int. J. Mass Spectrom. Ion Phys.* **1983**, *50*, 331

IriBarne, J. V., Thomson, B. A. *J. Chem. Phys.* **1976**, *64*, 2287

Janz, G. J., Tomkins, R. P. T. *Nonaqueous Electrolytes Handbook*, Academic Press

New York, 1972 Vol 1

Johnson, K A., Shira, B A, Anderson, J L, Amster, I J *Anal. Chem* **2001** *73* 803

Juvra, U, Wikstrom, H V, Bruins, A P *Rapid Commun. Mass Spectrom* **2000** *14* 529

Kebarle, P *J Mass Spectrom* **2000** *35* 804

Kebarle, P, Tang, L *Anal. Chem* **1993** *65* 972A.

Kertesz, V Van Berkel G J *J Mass. Spectrom* **2001** *36*, 204

Kihara, T, Sasaki, K., Shiba, H *Bull Chem Soc. Jpn* **1971** *44* 3457

Kim, I S Sasinos, F I Stephens R D Brown M A *J Agric. Food. Chem* **1990** *38* 1223

Kissinger P T Heineman W R *Laboratory Techniques in Electroanalytical Chemistry* Marcel Dekker Inc New York, 1984

Kleintop, B L, Eades, D M, Yost R A *Anal Chem* **1993** *65* 1295

Knight, L B *Acc Chem Res.* **1986** *19* 313

Krahmer M T Johnson, Y A, Walters, J J, Fox, K F Fox, A, Nagpal, M *Anal Chem* **1999** *71* 2893

Lesage S *J Chromatogr* **1993** *642* 65

Li, Y Koropchak, J A *Instrumentation Science & Technology* **1998** *26* 389

Limbach P A, Grosshans, P B Marshall A G *Int J Mass Spectrom Ion Processes* **1993** *123*, 41

Limbach, P A, Schweikhard L, Cowen, K A McDermott M T, Marshall A G, Coe, J Y *J Am Chem. Soc.* **1991** 113 6795

Lu, T Y, Shiu, L L, Liah, T Y, Her G R *Rapid Commun. Mass Spectrom* **1995** *9* 93

Lu W, Xu, X, Cole R B *Anal Chem* **1997** *69* 2478

Lund, H *Acta Chem Scand.* **1957**, *11* 1323

Majeski E J, Stuart J D Ohnesorge, W E *J Am Chem Soc* **1968** *90* 633

Malachesky, P. A., Marcoux, L. S., Adams, R. N. *J. Phys. Chem.* **1966**, *70*, 2054

Mann, C. K., Barnes, K. K. *Electrochemical Reactions in Nonaqueous Systems*; Marcel Dekker, Inc.: New York, 1970

Marcoux, L. S., Adams, R. N., Feldberg, S. W. *J. Phys. Chem.* **1969**, *73*, 2611

Marcoux, L. S., Fritsch, J. M., Adams, R. N. *J. Am. Chem. Soc.*, **1967**, *89*, 5766

Marshall, A. G., Hendrickson, C. L., Jackson, G. S. *Mass Spectrom. Rev.* **1998**, *17*, 1

McCarley, T. C., Lufaso, M. W., Curtin, L. S., McCarley, R. L. *J. Phys. Chem. B* **1998**, *102*, 10078

Meng, C. K., Mann, M., Fenn, J. B. *Proceedings of the 36th ASMS Conference on Mass Spectrometry and Allied Topics*: San Francisco, CA, June 5-10, 1988, p. 771

Mohilner, D. M., Adams, R. N., Argersinger, W. J. *J. Am. Chem. Soc.* **1962**, *84*, 3618

Moldovan, Z., Bayona, J. M. *Rapid Commun. Mass Spectrom.* **2000**, 14, 379

Murphy, M. M., Stojek, Z., O'Dea, J. J., Osteryoung, J. G. *Electrochim. Acta* **1991**, *36*, 1475

Nerkam, W. C., Dimeler, G. R., Desmond, M. M. *J. Electrochem. Soc.*, **1964**, *111*, 1190

Nelson, R. F., Adams, R. N. *J. Am. Chem. Soc.* **1968**, 90, 3925

Nelson, R. F., Feldberg, S. W. *J. Phys. Chem.* **1969**, *73*, 2623

Nelson, R. F., Philp, Jr., R. H. *J. Phys. Chem.* **1979**, *83*, 713

Niessen, W. M. A. *Liquid Chromatography-Mass Spectrometry*, 2nd ed.; Marcel Dekker, Inc.: New York, 1999

Oyama, M., Nozaki, K., Okazaki, S. *Anal. Chem.* **1991**, *63*, 1387

Pachuta, S. J., Kenttamaa, H. I., Sack, T. M., Cerny, R. L., Tomer, K. B., Gross, M. L., Pachuta, R. R., Cooks, R. G. *J. Am. Chem. Soc.* **1988**, *110*, 657

Parker, V. D. *Acta Chem. Scand.* **1970(a)**, *24*, 2757

Parker, V. D. *Acta Chem. Scand.* **1970(b)**, *24*, 3151

Peover, M. E., White, B. S. *J. Electroanal. Chem.* **1967**, *13*, 93

Phelps, J.; Santhanam, S. V.; Bard, A. J. *J. Am. Chem. Soc.* **1967**, *89*, 1752

Pretty, J. R.; Deng, H. T.; Goeringer, D. E.; Van Berkel, G. J. *Anal. Chem.* **2000**, *72*, 2066

Pross, A.; Moss, R. A. *Tetrahedron Lett.* **1990**, *31*, 4553

Pryor, W. A., Ed. *Free Radicals in Biology*. Academic: New York, 1984

Quenzer, T. L.; Emmett, M. R.; Hendrickson, C. L.; Kelly, P. H.; Marshall, A. G. *Anal. Chem.* **2001**, *73*, 1721

RamaKrishna, N. V. S.; Cavalieri, E. L.; Rogan, E. G.; Dolnikowski, G.; Cerny, R. L.; Gross, M. L.; Jeong, H.; Jankowiak, R.; Small, G. J. *J. Am. Chem. Soc.* **1992**, *114*, 1863

Ramakrishna, N. V. S.; Padmavathi, N. S.; Cavalieri, E. L.; Rogan, E. G.; Cerny, R. L.; Gross, M. L. *Chem. Res. Toxicol.* **1993**, *6*, 554

Razzazi-Fazeli, E.; Schmid, R. W. *Rapid Commun. Mass Spectrom.* **1998**, *12*, 1859

Regino, M. C. S.; Brajter-Toth, A. *Anal. Chem.* **1997**, *69*, 5067

Regino, M. C. S.; Brajter-Toth, A. *Electroanalysis* **1999**, *11*, 374

Regino, M. C. S.; Weston, C.; Brajter-Toth, A. *Anal. Chim. Acta* **1998**, *369*, 253

Ristagno, C.; Shine, H. J. *J. Org. Chem.* **1971**, *36*, 4050

Rogan, E. G.; Cavalieri, E. L.; Tibbels, S. R.; Cremonesi, P.; Warner, C. D.; Nagel, D. L.; Tomer, K. B.; Cerny, R. L.; Gross, M. L. *J. Am. Chem. Soc.* **1988**, *110*, 4023

Rooney, J. J.; Pink, R. C. *Trans. Faraday Soc.* **1962**, *58*, 1632

Schoener, D. F.; Olsen, M. A.; Cummings, P. G.; Basic, C. *J. Mass Spectrom.* **1999**, *34*, 1069

Seo, E. T.; Nelson, R. F.; Frisch, J. M.; Marcoux, L. S.; Leedy, D. W.; Adams, R. N. *J. Am. Chem. Soc.* **1966**, *88*, 3498

Shida, T.; Haselbach, E.; Bally, T. *Acc. Chem. Res.* **1984**, *17*, 180

Shiotani, M. *Magn. Reson. Rev.* **1987**, *12*, 333

Sumiyoshi, T. *Chemistry Letters* **1995**, 645-646

Symons, M. C. R. *Chem. Soc. Rev.* **1984**, *13*, 393

Tang, L., Kebarle, P. *Anal. Chem.* **1991**, *63*, 2709

Tang, L., Kebarle, P. *Anal. Chem.* **1993**, *65*, 3654

Thomson, B. A., Iribarne, J. V., Dziedzic, P. J. *Anal. Chem.* **1982**, *54*, 2219

Toriyama, K., Nunome, K., Iwasaki, M. *J. Am. Chem. Soc.* **1987**, *109*, 4496

Trippel-Schulte, P., Zeiske, J., Kettrup, A. *Chromatographia* **1986**, *22*, 138

Van Berkel, G. J. *J. Am. Soc. Mass Spectrom.* **2000**, *11*, 951

Van Berkel, G. J., Asano, K. G., Schnier, P. D. *J. Am. Soc. Mass Spectrom.* 2001, 12, 853

Van Berkel, G. J., Giles, G. E., Bullock, IV, J. S., Gray, L. J. *Anal. Chem.* **1999**, *71*, 5288

Van Berkel, G. J., McLuckey, S. A., Glish, G. L. *Anal. Chem.* **1992**, *64*, 1586

Van Berkel, G. J., Zhou, F. *Anal. Chem.* **1995 (a)**, *67*, 2916

Van Berkel, G. J., Zhou, F. *Anal. Chem.* **1995 (b)**, *67*, 3958

Van Berkel, G. J., Zhou, F. M., Aronson, J. T. *Int. J. Mass Spectrom. Ion Process.* **1997**, *162*, 55

Veith, H. J. *Org. Mass Spectrom.* **1983**, *18*, 154

Volk, K. J., Lee, M. S., Yost, R. A., Brajter-Toth, A. *Anal. Chem.* **1988**, *60*, 720

Volk, K. J., Yost, R. A., Brajter-Toth, A. *Anal. Chem.* **1989(a)**, *61*, 1709

Volk, K. J., Yost, R. A., Brajter-Toth, A. *J. Chromatogr.* **1989(b)**, *474*, 231

Volk, K. J., Yost, R. A., Brajter-Toth, A. *J. Electrochem. Soc.* **1990**, *137*, 1764

Volk, K. J., Yost, R. A., Brajter-Toth, A. *Anal. Chem.* **1992**, *64*, 21A.

Von Stackelberg, M., Pilgram, M., Toome, V. *Z. Electrochem.* **1953**, *57*, 342.

Voyksner, R.D., Smith, C. S., Knox, P. C. *Biomed. Environ. Mass Spectrom.* **1990**, *19*, 523

Voyksner, R. D., Straub, R., Keever, J., Freeman, H. S., Hsu, W. *Environ. Sci. Technol.* **1993**, *27*, 1665

Werst, D. W., Trifunac, A. D. *J. Phys. Chem.* **1991**, *95*, 3466

Werst, D. W., Trifunac, A. D. *Acc. Chem. Res.* **1998**, *31*, 651

Whitehill, A. B., George, M., Gross, M. L. *J. Am. Soc. Mass Spectrom.* **1996(a)**, *7*, 628

Whitehill, A. B., George, M., Gross, M. L. *J. Am. Chem. Soc.* **1996(b)**, *118*, 853

Wilkes, J. G., Freeman, J. P., Heinze, T. M., Lay Jr., J. O., Vestal, M. L. *Rapid Commun. Mass Spectrom.* **1995**, *9*, 138

Wilkes, J. G., Zarrin, F., Lay Jr., J. O., Vestal, M. L. *Rapid Commun. Mass Spectrom.* **1995**, *9*, 133

Willoughby, R. C., Browner, R. F. *Anal. Chem.* **1984**, *56*, 2626

Winkler, P. C., Perkins, D. D., Williams, W. K., Browner, R. F. *Anal. Chem.* **1988**, *60*, 489

Wu, Y., Huang, S. *Anal. Chem.* **1999**, *71*, 310

Xu, X., Lu, W., Cole, R. B. *Anal. Chem.* **1996**, *68*, 4244

Xu, X., Nolan, S. P., Cole, R. B. *Anal. Chem.* **1994**, *66*, 119

Yamashita, M., Fenn, J. B. *J. Phys. Chem.* **1984**, *88*, 4451

Yoshida, K. *Electrooxidation in Organic Chemistry – The Role of Cation Radicals as Synthetic Intermediates* John Wiley&Sons, New York, 1984

Yoshiyuki, H., Masakum, D. *Pharmacogenetics* **1995**, *5*, s80

Young, J. C., Lafontaine, P. *Rapid Commun. Mass Spectrom.* **1993**, *7*, 352

Zhang, T., Brajter-Toth, A. *Anal. Chem.* **2000**, *72*, 2533

Zhang, T., Brajter-Toth, A. *Anal. Chim. Acta* **2001**, *442*, 97

Zhang, T., Palii, S. P., Eyler, J. R., Brajter-Toth, A. *Anal. Chem.*, accepted, August 2001

Zhou, F., Van Berkel, G. J. *J. Am. Chem. Soc.* **1994**, *116*, 5485

Zhou, F., Van Berkel, G. J. *Anal. Chem.* **1995**, *67*, 3643

BIOGRAPHICAL SKETCH

Tianyi Zhang was born in Guannan, Jiangsu, P.R. China, on January 8, 1969. He received a Bachelor of Science degree in Chemistry from Nanjing University, P.R. China, in 1991, and obtained a Master of Science degree in analytical chemistry from the same university in 1994. After graduation, he worked as an analytical scientist at Jiangsu Institute of Nuclear Medicine for three years, during which he was promoted to an associate director position of the instrumental lab in 1995. He married his lovely wife, Shuhui Wang, in 1996. In 1997, he decided to pursue a Doctorate degree overseas. He was admitted to several US universities and two Canadian universities. His decision to come to the University of Florida was partly influenced by his graduate supervisor at Nanjing University, Prof. Shimin Zhu, who had been a visiting scientist in the Toth Group.

Tianyi Zhang began his graduate studies at UF in August of 1997, under the direction of Dr. Anna Brajter-Toth. The birth of his lovely son, Yang Zhang, marked 1998 as a special year in his life. He completed his research and received a Doctor of Philosophy degree in December 2001.

I certify that I have read this study and that in my opinion it conforms to acceptable standards of scholarly presentation and is fully adequate in scope and quality as a thesis for the degree of Doctor of Philosophy

Anna Brajter-Toth, Chair
Associate Professor of Chemistry

I certify that I have read this study and that in my opinion it conforms to acceptable standards of scholarly presentation and is fully adequate, in scope and quality as a thesis for the degree of Doctor of Philosophy

John R Eyler

John R Eyler
Professor of Chemistry

I certify that I have read this study and that in my opinion it conforms to acceptable standards of scholarly presentation and is fully adequate, in scope and quality, as a thesis for the degree of Doctor of Philosophy

Weihong Tan
Associate Professor of Chemistry

I certify that I have read this study and that in my opinion it conforms to acceptable standards of scholarly presentation and is fully adequate, in scope and quality as a thesis for the degree of Doctor of Philosophy

Jon D Stewart
Associate Professor of Chemistry

I certify that I have read this study and that in my opinion it conforms to acceptable standards of scholarly presentation and is fully adequate, in scope and quality as a thesis for the degree of Doctor of Philosophy

John P Toth
Associate Research Scientist of Food
Science and Human Nutrition

This dissertation was submitted to the Graduate Faculty of the Department of Chemistry in the College of Liberal Arts and Sciences and to the Graduate School and was accepted as partial fulfillment of the requirements for the degree of Doctor of Philosophy

December 2001

Dean, Graduate School